Experimental Investigation of Ice Cutting by High-Pressure Water Jet:

Deicing on Marine Vessels

by

Emmanuel Junior Arhin

A Thesis submitted to the Faculty of Graduate Studies of

The Memorial University of Newfoundland

in partial fulfillment of the requirements of the degree of

MASTER OF ENGINEERING

Faculty of Engineering and Applied Science

Department of Mechanical Engineering

Memorial University of Newfoundland

St. John's, Newfoundland, Canada

Abstract

Ice development on surfaces during winter or in severely cold climates affects several industries, including aviation, hydropower, telecommunications, navigation, electrical distribution, and transportation. The traditional technique of deicing maritime vessels with human labor is laborious and time-consuming especially when ice adhesion strength is high. Current alternative deicing technologies may be too expensive or impossible to implement. Since water is easily accessible to maritime operations and heat energy diverted from the engine to heat up the water, high-pressure water jet (HPWJ) is proving to be a useful deicing technology, which is the focus of our investigation. HPWJ is currently used in high-level precision manufacturing in the automotive, aerospace, building products, electronics, food, paper and steel industries. HPWJ has low efficiency in strong winds, especially when the stand-off distance is long and might damage equipment if the operation parameters are not adjusted appropriately.

The main objective of this study is to investigate the combined effect of operational parameters including operating pump pressure, nozzle geometry, water jet temperature, and standoff distance on the depth of cut through an ice block at certain time of cut. The significance of the main objective is to maximize depth and width of cut in order to facilitate the delamination of ice accrued on surfaces. Ice was simulated in the lab by making ice blocks that were kept at -10 °C throughout the experiment. Preliminary cases were acquired using a factorial design of experiment at different levels with five parameters, including the nozzle type, yielding biased results. New cases were developed, and the measured responses were used to generate regression model equations for the four nozzle types.

The models predicted depth of cut with a P-value less than 0.0001 and an F-value of 23.26 with 99% confidence, showing that the models are significant. Also, the Predicted R^2 of 0.7473 is in

reasonable agreement with the Adjusted R^2 of 0.8166; i.e. the difference is less than 0. 2. According to the findings, the nozzle geometry has the greatest impact on the maximum depth of cut, followed by the time of cut, pump pressure, water jet temperature, and stand-off distance. Whereas the models predicted width of cut with a P-value less than 0.0001 and an F-value of 44.67 with 99% confidence, showing that the models are significant. The respective Predicted and Adjusted R^2 values of the width of cut are 0.8635 and 0.8973 and are in reasonable agreement with a difference of less than 0.2. Also, the nozzle geometry has the greatest impact on the maximum width of cut, followed by the stand-off distance, pump pressure, time of cut and water jet temperature.

This study investigated the effectiveness of HPWJ deicing on maritime vessels. The optimization of operational parameters is used to develop a cuttability chart for various thicknesses of accumulated ice on the deck and various vessel surfaces. To the best of authors' knowledge, this is the first research on the combined effect of operating pump pressure, water jet temperature, stand-off distance of the different nozzle geometries ($0°, 15°, 25°$ and $40°$) on the depth and width of cut in ice blocks.

Keywords: *Depth of cut, width of cut, high-pressure water jet, de-icing, ice block, ice accretion, optimization*

Acknowledgement

I would like to thank the Almighty God for giving me this opportunity to complete this chapter of my life. I would also want to thank Professor Yuri Muzychka for allowing me to work on this project. His excellent expertise of thermo-fluids and heat transfer has kindled an insatiable interest in these subjects in me. I have learnt so much from the process of finishing this thesis, and I am confident that the range of duties required to accomplish this project will be useful to me in the future. Many thanks go to Dr. Nana Baafour for providing excellent advice and patiently and humorously answering all of my questions and concerns. His scrutiny and refining of every piece of information is amazing; he wants everything to be exceedingly refined and polished to ensure distinctive quality work. I am appreciative to the American Bureau of Shipping and Mitacs for their financial support and to the technicians at Memorial University of Newfoundland's Thermo-Lab for their technical assistance.

Special thanks to my graduate friends, particularly Saroj Gautam, for his constructive criticism and reviews, as well as Fredrick Nana Oppong and Michelle Kwegyir-Aggrey for spending approximately 18 hours with me at the lab collecting data.

I am grateful for the love and prayers of my parents, Rev. Isaac Kofi Annan and Alberta Efua Annan, as well as my aunt Lucy Biney and sister Joyce Amankwaah, and my girlfriend Regina Ofori Boateng. I cannot ignore my friend Samuel Adade's wisdom and unwavering support.

Table of Contents

Tables of Figures

List of Tables

Nomenclature

e_B	Bias error	[-]
e_P	Precision error	[-]
e_T	Total error	[-]
U_c	Mean velocity	[ms^{-1}]
U_o	Exit velocity	[ms^{-1}]
$V_{o,v}$	Impact velocity	[ms^{-1}]
$c_{o,c}$	Sonic Velocity	[ms^{-1}]
ρM_o	Momentum flux	[Kgm^{-1} s^{-1}]
ρm_o	Volume flux	[ms^{-1}]
d_{ne}	Nozzle equivalent diameter	[m]
C_f	Nozzle flow coefficient	[-]
Q_f	Fluid flow rate	[m^{3}s^{-1}]
l	Length	[m]
N	Number of experimental cases	[-]
R	Responses	[-]
T	Temperature	[°C]
P	Pressure	[psi]
t	Time	[s]

r	Wave distance travelled	[m]
D, d	Diameter	[m]
A', C'	Stable points of vessel	[-]
A, C	Tilted points of vessel	[-]
G	Centre of gravity	[kgms^{-2}]
B_o	Buoyancy	[kgms^{-2}]
B	New center of buoyancy	[kgms^{-2}]
M	Metacenter	[m]
W	Weight of vessel	[kgms^{-2}]
X'	Distance between stable & tilted metacenter	[m]

Greek Symbols

ρ	Density	[kgm^{-3}]
$\Delta \tau$	Peak pressure duration	[s]
μ	Dynamic viscosity	[Pa.s]
π	Pi	[-]
α	Contraction angle	[°]
σ	Standard deviation	[-]

List of Abbreviations

SHP   Super-hydrophobic

HPWJ   High-pressure water jet

PMMA   Polymethyl methacrylate

CEL   Coupled Eulerian-Lagrangian

AWJ   Abrasive water jet

RANS   Reynolds-average Navier Stokes

gpm   Gallon per minute

Psi   Pound-force per square inch

DOE   Design of experiment

Std. Dev   Standard Deviation

ANOVA   Analysis of variance

P-value   Probability value

F-value   Fisher value

Df   Degree of freedom

Indices

i, j & k Direction along x, y and z respectively

1.0 Introduction

This chapter details the motivation and objective of this study. Ice accumulation on surfaces creates problems for many industries, including aviation, hydropower, telecommunications, navigation, electrical distribution, and transportation (Frankenstein & Tuthill, 2002).

1.1 Background and Problem Statement

The issue of ice accretion has driven the Marine Icing Group of the Memorial University of Newfoundland, to investigate the potential of high-pressure water jets to cut slots in ice blocks, primarily for possible usage as an aid to ice removal on marine vessels. The traditional approach of deicing shipping vessels manually requires tremendous effort and long hours, which at times yield unsatisfactory results when ice adhesion strength is high. Harsh weather makes the work environment even harsher to deice. With a practical setup of a high-pressure water jet aboard marine vessels, deicing could be done quickly- even in intricate areas of the ship, without causing any damage to decks and bulkheads.

This study investigates the possibility and effectiveness of a high-pressure water jet cutting through an ice block from a pressure washer with different nozzle spray angles. The penetration rate is measured under the influence of varying conditions: nozzle type (spray angle), operating pump pressure, temperature of water jet and stand-off distance. The positive findings will serve in developing an innovative, faster deicing method and integrated deicing equipment aboard marine vessels.

1.2 The Need for Deicing on Shipping Vessels

Deicing is an essential process for ships operating in cold climates or navigating through icy waters. During winter, ice can accumulate on a ship's surfaces, leading to multiple issues that may jeopardize the vessel's safety and efficiency.

One primary concern with ice build-up on a ship is the increased weight. Ice formation on board vessel can add to the ship's mass, reducing maneuverability (Andrei, 1975; Ryerson, 2013). Furthermore, ice can also impact the ship's stability, making it more susceptible to capsizing or rolling in turbulent waters (Ryerson, 2013).

This issue is especially significant in the 21st century, as oceans and seas have gained strategic importance worldwide. The shipping industry, crucial to the maritime economy, now plays a vital role in many countries' maritime strategy (Zhou et al., 2022). With the melting of Arctic ice, new shipping lanes are emerging, decreasing dependence on traditional routes and substantially reducing shipping times and costs. Additionally, due to intense global competition for resources, the Arctic region, rich in oil and natural gas, is highly coveted (Donald et al., 2009). Consequently, marine vessels and drilling rigs are expected to increase their activity in the area. The shipping and oil and gas industries face challenges from extreme weather conditions, particularly in the Arctic, where cold snaps can create problems. Icing is a significant hazard that can interfere with communication equipment, make handrails, ladders, and decks slippery, render life-saving and firefighting equipment inoperable, and compromise the stability and integrity of vessels (Samuelsen et al., 2015). When avoidance of ice accretion is not possible and anti-icing is not applied, a deicing solution may be necessary.

Figure 1.1 displays the metacenter of ships and how ice accumulation can alter the center of buoyancy. Ice buildup on ship decks and exposed surfaces is frequently uneven, changing the

vessel's center of gravity and increasing rolling moment, compromising stability (Ryerson, 2013). In such events, the ship may likely capsize (Garry & Ivana, 1963), resulting in fatalities and loss of goods (Lagerveld et al., 2013). The points A and C of a vessel in a stable posture and steady waters coincide with the water's surface. In a neutral stance, the centers of gravity G and buoyancy B_o are above and below the water surface, respectively, in most cases. Because of the ice formation on one side of the vessel, the center of gravity G raises, which increases the rolling moment of the ship, giving it a metacenter M and a new center of buoyancy, B. The ship will capsize if the point M falls below G. As a result, vessels must be deiced as soon as possible before any catastrophe occurs.
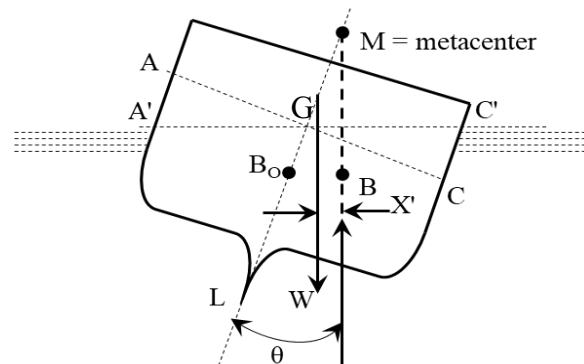
Figure 1. 1: The centers of gravity and buoyancy of ships, when ice accrued on ships, shifts its center of buoyancy

1.3 Sources of Ice Accretion on Shipping Vessel

The term "ice accretion" describes the process where ice forms and builds up on a ship's surface, potentially leading to unsafe and even disastrous situations. Ice formation on a vessel can occur through various means, such as freezing spray or seawater solidifying upon contact with the ship's superstructure. Ice accretion poses a considerable risk to a ship's stability and manoeuvrability and

presents a significant danger to vessels operating in frigid environments. Figure 1.2 shows ice accumulation on marine vessels.
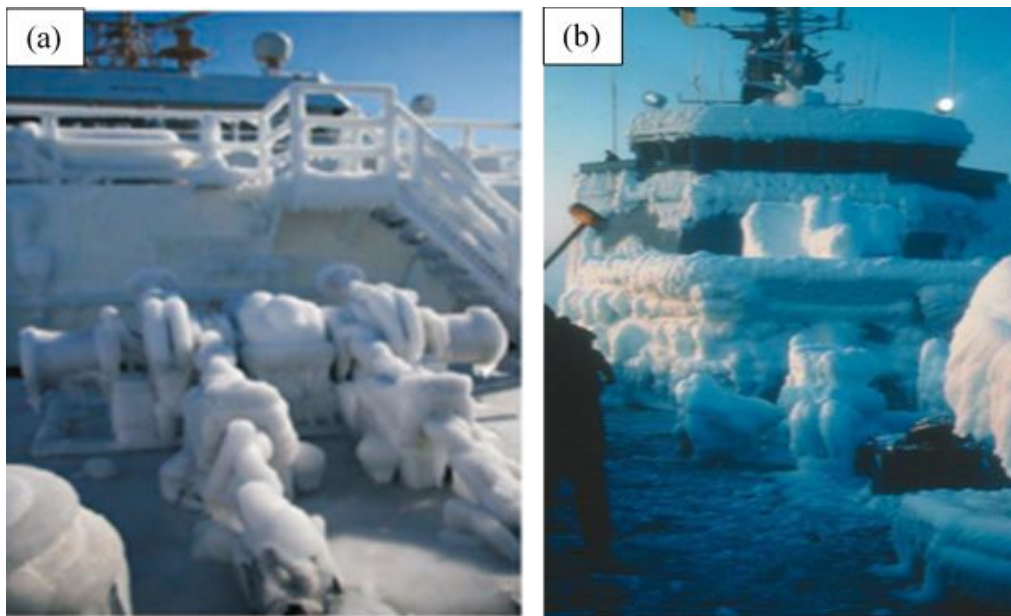
Figure 1. 2: Ice accretion on shipping vessels (a) (Cammaert, 2013) ; (b) (Samuelsen et al., 2015)

According to literature (Kulyakhtin & Tsarau, 2014), multiple factors contribute to ice accumulation on ships, including low temperatures, which cause airborne moisture to freeze on the ship's surface; high humidity, which allows moisture in contact with the surface to freeze and build up as ice; strong winds, which cause waves to splash and subsequently freeze on the ship's surface; sea spray, which occurs when high waves or heavy seas result in spray contacting and freezing on the ship's surface, among other factors. However, after examining several icing incidents in shipping vessels documented in the relevant literature (Dehghani et al., 2016), it was discovered that sea spray icing and atmospheric icing are the two most common causes/sources, among several others. Sea spray icing was found to be responsible for 89.8% of all ice-related occurrences. In contrast, atmospheric icing accounted for 2.7%, sea spray icing accompanied by rain or fog accounted for 6.4%, and sea spray icing accompanied by snow accounted for 1.1%

(Borisenkov & Panov, 1972; Dehghani et al., 2016). A summary of these two most frequent sources is recapitulated in Table 1.1.

Table 1. 1: Summary of causes of icing in shipping vessels

Icing Cause/Source	Percentage of Occurrences
Sea spray icing	89.8%
Atmospheric icing	2.7%
Sea spray icing with rain or fog	6.4%
Sea spray icing with snow	1.1%

1.4 Physics of Vessel Icing

Several processes are involved in the two most common sources of ice accretion (sea spray icing and atmospheric icing). The following points highlight the various processes involved. These are summarized in Figure 1.3.
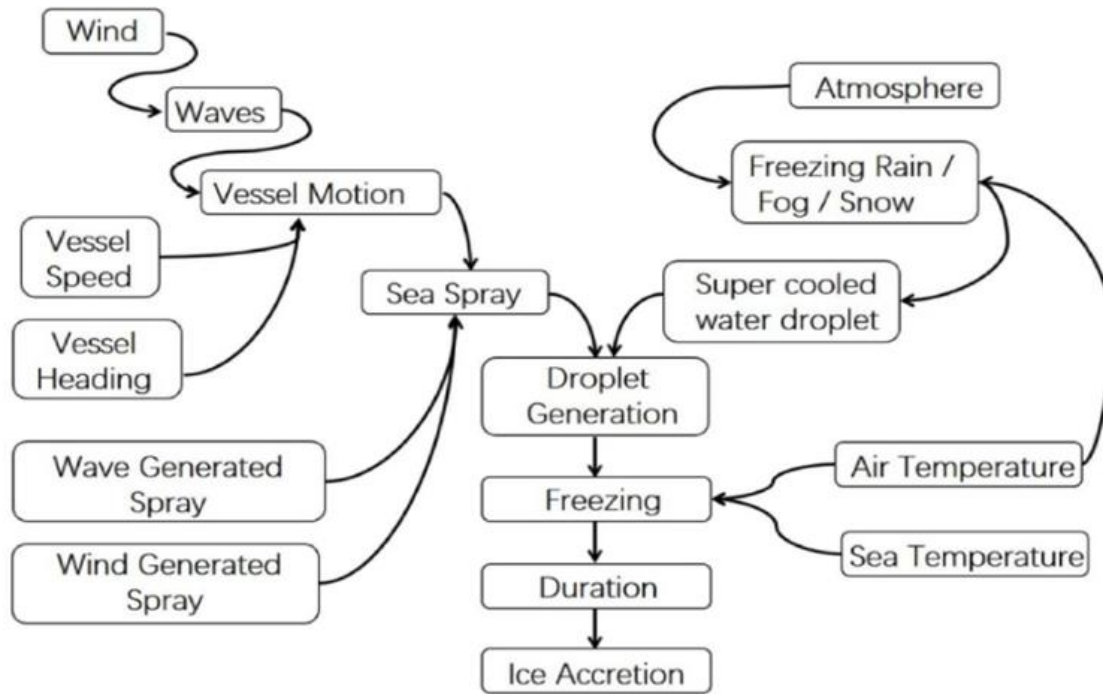
Figure 1. 3: Ice formation process on marine vessels (Mintu et al., 2016)

1.4.1 Sea Spray Icing

Sea spray icing is a phenomenon that occurs when seawater droplets in the air come into contact with ships or offshore structures and then freeze. There are two types of sea spray: wind-generated and wave-generated (Ryerson, 1995; Hansen, 2012). The interaction of waves with the structure wall generates sea spray, as the wave energy causes the water to move upward and separate into small droplets. This process of spray generation is primarily caused by wave energy dissipation. According to Jones and Andreas (2012), wind can also contribute to spray creation by pulling seawater from the wave crests. The process of sea spray icing begins with the formation of sea spray, which occurs when strong winds create waves that break and produce droplets of water carried by the wind. These droplets can travel long distances and may be transported to areas where the air temperature is below freezing, which can cause them to freeze on contact with any surface. Figure 1.4 shows a ship colliding with boisterous waves to create sea spray droplets.

6

Figure 1. 4: How icing occurs through sea spraying (Kulyakhtin & Tsarau, 2014)

When sea spray droplets come into contact with a cold surface, such as a ship's deck or a bulkhead, they freeze and form a layer of ice. This ice layer can grow rapidly and become very thick, which can cause serious problems for ships and offshore structures.

Sea spray may create ice on both decks and superstructures, which can cause communication, navigation, and radar difficulties due to antenna icing and ice on the wheelhouse windows. It can also cause damage to structures, as the weight of the ice can place significant stress on the object, leading to deformation or even collapse.

Wind-generated spray is formed when the wind blows water droplets from the whitecaps on the ocean surface. It appears as a layer of mist, and the water content of the droplets remains small and constant regardless of the wind conditions. On the other hand, wave-generated spray is created by the collision of ships or marine structures with waves. Wave-generated spray is the most important source of spray icing, while wind-generated spray produces less icing. This is because wave-generated spray has a higher water content and a larger quantity than wind-

generated spray. Additionally, wave-generated spray is formed when there is a collision between the wave and the ship or offshore structure, which provides a surface for the droplets to freeze on (Zakrzewski, 1987; Paul Zakrzewski et al., 1988).

Sea spray icing is a significant issue for ships and offshore structures operating in cold environments. Understanding the different types of sea spray and their characteristics is essential to develop effective strategies for mitigating the effects of sea spray icing.

The sea spray icing process has three main sub-processes, as outlined by Kulyakhtin (2014). The first sub-process is spray generation, which involves the formation of a water film and droplets. Dehghani et al. (2016) provide a detailed explanation of the formation of wave-generated spray during this process. The second sub-process is spray flow, where the wind carries the water film and droplets upward. During this process, the water film breaks into droplets (Ryerson, 2013; Dehghani et al., 2016), which may remain in a super-cooled state. The third sub-process is wet growth, where the super-cooled water droplets collide with the surface of the structures, creating ice followed by a liquid water film. As the ice thickness increases, the salt in the water precipitates, forming brine pockets and pure ice. Most of the unfrozen liquid water film is removed by gravity as runoff (Rashid et al., 2016), and only a small amount is intercepted. The process of ice formation on structures is called wet growth (Makkonen, 1987).

1.4.2 Atmospheric Icing

Atmospheric icing in shipping vessels occurs when super-cooled water droplets in the air come into contact with a surface that is below freezing temperature, such as a ship's deck, rigging, or antennas. Super-cooled water droplets are water droplets that are still in a liquid state but have a temperature below the freezing point of water (Wang, 2008).

When a vessel travels through areas with very low temperatures and high humidity, such as in Arctic or Antarctic waters, the super-cooled water droplets can freeze upon contact with the ship's surfaces. As more water droplets freeze, the ice can accumulate and form a thick layer. This is known as atmospheric ice accretion or atmospheric icing (Zhou et al., 2022).

The rate at which atmospheric icing occurs depends on a number of factors, including the temperature and humidity of the air, the speed and direction of the wind, and the shape and orientation of the ship's surfaces (Jorgensen, 1982). For example, surfaces that are exposed to the wind and are perpendicular to its direction are more likely to experience atmospheric icing than those that are sheltered or at an angle to the wind.

Atmospheric icing on shipping vessels can occur when the surface temperature of the ship is below the freezing point of water and the relative humidity of the surrounding air is high. When these conditions are met, water droplets or water vapor in the air can freeze onto the ship's surfaces, leading to the formation of ice (Rashid et al., 2016).

According to Ryerson (2013), the different components of atmospheric icing are glaze, snow, frost and rime. A summary table of these types of atmospheric icing is summarized in Table 1.2.

Glaze is a hard and transparent ice that forms from freezing rain or drizzle, with a density of approximately 900kg/m^3 (Brown et al., 1988). It can form on horizontal surfaces exposed to precipitation and vertical surfaces affected by wind and runoff. Glaze has a smooth and homogeneous texture that is difficult to remove, and even a thin layer less than 1mm thick can pose a danger to stairs and decks (Liljestrom and Lindgren, 1983). Accumulation of glaze on

machinery, such as winches and cranes, can cause cables to become locked in continuous ice, leading to equipment failure.

Snow is a type of precipitation consisting of small white ice crystals that form directly from vapor or liquid water in the air. It is the most common and serious form of atmospheric icing that can affect ships. The melting and re-freezing of snow may result in falling ice, which can be harmful to people and equipment. Moreover, snow on a ship's structure can become compressed to form white ice under certain weather conditions (Ryerson, 2011).

Frost is formed when water vapor directly sublimates into ice crystals. It can occur on various ship structures, such as decks, antennas, cranes, vents, railings, stairs, and cables, among others (Ryerson, 2013). Frost can create slipping hazards, even with a thickness as thin as 0.05mm (Ryerson, 1995; Haavasoja et al., 2002).

Rime is a type of atmospheric icing that forms when super-cooled fog or cloud droplets are carried by the wind (Ryerson, 2013). It can be categorized as either hard or soft rime, depending on the rate of heat loss during formation. Rime is the second-most common form of atmospheric icing that affects ships, usually forming first on windward objects and growing to maximum thickness (Makkonen, 1984). Rime can accumulate on both vertical and horizontal surfaces, potentially causing communication equipment failure and creating slippery surfaces (Fett et al., 1993). The most significant danger posed by rime on board ships is the risk of collapse and falling of large ice pieces, which can result in personal injury and equipment damage.

Table 1. 2: Summary of types of atmospheric icing

Type of Atmospheric Icing	Formation Process	Density	Impact on Ships
Glaze	Forms from freezing rain or drizzle	~900 kg/m³	Creates slippery surfaces, difficult to remove, can cause equipment failure

Snow	Forms from vapor or liquid water in the air	Varies	Adds extra weight and instability, damages deck machinery, creates slippery conditions, can result in falling ice		
Frost	Forms when water vapor directly sublimates into ice crystals	Varies	Creates slipping hazards, can occur on various ship structures		
Rime	Forms when super-cooled fog or cloud droplets are carried by the wind	Varies	Can cause communication equipment failure, creates slippery surfaces, risk of collapse and falling ice pieces		

1.5 Impact of The Various Hazard Rating Caused by Ice Accretion on Offshore Structures

As stated in earlier sections these two-icing source of ice accretion (sea spray icing and atmospheric icing) affect the safety of marine vessels and crew members. Table 1.3 provides the safety rating of how both atmospheric icing and sea spraying affect offshore structures. In order of priority, the following bullets highlight the various impact of the potential hazards on marine structures discussing the impact of these hazards. This matrix is connected to offshore platforms, and distinct ratings may apply to marine-specific matrices.

Table 1. 3: Safety consequences associated with various ice types and platform elements or functions, where higher figures represent a greater safety risk (Ryerson, 2013).

Hazard rating	Safety rating	Sea spray 10	Snow 8	Glaze 7	Rime 6	Frost 4
Stability	10	100	80	70	60	40
Integrity	10	100	80	70	60	40
Fire and rescue	9	90	72	63	54	36
Communications	8	80	64	56	48	32
Helicopter pad	8	80	64	56	48	32
Air vents	8	80	64	56	48	32
Flare boom	7	70	56	49	42	28
Handles, valves	6	60	48	42	36	24
Windows	5	50	40	35	30	20
Cranes	4	40	32	28	24	16

Winches	4	40	32	28	24	16
Stairs	4	40	32	28	24	16
Decks	3	30	24	21	18	12
Railings	3	30	24	21	18	12
Hatches	2	20	16	14	12	8
Cellar deck	1	10	8	7	6	4
Moon pool	1	10	8	7	6	4

1.5.1 Integrity

This pertains to a marine structure's (rigs, offshore wind turbine farms) likelihood of breaking apart due to the structural strain from ice accumulation on parts of the structure (Ryerson, 2011). Marine structures such as rigs are engineered to withstand oscillatory stresses resulting from wave movement; however, ice build-up can affect aspects like, inertia, drag, diameter, flexural response, roughness potentially altering the structure's resilience to waves (Crowley, 1988). However, ice accretion leads to stress that may lead to fatigue in the supports beneath the main deck, possibly causing the rig's collapse. Thus, the integrity of offshore structure tends to pose a risk causing issues such as sinking of the structure, rig's total loss, potential large-scale oil and drilling chemical spills and loss of personnel (Crowley, 1988).

1.5.2 Stability

The stability of marine vessels can be jeopardized by substantial ice accumulation on the superstructure, causing increased rolling moments and reduced freeboard. Uneven ice accumulation may lead to tilting, and marine vessels destabilization poses a high hazard due to potentially disastrous outcomes such as loss of lives and significant oil and chemical spills. The build-up of ice on components such as platform legs, bracing, blowout-preventer guidelines, mooring chains, marine risers, and kill and choke lines in the splash zone, especially in moderate sea conditions, presents a considerable issue (Baller, 1983).

1.5.3 Fire and Rescue Safety

Ice accretion poses the risk of fire danger. In that, if a fire or explosion occurs, ice accretion could lead to encasement which could result in difficulty to access rescue tools, including life rafts, fire and gas sensors, and firefighting equipment among others (Nauman, 1984). On decks that are slick and partially ice-blocked, crew cannot move quickly because of slips and falls causing slow movement with lots of tripping hazards. Additionally, ice build-up may make it more difficult to deploy lifeboats using passageways or davits (Ryerson, 2011).

1.5.4 Helicopter Landing Pad Hazard

The inability to use the helicopter landing pad due to icing hampers the supply of vital safety or medical supplies as well as the rapid rescue of injured or in danger crew members (Ryerson, 2011). In addition, employees may slip on landing platforms that lack safety railings, causing the helicopter to slide on the pad and making it harder to tie the chopper down (Zhou et al., 2022).

Boston (1985) reported that icing occurs on the U.S. Navy's Recovery Assist Securing Traversing (RAST) system that guides helicopters between hangars and launch and recovery positions on the flight deck.

1.5.5 Communication Hazard

Although it would be unlikely for an offshore platform to be lost due to a loss of communications, it could endanger the lives of crew members in the event that a life-threatening situation necessitated rescue or assistance. Due to their tiny diameters and exposed locations, whip and dipole communication antennas can accumulate ice. When water is trapped in ice, especially saline ice with pockets of brine, the dielectric constant rises and signals may be obstructed. Ice has the potential to bridge insulators and small antennae. Radio and radar outages make it impossible to contact potential rescue boats and aircraft. Due to bad weather and rough seas, supply boats and

helicopters may not be able to access platforms during icing episodes, however ice can continue after the weather clears up and keep communication open (Ryerson, 2011).

1.5.6 Ventilation Hazard

Due to the risk of dangerous or catastrophic gas concentrations, ventilation is essential on offshore structures. Blocking air intakes can make it more dangerous for combustible or deadly gases to build up in living spaces or other areas with ignition sources. Additionally, ventilation is frequently needed when operating machinery for cooling, exhaustion, and ignition. Essential operations could fail as a result of ventilation loss, and one or more crew members could perish. In severe cases, a power outage brought on by a machine shutdown could result in the structure being lost (Carstens, 1983).

1.5.7 Flare System Hazard

A flare system enables the safe combustion of petroleum products that cannot be safely gathered while oil is being extracted from the wells of an offshore drilling rig. It is extended at one end away from the main oil platform to keep the blazing flame as far away from the structure as is safe, protecting people, property, and the platform from the intense heat and burns. Since they stretch over water, flare booms are more susceptible to ice than many other platform structural components. They are consequently subjected to atmospheric and sea-spray ice. Flare systems are frequently lattice frameworks, which offer a lot of surface space for the accumulation of ice and snow. Flare booms release explosive gases, thus if the boom structure is damaged by ice or snow or the burner nozzles are blocked, an explosion, fire or concentrations of hazardous gases may result (Fagan, 2004). The safety of the crew and even the entire rig may be seriously jeopardized by ice effects on the boom.

1.5.8 Controlling Parts Blockage (valves, and ship handles and windows) Hazard

Critical parts that affect the safety of the rig or person could not operate due to frozen valve handles. Therefore, iced valves and handles may be tough to manipulate or may not turn at all, which is of a risk in shipping vessels (Ryerson, 2011). For workers operating cranes and other staff working in enclosed control stations, ice-covered windows reduce vision. Loss of visibility can be hazardous, yet most accidents and injuries it results in are not fatal. However, if a crane or other catastrophe resulted in an explosion or fire, the platform and the entire crew might be in danger (Ryerson, 2011).

1.5.9 Cranes, Stairs, Winches

Cranes are used to transport commodities and people to and from maritime vessels in addition to moving and handling other heavy loads. These are important to the shipping industry. Cranes are some of the tallest structures on platforms that can extend over 100 meters above sea level. Their open lattice booms are susceptible to rime and glaze icing and dangerous falling ice due to refreezing meltwater in structural gaps (Ryerson, 2013). Although not necessarily life-threatening, crane issues related to ice can result in injuries or operational disruptions. A falling crane derrick could potentially trigger a disastrous chain reaction.

Icy stairs present a falling hazard for workers due to slipperiness and irregular shapes that can lead to loss of footing.

Additionally, frozen winches can disrupt crane operations and other lifting or dragging tasks, posing risks to personnel.

1.6 Methods of Deicing/Anti-icing

In cold weather conditions, ensuring the safety and performance of structures depends on the application of both deicing and anti-icing techniques. Deicing is the act of eliminating existing ice

from various surfaces, while anti-icing is a preventive measure designed to inhibit ice formation on those surfaces from the outset.

An overview of some anti-icing and deicing methods cited in the literature have been presented in Table 1.4, along with their applications, advantages and disadvantages. Table 1.4 lists some deicing technologies investigated by researchers over the years in a variety of applications. It is demonstrated that the method of "high-velocity fluids," is very efficient but has the danger of damaging equipment and surfaces. This necessitates the characterization of operational parameters for the deicing equipment, in our case the commercial pressure washer.

Table 1. 4: Overview and applications of anti-icing and deicing methods

Reference	Methods	Highlights	Applications	Advantages	Disadvantages
Farzaneh & Ryerson (2011)	Coatings	Coatings provide passive ice protection and many have been shown to reduce the adhesion of ice to substrate	Large areas such as decks and bulkhead	No additional energy	Short effective time
Yu et al. (2021)	Covers	Handy and useful for preventing ice accumulation on outdoor equipment	Outdoor machinery	Low cost and convenience	Additional deicing and storage space for covers
(Li & Ye, 2009)	Manual deicing	Human labour is used to clear accumulated ice using a rod, hammer, and other tools.	Places where people can reach	Low cost and simple operation	Low efficiency and equipment damage risk
(Zaki & Barabadi, 2014)	High-velocity fluids	High-pressured fluid is used to lacerate ice accretions, making them easier to remove mechanically.	Open places such as decks and bulkheads	High efficiency and low energy exhaust	Relatively low efficiency under wind and equipment damage risk
Zdobyslaw Goraj (2004)	Pneumatic boots	Inflating and deflating tubes attached to the leading edges of aircraft wings and stabilizers and other structures with air.	Plane structures (e.g. bulkhead) and tubular structures (e.g. railings)	Low cost, simple operation, robustness and easy installation	Frequent replacement
Pommier-Budinger et al.(2018)	Piezoelectric actuators	Vibrating the ice structure to induce high-level stresses that result in delamination or cracking	Areas made of relatively thin and flexible materials	Low energy consumption and high efficiency Outdoor	Additional electric circuits and regular maintenance
Yehia & Tuan (1998)	Chemicals	Usage of chemicals such as salt on surfaces to avoid freezing by	Outdoor areas with little impact on people	Low cost and simple operation	Environment pollution and metal corrosion

		creating osmotic pressure, which causes water to flow toward the top layer of the slab where freezing occurs			
Zhao et al. (2020)	Electric heating	Using electricity to heat surfaces to prevent ice accumulation by reduce ice adhesion strength	Priority is given to critical equipment and areas	Good deicing effect	High energy consumption and risk of secondary icing
(Charles C. Ryerson, 2011)	Gas heating	Use of gases such as hot air to melt the ice on surfaces	Bulkheads, railings, decks, portholes, etc.	Full of waste gas	Additional air circuits required
(Zhou et al., 2022)	Water heating	Submerging the surface in water or passing water through heat exchangers to deice	Deck, forecastle winch, windlass and anchorage, etc.	Large heat capacity	High energy consumption
(Sollén et al., 2022; Zhou et al., 2022)	Infrared heating	Heat transfer via infrared emitters to be absorbed by ice or substrate	Heating for small areas	Ability to heat remotely	High energy lost in the medium

Figure 1.5 shows the different traditional de-icing and anti-icing techniques. Deicing techniques can be grouped into categories such as thermal, design, coatings, cover, and chemicals, while anti-icing methods can be classified under mechanical, thermal, and chemical approaches. More advanced deicing/anti-icing approaches include advanced electrical, ultrasonic, improved coating, among others.
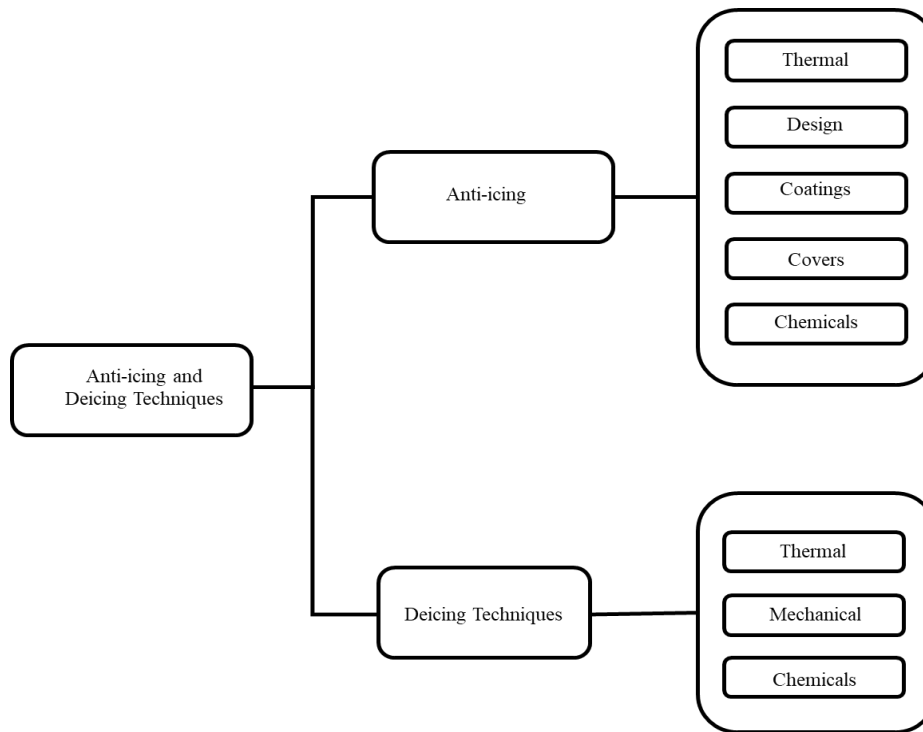
Figure 1. 5: Anti-icing and deicing methods (Zhou et al., 2022)

1.6.1 Conventional Methods of Deicing/Anti-icing.

1.6.1.1 Thermal

Various methods have been proposed to as a deicing/anti-icing technique. These include gas, electrical, infrared and water based thermal techniques. Discussing water-based strategies, which leverage its high heat capacity, water serves as an efficient solution for deicing and anti-icing purposes. Typically, there are a couple of ways to apply water on coated surfaces. The first method entails using a heat exchanger. A dependable heat exchanger system, able to operate at -45°C, is now available for melting ice on areas like the deck, forecastle winch, windlass, and anchor points (Esoy et al., 2019). The alternative technique involves completely covering the surface with water.

The electrical thermal approach includes heating surfaces above 0°C with a resistance wire to dissolve ice or prevent ice formation. The implanted resistance heating element is a popular appliance. Although electro-thermal devices are efficient for deicing and anti-icing operations, their high energy consumption and risk of re-icing restrict their use in more general circumstances. These systems are typically put in key locations, such antennae and portholes, to prevent ice collection (Makkonen, 2012).

Ice or the underlying surface can absorb heat emitted by infrared sources. According to Farzaneh & Ryerson (2011), the infrared heating is a form of remote heating technique. As noted by Ryerson (2011), the primary infrared radiation employed for ice protection falls within the wavelength range of approximately 3 to 15 micrometers. There are difficulties with heat loss during transmission, the possibility of materials overheating, and reliance on absorbent substrates. Consequently, infrared emitters should be positioned as close to the surface requiring heat as possible, and the chosen substrate material should exhibit an absorption spectrum outside the infrared range. This method is currently applied to small areas on ships.

According to Ryerson (2013), gas remains a valuable method for combating ice formation and accumulation notwithstanding its relatively low heat capacity and thermal conductivity. These gas heating systems are designed to capture exhaust gas directly from the engine compartment, changeling it upwards to areas in need of anti-icing and de-icing measures, such as bulkheads, decks, railings and viewports.

1.6.1.2 Chemical

Various industries rely heavily on chemicals for deicing and anti-icing applications, and these can be employed on ships as well. Chemical deicing agents include alcohol, bio-based compounds, chloride, acetic acid, among others. For open spaces such as decks, stairways, and other surfaces,

devices like garden sprayers for liquids or spreaders akin to those used in distributing lawn fertilizer can effectively address anti-icing and deicing needs occurs (Rashid et al., 2016). Meanwhile, more specialized, and fixed spray systems are necessary for tight spaces, including latticed structures and moon pool areas. There are different types of chemicals, some designed to melt ice and others intended to hinder ice formation on surfaces before freezing occurs. To reduce environmental pollution and material degradation, researchers are continually developing and assessing new chemicals (Kenzhebayeva et al., 2021).

1.6.1.3 Design

According to Ryerson (2011), optimizing the structural design may be the most effective way to minimize ice-related hazards. Emphasis should be on modifying the structure's geometry to decrease sea spray caused by wave-structure interactions (Deshpande et al., 2021). Enhanced bow rake and tumblehome can efficiently restrict ice accumulation on the bow deck by redirecting spray. A protective cover enclosing the forecastle deck at the bow helps prevent the internal structure from freezing. Elevated bulwarks and bows help reduce spray, subsequently decreasing the icing area through a simpler onboard layout.

1.6.1.4 Covers

This method of de-icing/anti-icing includes metal buildings and tarpaulins. Tarpaulins are created from ice-repellent or anti-icing materials. When tarpaulins that are freely fastened to the protected objects they are simpler to de-ice than those that are tightly tied (Ryerson, 2011). Crews use covers to cover lifting poles, anchor lifts, winches, and outdoor apparatus when travelling through cold climates to prevent ice (Zhou et al., 2022).

1.6.1.5 Coatings

Ice-repellent coatings and anti-icing coatings are the two main categories of coatings. To make ice less likely to stick to the surface, an ice-repellent coating is used. According to Ryerson (2013), an ideal ice-repellent coating should be able to greatly reduce the ice adhesion strength, be highly durable, be reasonably priced, and be simple to apply. Anti-icing coating on the other hand is used to encourage water droplets to run off before they freeze. According to Heydari et al. (2013), surfaces that can be waterproof may also be ice-proof. Ice-resistant coatings are typically rated for ability to reduce ice adhesion strength to substrates; however, their ability to endure repeated washings by saline water and abrasion before renewal are critical durability concerns for the use of these coatings, as is slipperiness when applied to trafficked areas and ability to function when contaminated (Ryerson, 2013).

1.6.1.6 Mechanical Techniques

This technique encompasses a broad varieties of techniques pneumatic boots, electro-expulsive separation, piezoelectric actuators, manual, and high-speed fluids/velocity (Zhou et al., 2022). Significant volumes of ice can be mechanically removed by high-velocity fluids. This technique works well since the ice may be broken up with just a tiny cut made by the fluids. Deicing fluid, water, air, or any mix of these can be used as the fluid (Villeneuve et al., 2015). On the other hand, manual mechanical deicing involves crews with the use of shovels, mallets and sticks. The "five-point chisel," a special instrument, is made to quickly shatter and remove ice off surfaces with little risk of damaging the composite materials (Ryerson, 2013). However, a major, disadvantage of manual mechanical is that this method is difficult in severe weather conditions. Also, although this method is cost-effective, the expense to the staff is substantial (Zhou et al., 2022).

Moving on to, piezoelectric actuators, these are transducers that transform electrical energy into mechanical movement or stress, or the other way around (Adriaens et al., 2000). When a unidirectional current flows through a piezoelectric crystal, the crystal is forced to bend. Thus, the substrate vibrates at a very high frequency when a high-frequency alternating current is delivered to piezoelectric actuators (Adriaens et al., 2000).

1.6.2 Advanced Methods of De-icing/Anti-icing

1.6.2.1 Icing Sensors

This is an advanced technique that employs a thin film capacitive-based sensor (Goraj, 2014). These icing sensors are composed of a copper electrode encased within a polyimide laminate, attached to the host airfoil. A minor electric field is established on the sensor's exposed surface. When ice forms on the sensor surface, the field characteristics change, and these alterations are detected by the sensor electrodes. The sensing area spans 1.5 inches chord-wise and 4.5 inches span-wise (Goraj, 2014). Figure 1.6 shows the schematic workflow of icing sensors.
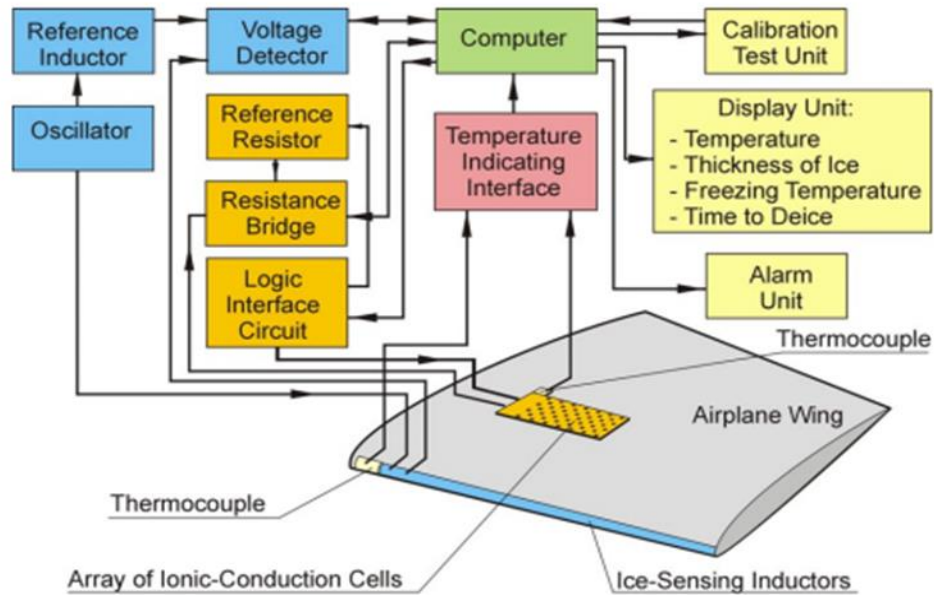
Figure 1. 6: Ice sensor monitoring system as a de-icing method developed by NASA (Goraj, 2014)

1.6.2.2 Ultrasound Technology

This technology has several applications both in maritime and aerospace industry. Some of its wide application include windscreen ice protection, freezer rime removal, mussel removal among others (Goraj, 2014). The most used ultrasonic wave for this application is the shear horizontal waves and the Lamb waves (Palacios et al., 2011). Based on the principles of wave propagation within a plate, ultrasonic waves have the potential to generate strains and displacements at the junction between ice and the primary structure (Zhou et al., 2022). Consequently, these forces could cause the ice to dislodge from the structure. Lamb waves experience less attenuation than conventional ultrasonic waves over the same propagation distance. This is due to a Lamb wave's energy attenuation ratio being $1/r$, as opposed to a standard ultrasound's $1/r^2$, where r represents the distance, the wave is traveling (Willberg et al., 2009) .

23

1.6.2.3 Microwave Technology

Concrete surfaces are warmed by microwave de-icing, which quickly heats magnetic and dielectric materials. Microwave radiation penetrates the ice, heats the road, and weakens the link between the ice and pavement, making it easier to remove ice off roadways when a truck-mounted microwave generator is used. The microwave heating principle is mainly used in microwave deicing. The method is based on molecular friction and heat production brought on by electric and magnetic dipoles in magnetic and dielectric materials aligning with an electric field (Lu et al., 2017). Microwave deicing operates by exposing dielectric and magnetic materials to an electric field, causing their electric or magnetic dipoles to align. This alignment, or polarization, generates a secondary electric field, reinforcing the primary one. As the electric field changes direction, molecular friction occurs, producing heat—faster changes yield more heat (Lu et al., 2017). A dielectric polarization diagram that exemplifies this process is seen in Figure 1.7. By absorbing microwaves, the substrate's temperature rises. As a result, the ice melts and the adhesion strength between the ice layer and the substrate weakens (Liu et al., 2020).

(a) No electric field   (b) Electric field
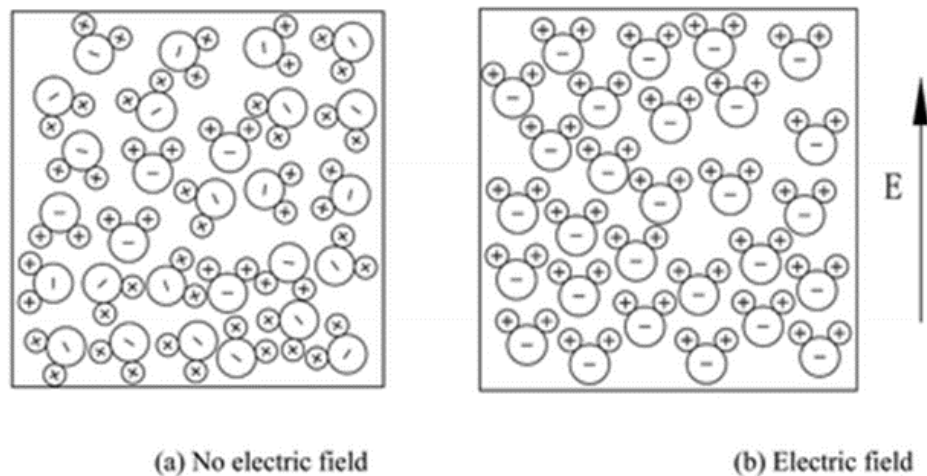
Figure 1. 7: Dielectric polarization process

1.7 Objectives

The main objective of this study is to investigate the combined effects of operational parameters, including pressure, nozzle geometry, water jet temperature, and standoff distance, on the depth and width of cut (penetration) through an ice block. The significance of the main objective is to maximize the depth and width of cut to facilitate the delamination of ice accretion on surfaces. As stated previously in the section 1.1, a realistic installation of a high-pressure waterjet aboard marine vessels will aid in rapid deicing, even in the most intricate areas of the ships, without causing any damage to walls or surfaces upon research breakthrough. The following are the objectives set for this project:

- Develop an experimental setup to measure the width of cut and penetration depth.
- Use statistical approach to obtain the optimum parameters that yields maximum width of cut and maximum penetration depth.
- Use statistical approach to develop correlations to characterize depth of cut and operational parameters of the deicing equipment.

- Use statistical approach to develop correlations to characterize width of cut and operational parameters of the deicing equipment.

- Determine significant parameters that affect the width and depth of cut.

- Develop a cuttability chart for ice cutting.

1.8 Organization of Thesis

This thesis is divided into five chapters, which are listed in the following order: introduction, literature review, methodology, discussion and results, and conclusions and recommendations.

Chapter 1: This chapter presents and describes the motivation behind this study. It states the background and problem statement for this research. The chapter also discusses various methods of deicing as well as the objectives for the study.

Chapter 2: This chapter examines a review of the literature on water jet technology, liquid jets, nozzles, and the equations that govern the flow of high-pressure fluids through nozzles. The chapter also discussed the principles of ice breakup and high-pressure fluid penetration.

Chapter 3: Details of the experimental setup are discussed in this session. The chapter also presents the design of experiment and the use of statistical tool to optimize the data of the parameters under investigation.

Chapter 4: This chapter presents discussion of the effects of the various parameters on the depth and width of cut. It provides statistical analysis of data to predict the most influencing parameters on the depth and width of cut. The statistical analysis was able to predict depth and width of beyond the parameter settings of this experiment.

Chapter 5: This chapter includes the study's conclusion, as well as future research recommended in the chapter.

2.0 Literature Review

This chapter summarizes previous research on ice-cutting and liquid jets. A detailed assessment of related literature is conducted to identify and address the knowledge gap.

2.1 Water Jet Technology

Waterjet technology, developed in the late 1960s by Dr Norman C. Franz at the University of Michigan, was first commercialized and installed by the McCartney Company in 1971 (Miller, 1990). Waterjet technology has since been popularized. Waterjet cutting technology has many applications in high-level precision manufacturing in the automotive, aerospace, building products, electronics, food, paper and steel industries (Miller, 1990). Since water is a coolant, using waterjet technology to cut temperature-sensitive materials is a viable option compared to other methods (Sharma et al., 2009). This process is readily accessible due to the availability of water, which can be recycled after cutting the material (Thakur et al., 2022). Also, this process leads to significantly less stress concentration on the cut surface, which makes it unique (Yuvaraj & Kumar, 2016). The cutting can be done either with water alone or with an abrasive additive, which is significant in the cutting process of more rigid materials (Engin, 2012; Gryc et al., 2014; Yuvaraj & Kumar, 2016; Liu et al., 2019; Bruno Arab & Barreto Celestino, 2020; Jerman et al., 2022). Water jet technology has advanced quickly and is utilized in many applications, such as rock cutting, mining, oil and gas drilling, and cleaning. These applications are based on theoretical and experimental investigations of the loads and damaging capabilities of the high-speed liquid jet (Zhaolong et al., 2014).

2.2 Impact of Liquid Jet: Pressure

Before introducing ice shattering by a high-speed water jet impact, it is vital to examine the load characteristics of the liquid jet colliding on a rigid or elastic wall, typically the two normal

boundaries. The simplest border is an impermeable wall. Due to the fluid's compressibility and shock wave propagation in various mediums, a high-speed liquid jet striking a flat wall causes an initial pressure peak on the wall within the stagnation region (Pingping et al., 2022). Previous studies investigated high-pressure water jet (HPWJ) and have presented several theories, such as, the water hammer effect, stress wave effect, impact effect, water wedge effect, cavitation effect, and pulsed load-induced fatigue damage(Zhao et al., 2019; Lu et al., 2021).

Semenov et al. (2013) investigated the formation of splashing jet at the initial stage following the collision of two liquids with the same density using the velocity potential theory with fully nonlinear boundary conditions and the assumption that the liquid was incompressible and inviscid. When the two jets were symmetrical, it looked like a jet hitting a hard wall. Dyment (2015) investigated the interaction between a compressible liquid and a rigid body by developing a model with compressible effects that could be applied to body profiles and jet fronts of any shape. Zhao et al. (2021) used theoretical and finite element methods to analyze how the geometric shape of a rigid body is affected by the impact pressure caused of a water jet. Additionally, they discovered a connection between the peak pressure and the opening angle, jet velocity, jet radius, and concave sphere radius under various concave surfaces.

The damage characteristics of the high-speed liquid jet on complicated boundaries are the subject of another significant area of research. Foldyna et al. (2009) investigated the effect of pulsating water jets on aluminum samples. They used a pressurized tap water from plunger pump to determine the impact pressure of a water jet striking the solid surface. Pulsating water jets created at pressures as low as 20 MPa were discovered to erode deeply and efficiently the aluminum surface due to repeated impacts of the water jet. According to Field et al. (2012), some of the cavities generated inside the liquid falling onto the solid surface may be the cause of the erosion

of metals and alloys at a lower impact. Additionally, when erosion progresses, lateral fluid movement may increase shear stresses on the surface, and hydraulic loads applied in cracks and crevices may hasten the destruction. Sun et al. (2013) examined the deformation caused by a water jet with a spherical head striking a plate made from Polymethyl methacrylate (PMMA), stainless steel, and aluminum. They then used the Coupled Eulerian-Lagrangian (CEL) method to summarize the relationships between the diameters and depths of the depressions and the mechanical characteristics of these materials.

Due to the demands of engineering applications, Wang et al. (2017) explored the interaction between a water jet and rocks. They concluded that the pressure of underwater jets has an impact on rock-breaking behaviors. Their research also investigated the effects of boundary conditions, impact velocity, and micro-structural and micro-mechanical aspects on rock-breaking behaviors.

2.2.1 Water Hammer Effect

The concept of water-hammer pressure is the fundamental principle behind the deformation of solid structures upon the imminent impact of a high-pressure liquid jet with the solid surface. The water hammer theory describes how pressure waves propagate in fully liquid-filled pipe systems (Tijsseling et al., 2008). The initial pressure of a water jet striking a flat solid is comparable to the water-hammer pressure (Parsons et al., 1928). The empirical formulation for water-hammer pressure, including the hypothesized assumptions, as presented by Hsu et al. (2013) is:

$$P = \rho v c \qquad (2.1)$$

Where P is the pressure, ρ is the liquid density, v is the impact velocity, and c is the sonic velocity of liquid. The initial high pressure predicted by the pressure equation rapidly diminishes due to release waves propagating into the jet from the circumference. They reported that the

pressure approaches hydro-dynamic pressure if impingement persists until a steady condition is established;

$$P = \frac{1}{2}\rho v^2$$

(2.2)

According to Brunton (1966), the water-hammer pressure represents the maximum pressure for the impingement of a spherical liquid drop:

$$P = \frac{\alpha}{2}\rho vc$$

(2.3)

Where α depends on impact velocity and approaches unity for high velocities.

They concluded that the water-hammer pressure only persists for as long as it takes the release wave, produced at the contact edge of the jet, to travel to the center. The duration, $\Delta\tau$, of this peak pressure with respect to the diameter, d, of the water jet is shown in the following equation:

$$\Delta\tau = \frac{d}{2c}$$

(2.4)

Raudensky et al. (2007) present an illustration of the mechanism of the water-hammer effect, shown in Figure 2.1, based on shock wave propagation. They noted that the impact shock wave propagation happens at sonic velocity soon after the hit, resulting in a rapid initial pressure

increase.
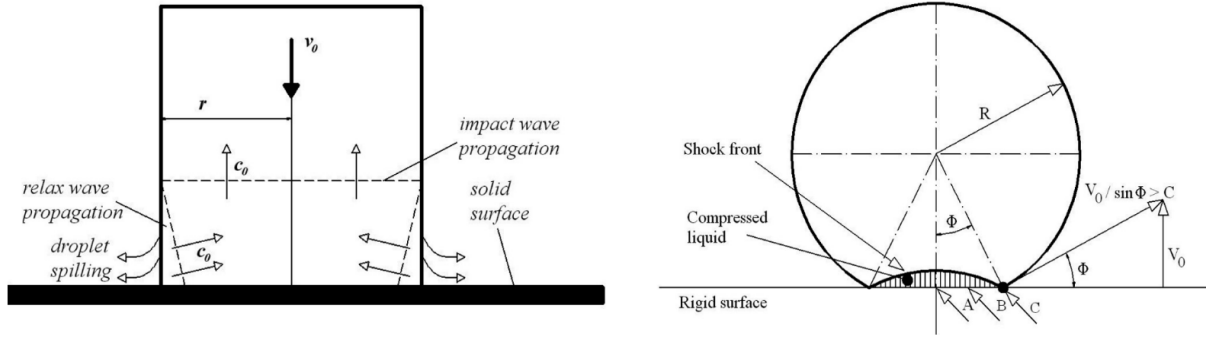
Figure 2. 1:Droplet impact, water-hammer effect (Raudensky et al., 2007).

The presented models by Raudensky et al. (2007) agree with the aforementioned formulas of maximum impact pressure, $P = \rho v c$, $P = \dfrac{\alpha}{2} \rho v c$, and duration, $\Delta \tau = \dfrac{d}{2c}$ by Brunton (1966); Hsu et al. (2013). Where $r = \dfrac{d}{2}$, $v \sim v_0$, and $c \sim c_0$.

2.3 Influence of Nozzle Geometry on Jet Impact

The nozzle shape significantly impacts a liquid jet's impinging capabilities. A wide range of nozzle geometry has been examined to investigate the effect of geometry, particularly the shape of the nozzle's inlet and outlet, on flow development and the impact on surfaces. Many studies have found that nozzle shape can somewhat influence turbulent jet flow (Mi et al., 2005; Deo, Mi, et al., 2007; Deo, Nathan, et al., 2007; Gentz et al., 2015; Nyantekyi-Kwakye, 2016). For example, in terms of centerline mean velocity, Uc, the jet emitted by a circular jet varies as $Uc \sim x^{-1}$ but the far field centerline velocity of a plane rectangular jet varies as $Uc \sim x^{-0.5}$ (Pope, 2000).

31

Lu et al. (2021) established the velocity and impact stress distribution at various target distances in their research. The jet velocity and the impact force decreases gradually as the target distance increases. They discovered that the contraction angle α, length-diameter ratio l/d, contraction section length, and outlet diameter are the most important nozzle characteristics influencing jet impact performance in coal crushing. They found that when the pressure is constant, the jet diffusion angle increases noticeably as the nozzle diameter increases, and when the nozzle diameter is constant, the diffusion angle changes little as the water pressure fluctuates.

The impinging performance of high-pressure water jets emerging from various nozzle orifice shapes was examined by Huang et al. (2020). Their study includes circular, triangular, square, elliptical, and crossed-shaped nozzles. They discovered two things: (i) the peak pressure of the circular jets is the highest, and the peak pressures of the square, triangular, crossed-shaped, and elliptical water jets drop in turn; and (ii) The circular water jet has the highest center velocity, the elliptical water jet has the lowest, and the square, triangular, and crossed-shaped jets are in the middle. They concluded that the peak pressure might be a combined action of the liquid velocities and the jet head shapes.

In another study on flat, round, and abrasive waterjet (AWJ) cutting nozzles by Srivastava et al. (2016), the magnitude of the compressive residual stresses induced at the subsurface at 50 microns was found to be approximately 15% greater than the base material hardness, and flat nozzles were found to be more efficient in terms of higher compressive residual stresses induced on the treated surface. Begenir et al. (2004) examined water jet profiles to establish breakup lengths and spray angles for various nozzle geometries. They provided a comprehensive evaluation of cone-down, cone-up, and cylindrical nozzles. Compared to the other two geometries, their results showed that

the cone-up nozzle creates water jets with significantly shorter intact lengths, slightly higher spray angles, and a higher discharge coefficient.

2.4 Ice Mechanics

Ice is viewed as one of nature's most complex materials from the perspective of ice mechanics (Timco & Weeks, 2010). Numerous flaws can be found in a natural ice sheet, including pre-existing fissures, inclusions, pores, grain boundaries. The flaws significantly affect the ice sheet's characteristics and mechanical behavior, making it challenging to accurately replicate the natural ice sheet in a lab setting. An alternate way in a lab is to create a purportedly "clean" ice sheet using de-aired fresh water to eliminate the effects of these faults (Ni et al., 2021). This study uses an ice block created from fresh tap water.

One of the challenges faced by ships and other equipment operating in an ice-covered ocean region is ice breaking (Xue et al., 2020). Breaking ice using a rod, which may be viewed as either a concentrated load or a distributed load depending on the ratio between the rod's diameter and the ice thickness, is one of the simplest and earliest icebreaking techniques (Masterson, 2009). It is widely accepted that there are three stages of ice cover failure under static concentrated and distributed loads: the radial cracking, caused by significant bending moments; the circumferential cracking at a distance from the load; and the breakup of an ice plate along the radial and innermost circumferential cracks. Although the reasons are different, these three stages—considered adequate for the high-speed water jet loads in this paper—are typical for breaking an ice plate under a vertical force (Sodhi, 1995; Gold, 1971; Lu et al., 2015; Ni et al., 2021).

To increase the ability to break through ice to pave way for ship movement, new auxiliary technologies, such as icebreakers, are constantly being pursued and researched (Ni & Wu, 2020). Future icebreakers may be equipped with high-speed water jet generators to shatter or crack the

thick ice in a significant portion of the area in front of the vessels. As a result, the icebreaker cruising in the ice area will have less "breaking ice resistance." For theoretical and numerical research, cracking ice with a high-speed water jet poses a complex interaction problem with several interfaces, including the water-gas and ice-water interfaces. Additionally, it has been demonstrated that the shock wave and the bubble jet are efficient at breaking ice using high-pressure bubbles (Yuan et al., 2020), which establishes a solid foundation for icebreaking utilizing a high-speed water jet.

2.5 Jet Flow Governing Equations

2.5.1 Equations of Flow

For an incompressible Newtonian fluid with viscosity μ, density ρ with hydrostatic pressure P, the continuity, and Reynolds-averaged Navier Stokes (RANS) equation in tensor notation can be written in the form:

$$\frac{\partial u_i}{\partial x_i} = 0 \tag{2.5}$$

$$\frac{\partial U_i}{\partial t} + U_j \frac{\partial U_i}{\partial x_j} = -\frac{1}{\rho}\frac{\partial P}{\partial x_i} + \frac{\partial}{\partial x_j}\left(\upsilon \frac{\partial U_i}{\partial x_j} - \overline{u_i u_j} \right) \tag{2.6}$$

where, $i = 1, 2$ and 3 and $j = 1, 2$ *and* 3. The indices 1, 2, and 3 denote x, y and z directions, respectively. The Reynolds stresses in the tensor equation are denoted by $\overline{u_i u_j}$.

2.5.2 Jet Flowrate and Pressure

The flow properties of the fluid and the parameters of the nozzles can be used to characterize the flow via nozzles. The following equation (Bajaj & Garg, 1977) was used to express the relationship between water pressure and flow rate for a nozzle:

$$Q_f^2 = \frac{C_f^2 d_{ne}^4 P_b}{0.081 \rho_f} \tag{2.7}$$

Where Q_f^2 is the fluid flow rate, C_f is the nozzle flow coefficient, d_{ne} is the nozzle equivalent diameter, P_b is the nozzle pressure and ρ_f is the fluid density.

Since the flow rate is a function of the pump's pressure, we can use the Bernoulli equation to calculate the jet outflow pressure. The Bernoulli equation for an ideal incompressible fluid is as follows:

$$P + \rho \frac{v^2}{2} = \text{constant} \tag{2.8}$$

Where P is pressure of fluid, ρ is density of fluid and v is velocity of fluid.

Since the flow in the washer gun and the nozzle outlet share the same axial position, the Bernoulli equation between those two places is:

$$P_1 + \rho \frac{v_1^2}{2} = P_2 + \rho \frac{v_2^2}{2} \tag{2.9}$$

The P_1 denotes pump operating pressure, P_2 is water jet exit pressure, v_1 is velocity of fluid in the pipe hose (wand) connected to pump and v_2 is jet exit velocity.

2.5.3 Equations for Impact Force, Volume and Momentum Flux

The known equation, according to momentum theory, for the impact of liquid impacting a solid surface is:

$$F = \rho Q v(1 - \cos\theta) \tag{2.10}$$

where ρ is the density of the fluid, Q is the flow rate, v is the vet velocity, and θ is the angle between the solid surface (in this paper, the ice block) and the reflecting direction of the fluid after the impact. According to theory, the momentum loss of the fluid jet is equal to the impact force F acts on the surface of the solid. The impact pressure can then be calculated using the pressure formula $P = F / A$. The area A is the region of contact of the jet. In this study, the area is deduced from the cavity created after impact.

According to the momentum principle, the rate of change in momentum flux for a given control volume equals the sum of the forces operating on the control volume (Chanson, 2004). In an experiment to quantify velocity in a high Reynolds number, an axisymmetric turbulent jet using the momentum principle, Hussein et al. (1994) expressed the relationship between volume flux, ρm_0, momentum flux, ρM_0, jet exit velocity, U_0, and diameter, D, as follows:

$$\rho m_0 = \frac{1}{4}\pi U_0 D^2 \tag{2.11}$$

$$\rho M_0 = \frac{1}{4}\pi U_0^2 D^2 \tag{2.12}$$

2.6 Jet Formation

Liquid jets, observed experimentally or naturally, alter shape as they emerge from their outlets. The pressure exerted on the fluid or the shape of the orifice characterizes the shape of a jet. For example, the sudden opening of valves installed vertically on top of each other on the side of a

water-filled tank. Since pressure increases with depth, the valve at the bottom will issue liquid jet with more intensity than the other valves above it.

Figure 2.2 shows an image illustrating the formation of a jet exiting a nozzle. The laminar flow is seen in the first two columns in (a) and in the "core of jet" column in (b). Turbulent flow is observed after these two columns, where the jet breaks up or atomizes depending on flow conditions. Some literature attributes the breakup length and the atomization conditions to aerodynamic interaction effects, liquid turbulence, jet velocity, cavitation phenomena, and fluctuating liquid supply pressure. However, these factors are still unclear (Reitz & Bracco, 1982; Kalaaji et al., 2003).
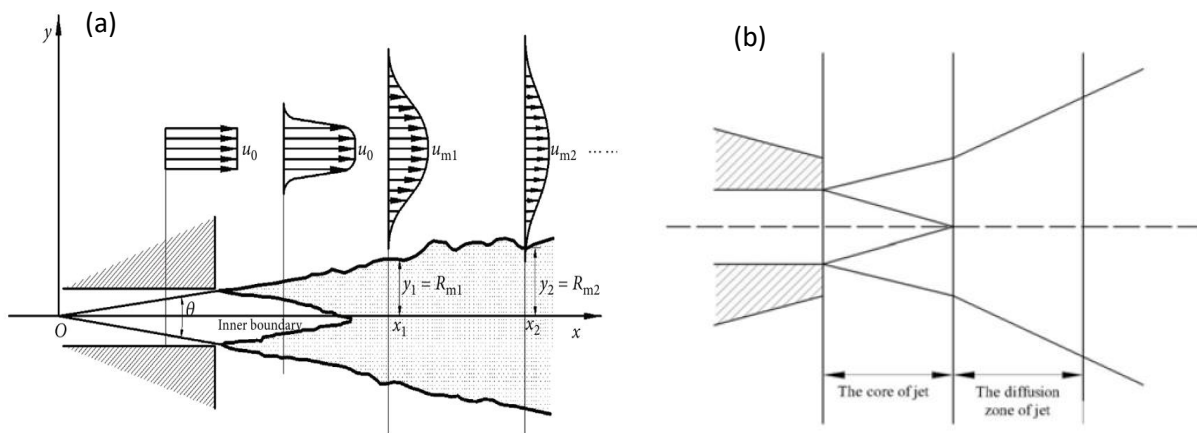
Figure 2. 2:Formation of jet exiting a nozzle (a) type of flow (b) breakup/diffusion zone (Hu et al., 2014; Huang et al., 2020)

2.7 Summary of Literature

This chapter provided an overview of previous research on water jet technology, the impact of liquid jet pressure, the water hammer effect, the influence of nozzle geometry on jet impact, ice mechanics, jet flow governing equations (equations of fluid, jet velocity, and pressure, equations for impact force, volume, and momentum flux), and jet formation. The literature reviewed on the

aforementioned subjects had the objective of exploring fundamentally the pressure and temperature effect of water jets to cut through a solid structure, primarily rock, coal, metals and ice. Although several correlations have been investigated in recent literature, their goals were not to characterize the spray angle of the different nozzles ($0°, 15°, 25°$ and $40°$) in relation to operating pump pressure, water jet temperature, stand-off distance, and depth and width of cut in successive time increment. Based on the gap mentioned above in the literature, the current study aims to characterize the various nozzles of the pressure washer and examine the correlations between the parameters above using multiple linear regression.

Tables 2.1 and Table 2.2 provide a summary of important literature on ice cutting utilizing high pressure water jets. Table 2.1 shows the aims, and results of the literature, whereas Table 2.2 shows the technique and parameters utilized in the examination of ice cutting using a high pressure water jet.

Table 2. 1: Relevant literature on ice cutting using high-pressure water jet

Author	Aims	Results
Shvaishtein (1973)	Determine the most important parameter of jet.	Ice cutting with continuous high-pressure water jet was extremely effective using high dynamic jet pressure. Nozzles with higher diameter required higher force to eject high pressure jet.
(Mellor et al., 1973)	Determine hydraulic power requirement for cutting two feet of fresh water ice.	Results showed extremely high power requirement with pump pressure at 100000 psi. Concluded that ice cutting with high pressure water jet is not a feasible method.
Gilpin (1973)	Determine effect of water jet temperature on ablation rate of ice	The rate of penetration of ice depended linearly on the temperature of water jet. Convective heat transfer controlled the ablation rate.
(Coveney & Brierley, 1978)	Determine the correlation of test results by regression analysis.	Regression analysis using four parameters to deduce depth-of-cut equation indicated good correlation. Suggested measurement of penetration should be done at specific intervals to provide statistically more useful measurement.
(Coveney, 1981)	Determine the correlation of test results by regression analysis by reintroducing nozzle stand-off distance.	The reintroduction of nozzle stand-off distance resulted in a significant correlation and improved the overall relationship.

(Takahashi et al., 2004)	Evaluate the practicality and effectiveness of water jet to remove ice buildup on different surfaces.	Jet discharges with a 30 degree offset provided better penetration depths and wider regions of ice removal, particularly on the rubber sheet, compared to the steel and concrete sheets.
(Guo et al., 2014)	Evaluate the breakthrough time to penetrate through 10-cm-thick ice block.	Breakthrough time increases as stand-off distance decreases, increasing impinging pressure. Maximum deicing efficiency was obtained at an optimal distance of about 90 cm.
(Yuan et al., 2021)	Characterization of ice cracking and fracturing under various parameters.	Reduction factor between 0.302 and 0.3045 was found between the compressible and water-hammer pressure.

Table 2. 2: Technique and parameters considered in study

Author	Technique	Temperature ($^\circ C$)	Pressure (psi)	Nozzle geometry	Stand-off distance (cm)	Time (s)
(Shvaishtein, 1973)	Experiment	50	29392-36740	Round/---	20-80	---
(Mellor et al., 1973)	Experiment	---	20000-100000	Round/13	1.95-2.54	---
(Gilpin, 1973)	Experiment	25-60	100	Round	---	---
(Coveney & Brierley, 1978)	Experiment	--	1050-1640	---	15.24-152.4	---
(Coveney, 1981)	Experiment	---	595-10298	---	3-152	---
(Takahashi et al., 2004)	Experiment	---	725-1885.5	---	50-200	60
(Guo et al., 2014)	Experiment	---	---	---	30-110	---
(Yuan et al., 2021)	Experiment	---	4687.62-6152.5	---	3-11	---

The novelty of this study is to investigate the combined influence of operating pump pressure, water jet temperature, and stand-off distance of the four nozzles ($0^\circ, 15^\circ, 25^\circ$ and 40°) at precise time intervals that prior studies listed in Tables 2.1 and 2.2 did not capture all at once. The

combined influence of cutting parameters was reported in earlier work (Ozcelik et al., 2012) but their target object was a sample of Sardinian basalt, and the parameters were nozzle diameter, traverse velocity, standoff distance, and pump pressure.

3.0 Methodology

3.1 Experimental Setup

The water jet technology setup is simplified in the form of a pressure washer. This study uses a commercial pressure washer with a maximum flow rate of 3.5 gpm (0.220 L/s) and maximum pressure of 4000 psi (27.6 MPa) shown in Figure 3.1

Figure 3. 1:Pressure washer (Water jet-producing system)

The Kohler motor powers the pump that pressurizes water through the reinforced high-pressure exit hose. Pressurized water exits through a specialized nozzle attached to the hose with a high kinetic energy which can cut through various materials depending on the intensity of the pressure. The pressure washer comes with a spray gun that is mounted at a fixed position on a tripod stand. As shown in Figure 3.2, the pump outlet hose connects to the spray gun mounted on the tripod. The internal diameters of the outlet hose and the gun's wand are the same. Flow in the wand is the inlet to the nozzle attached to the wand's tip.

Figure 3. 2: Experimental Setup

3.2 Sample Preparation

An experimental ice block is made by freezing tap water which is contained in three different aluminum rectangular molds. The molds measure 60 cm in length, 20 cm in width, and 50 cm in height for the first, 50 cm in length, 20 cm in width, and 30 cm in height for the second, and 60 cm in length, 20 cm in width, and 100 cm in height for the third. Aluminum was chosen for the mold because it is hydrophilic and has a high thermal conductivity, which defines its ability to be wetted by water droplets and conduct heat. Aluminum also has a liquid contact angle less than 90 degrees. The mold is 0.25in thick, which is sufficient to withstand the expansion of water as it turns to ice. The frozen ice block is removed from the freezer and placed on a table facing the tripod stand that holds the spray gun, as illustrated in the experimental setup, Figure 3.2. The setup is carried out in a cold room with a regular ambient temperature of 10 degrees Celsius. The ice surface is levelled and smoothened to match the interior height of the molds. The temperature of the ice is measured by drilling a hole in its center and using a thermocouple probe. A temperature of -10 degrees Celsius is reached and maintained. Crevices in ice are treated by pouring hot water

into them, which melts the ice surfaces between that crack and cures it without further cracks. The figure 3.3 shows a picture of the molds and ice blocks.
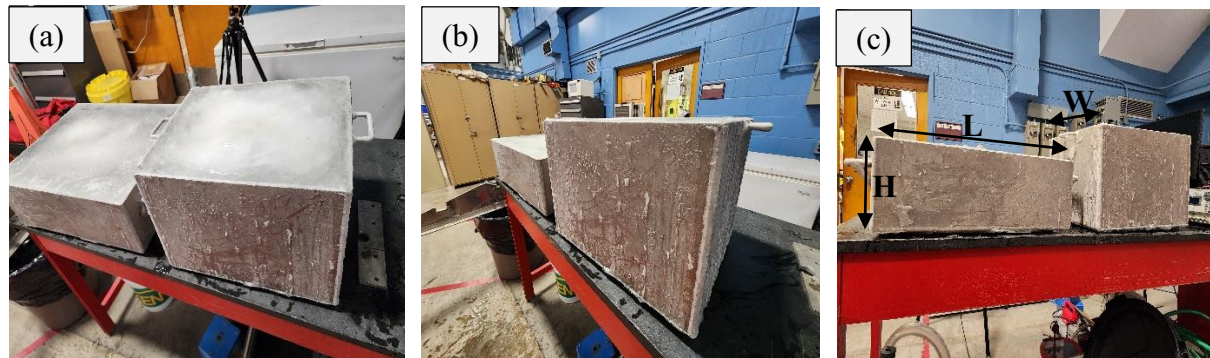
Figure 3. 3: Ice block samples (a) molds containing ice blocks, (b) levelled ice block, (c) dimensions of molds

3.3 Design of Experiment

The design of experiments is an effective analysis tool for modelling and analyzing the effects of process factors on a specific variable that is an unknown function of these process variables (Murti & Philip, 2007).

According to a study by Cui et al. (2022), the key influencing variables of water jet cutting include pump pressure, stand-off distance, nozzle transverse speed, nozzle structure, and so on. Pump pressure, stand-off distance, nozzle structure (spray angle) and water temperature were all evaluated in these tests. The nozzle parameters in this study are the properties of the nozzle and its configuration, such as the nozzle spray angle, nozzle pressure, and stand-off distance. The experimental design cases developed using Taguchi's technique are depicted in Table I.1 in the appendix, with factors and levels recorded in Table 3.1. The use of Taguchi's technique to examine the parameters with the minimum number of experiments was necessary because preliminary experimental cases created using Factorial design with varied levels yielded biased results.

Table 3. 1: Experimental design factors and levels

Temperature (^{o}C)	Pressure (psi)	Distance (cm)	Time (s)
10	1000	5	10
30	2000	10	20
50	3000	15	30

In the preliminary study, 59 water jet penetrations were measured using a minimum of two levels and a maximum of six levels, as well as five factors: water jet temperature, operational pump pressure, stand-off distance, nozzle spray angle, and time of cut. The nozzle type was not taken into account as a parameter in the Taguchi technique, which gave 36 experimental instances with three levels for each parameter. This revised DOE method (The Taguchi technique) enabled all four nozzle types to operate with the same variable parameters, enhancing the analysis.

The design tree for the experiment is shown in Figure 3.4. The order of selection of parameter is:

Nozzle type ⟶ Distance ⟶ Temperature ⟶ Pressure ⟶ Time of cut.
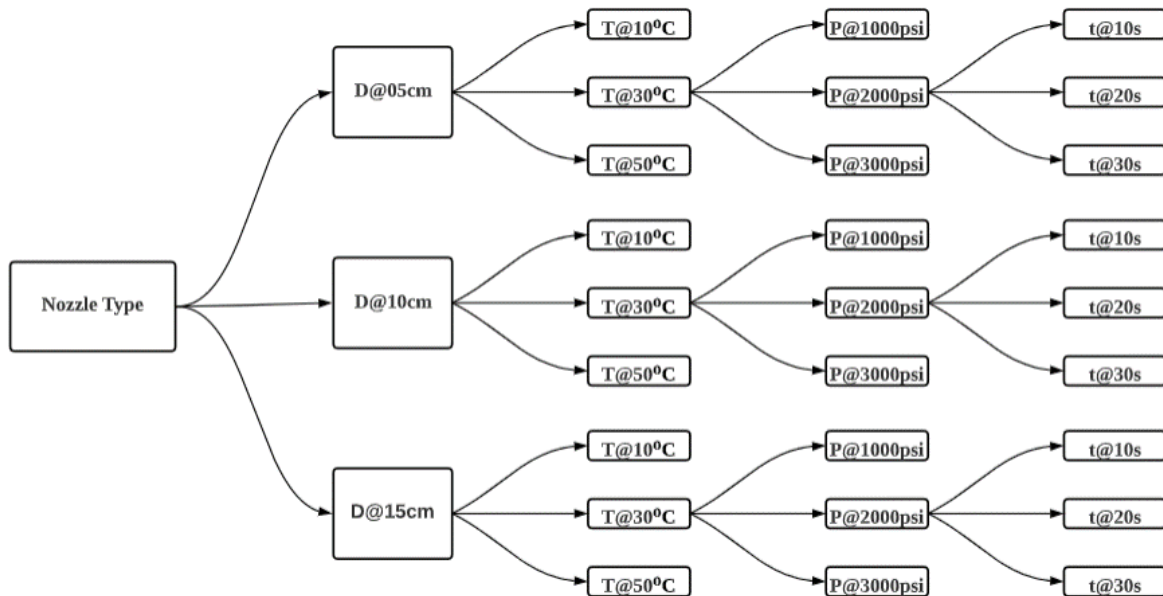
D-distance; *T*-temperature; *P*-pressure; *t*-time

Figure 3. 4: Experimental design tree

3.4 Experimental Procedure
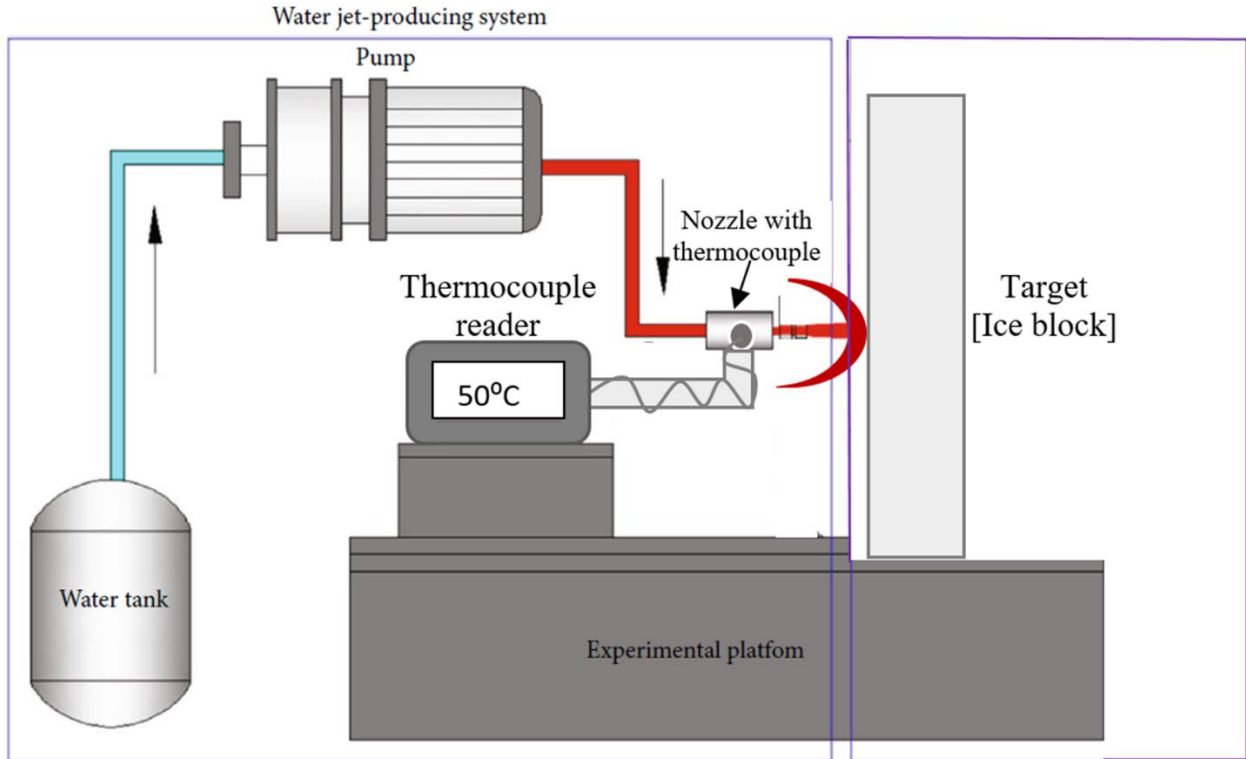
Figure 3. 5: Schematic of experimental setup

Freshwater from the tap is routed to the pump, which pressurizes the water to the necessary pressure, as illustrated in the schematic. For each experiment, the water temperature is adjusted via the handle of the tap and measured using a thermocouple coupled to the spray gun installed on the tripod. Temperature is measured both before and after to confirm that the desired temperature is not altered.

Before cutting begins for a set duration, the desired parameters (standoff distance, temperature, and pressure) are measured. The ice block sample in the mold is secured to the sturdy table to prevent movement. The spray gun's nozzle is preset to the desired distance. With each cut, the

depth of cut is measured using a depth gauge and validated with a measuring tape. The procedure

is repeated for every set of the cases in Table I.1 in the appendix. The duration of each experiment

is 2 hours and the overall duration is approximately 18 hours spanning over 10 weeks.

3.5 Measuring Tools

This section provides details of measuring instruments used to measure the temperature of water

jet, the operating pump pressure, the standoff distance, and the time of cut.

3.5.1 Temperature

The temperature of the water jet was taken by connecting the thermocouple probe to Fluke 52 II

dual probe thermocouple reader. Both instruments have a total sensitivity error of $\pm 0.75\%$.

3.5.2 Pressure

The operating pressure of the pump was measured using a pressure gauge connected between the

pump exit and the exit hose. The pressure gauge is graduated in 500 psi increment, making it

easier to set the operating pressure to the appropriate value. The pressure gauge has a sensitivity

error of $\pm 0.18\%$.

3.5.3 Distance

The standoff distance of the nozzle from the ice block surface was measured using a Vernier

caliper of sensitivity error of $\pm 0.017\%$. The tripod is adjusted forward while the Vernier caliper

is set to the desired value from the surface of the ice block.

3.5.4 Time

The timer is used to measure the time of cut through the ice block. Cutting was done in 10, 20

and 30 seconds. The timer used has a sensitivity error of $\pm 0.0005\%$.

3.6 Regression Analysis

A multiple regression analysis was carried out to determine the relevant parameter(s) that affect

the depth and width of cut, as well as the overall impact of these parameters on both the depth and

width of cut. The experimental cases generated by the factorial design tool are presented in Table

I.1. The recorded responses are documented in the column that represents the depth and width of

the cut, as measured in the laboratory.

The design summary encompasses the influential factors, responses, and design properties. Table

3.2 presents the design properties, whereas Tables 3.3 and 3.4 display the descriptive statistical

analysis of the factors and responses, correspondingly.

Table 3. 2: Design Properties

Study Type	Design Model	Runs	Blocks
Response Surface	Linear	36	No blocks

Table 3. 3: Descriptive analysis of factors

Factor	Name	Units	Type	Minimum	Maximum	Mean	Std. Dev
Temperature	T	C	Numeric	10	50	30.00	16.56
Pressure	P	Psi	Numeric	1000	3000	2000	828.08
Distance	dx	cm	Numeric	5	15	10.00	4.14
Nozzle	N	-	Nominal	Red	White	Levels	4
Time	t	s	Numeric	10	30	20.00	8.28

Table 3. 4: Descriptive analysis of responses

Factor	Name	Units	Observations	Minimum	Maximum	Mean	Std. Dev	Ratio
Depth of cut	*R1*	mm	36	86	825	305.81	219.97	9.59
Width of cut	*R2*	mm	36	26	175	89.62	43.30	6.73

3.6.1 Regression Analysis for Depth of Cut

Table 3.5 shows the results of a statistical study performed to predict the depth of cut. If the *P*-values at a 95% confidence level are less than 0.005, the results are highly significant; otherwise, they are regarded inconsequential and have no effect on output.

Table 3. 5: Statistic analysis for selecting the suitable model for depth of cut

Model (Transform)	*P*-value	Adjusted R^2	Predicted R^2	Results
Linear (Natural Log)	<0.0001	0.8166	0.7473	Suggested
2FI	0.2780	0.8484	0.5977	

The multiple regression analysis of the model and analysis of variance (ANOVA) results are given in the Table 3.6.

Table 3. 6: ANOVA of the regression model for depth of cut

Source	Sum of squares	Df	Mean Square	F-value	P-value	Result
Model	13.85	7	1.98	23.26	<0.0001	significant
N- Nozzle	7.05	3	2.35	27.63	<0.0001	
T-Temperature	3.59	1	3.59	42.21	<0.0001	
P-Pressure	0.6212	1	0.6212	7.31	<0.0001	
dx-Distance	0.3517	1	0.3517	4.14	0.0516	
t-Time	2.24	1	2.24	26.29	<0.0001	
Residual	2.38	28	0.0850			
Correlation Total	16.23	35				

With a P-value less than 0.05, the F-value of 23.26 indicates that the model is significant. In this case, N, T, P, and t are more important model parameters than dx, which is distance. At 99% confidence, the model is statistically significant ($p = 0.0001$ alpha $= 0.01$).

Table 3. 7: Results of multiple regression analysis for depth of cut

Factor	Coefficient Estimate	Degree of freedom(Df)	Standard error
Intercept	5.49	1	0.0486
N[1]	0.7057	1	0.0842
N[2]	0.0277	1	0.0842
N[3]	-0.2789	1	0.0842
T-Temperature	0.3867	1	0.0595
P-Pressure	0.1609	1	0.0595
dx-Distance	-0.1211	1	0.0595
t-Time	0.3052	1	0.0595

According to Table 3.7, the model equation for the depth of cut for the individual nozzles is formulated below:

Table 3. 8: Regression equations for depth of cut

Nozzle	Regression Equations
Red	$\ln(\text{Depth of cut (mm)}) = 4.92654 + 0.019335T + 0.000161P - 0.024211dx + 0.030520t$
Yellow	$\ln(\text{Depth of cut (mm)}) = 4.24851 + 0.019335T + 0.000161P - 0.024211dx + 0.030520t$
Green	$\ln(\text{Depth of cut (mm)}) = 3.94189 + 0.019335T + 0.000161P - 0.024211dx + 0.030520t$
White	$\ln(\text{Depth of cut (mm)} = 3.76632 + 0.019335T + 0.000161P - 0.024211dx + 0.030520t$

Figure 3.6 below shows the relationship between the actual and predicted depth of cut values obtained. The Predicted R^2 of 0.7473 is in reasonable agreement with the Adjusted R^2 of 0.8166; i.e. the difference is less than 0.2.
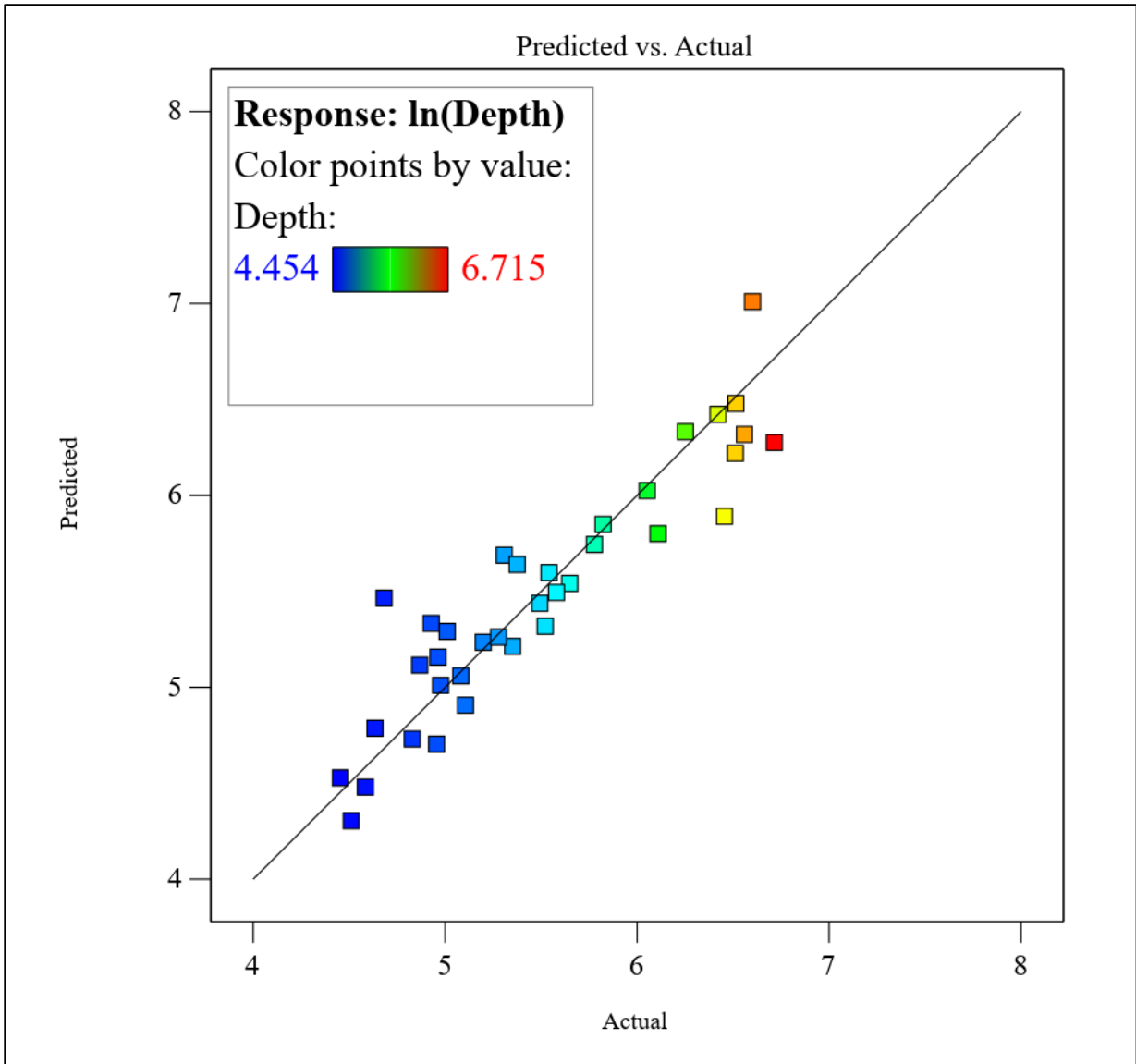
Figure 3. 6: Relationship between actual and predicted values for the depth of cut.

3.6.2 Regression Analysis for Width of Cut

Likewise, Table 3.9 shows *P*-values for width of cut at a 95% confidence level are less than

0.005, the results are highly significant. The linear model is therefore suggested for analysis.

Table 3. 9: Statistic analysis for selecting the suitable model for width of cut

Model	P-value	Adjusted R^2	Predicted R^2	Results
Linear (Natural Log)	<0.0001	0.8973	0.8635	Suggested
2FI	0.3955	0.9056	0.6659	

Also, the multiple regression analysis of the of the width of cut model and its analysis of variance (ANOVA) results are given in the Table 3.10.

Table 3. 10: ANOVA of the regression model for width of cut

Source	Sum of squares	Df	Mean Square	F-value	P-value	Result
Model	9.92	7	1.42	44.67	<0.0001	significant
N-Nozzle	8.85	3	2.95	93.05	<0.0001	
T-Temperature	0.6424	1	0.6424	20.25	0.0001	
P-Pressure	0.1935	1	0.1935	6.10	0.0199	
dx-Distance	0.0850	1	0.0850	2.68	0.1129	
t-Time	0.1429	1	0.1429	4.51	0.0427	
Residual	0.8881	28	0.0317			
Cor Total	10.81	35				

The width of cut recorded an F-value of 44.67 indicating that the model is significant. P-values recorded suggest that, N, and T are the most important model parameters affecting width of cut. At 99% confidence, the model is statistically significant ($p = 0.0001$ alpha = 0.01).

Table 3. 11: Results of multiple regression analysis for width of cut

Factor	Coeff. Estimate	Degree of freedom(Df)	Standard error
Intercept	4.36	1	0.0297
N[1]	-0.7703	1	0.0514
N[2]	-0.0492	1	0.0514
N[3]	0.2480	1	0.0514
T-Temperature	0.1636	1	0.0364
P-Pressure	0.0898	1	0.0364
dx-Distance	0.0595	1	0.0364
t-Time	0.0772	1	0.0364

According to Table 3.11, the model equation for the width of cut for the individual nozzles is formulated below:

Table 3. 12: Regression equations for width of cut

Nozzle	Regression Equations
Red	ln(Width of cut (mm)) = $2.89183 + 0.008180T + 0.000090P + 0.01190dx + 0.007717t$
Yellow	ln(Width of cut (mm)) = $3.61286 + 0.008180T + 0.000090P + 0.01190dx + 0.007717t$
Green	ln(Width of cut (mm)) = $3.91015 + 0.008180T + 0.000090P + 0.01190dx + 0.007717t$
White	ln(Width of cut (mm) = $4.23359 + 0.008180T + 0.000090P + 0.01190dx + 0.007717t$

Figure 3.7 below shows the relationship between the actual and predicted width of cut values obtained. The Predicted and Adjusted R^2 values of the width of cut recorded higher values than the depth of cut. The respective Predicted and Adjusted R^2 values of the width of cut are 0.8635 and 0.8973 and are in reasonable agreement with a difference of less than 0.2.
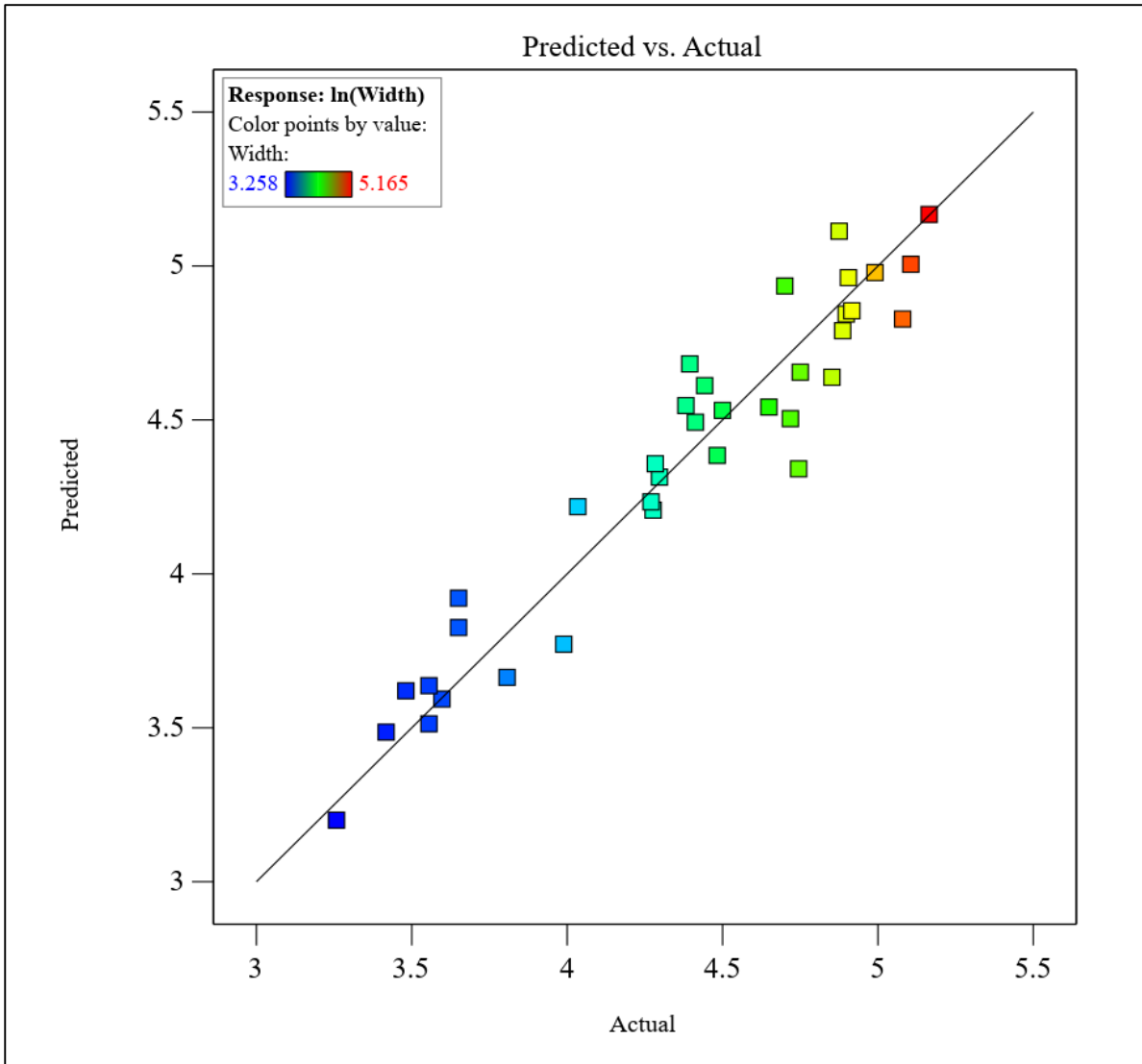
Figure 3. 7: Relationship between actual and predicted values for the width of cut.

3.7 Error Analysis and Experimental Uncertainty

The measurement error or uncertainty is the difference between the experimentally measured value and the true value. The total error in experimental measurements can be categorized into two main components: the bias, e_B, and precision, e_P, components. Some errors that may arise from this experiment may be calibration errors of instruments used, human error (inconsistent reading of scale at a horizontal level), and spatial errors (temperature changes in the room). Uncertainties

(bias errors) of measuring instruments are estimated through proper calibration by the manufacturers and given in Table 3.13.

Table 3. 13: Bias limits of instruments used

Parameter	Instrument	Sensitivity (error)
Temperature	Thermo-couple probe	±0.75%
Temperature	Temperature Reader (Fluke)	±0.05%
Pressure	Pressure gauge	±0.18%
Distance	Vernier caliper	±0.017%
Time	Timer	±0.0005%
	%Bias error	$e_T = 0.77\%$

The precision error is estimated from the mean and standard deviations of the data gathered. The precision error, e_P, of the measured variable, d is given by

$$e_P = \frac{z\sigma}{\sqrt{N}}$$

(3.1)

where z is the confidence coefficient having a value of 2 for 95% confidence level according to Holman (1994; 2001), N is the experimental cases (36) and σ is the standard deviation, defined as

$$\sigma = \sqrt{\frac{1}{n-1}\sum_{j=1}^{n}(d_j - \overline{d})^2}$$

(3.2)

where $\overline{d}$ is the mean and is given by:

$$\bar{d} = \frac{1}{n}\sum_{j=1}^{n} d_n \tag{3.3}$$

The standard deviations of the depth of cut was obtained. The standard deviation was approximately 1.998%. With known values of z, N and σ, the precision error was estimated from Equation (3.1) to be 0.67%.

The total measurement uncertainty, e_T, is the root-sum-square of the bias and precision errors and is given by

$$e_T = \sqrt{e_B^2 + e_P^2} \tag{3.4}$$

The total measurement uncertainty for the depth and width of cut was obtained to be 1.02%.

4.0 Results and Discussion

The effect of control factors such as pump pressure, water jet temperature, stand-off distance, and time-of-cut on depth and width of penetration was investigated using mean values of depth and width of penetration. The next sections discuss the trends observed under various cutting conditions. Other factors vary, whereas *x-axis* parameters change across all trends. As a result, the trend change is not the sole influence of the *x-axis* parameter. The data, however, was trained to predict the significance of each parameter on the depth and width of cut. Figure 4.1 depicts the parameter significance of the depth of cut. It is observed that the nozzle geometry has the most significant influence on the maximum depth of cut, followed by the time of cut, pump pressure,

water　　　　　jet　　　　temperature,　　　　and　　　　stand-off　　　　distance.

Impact of Parameters
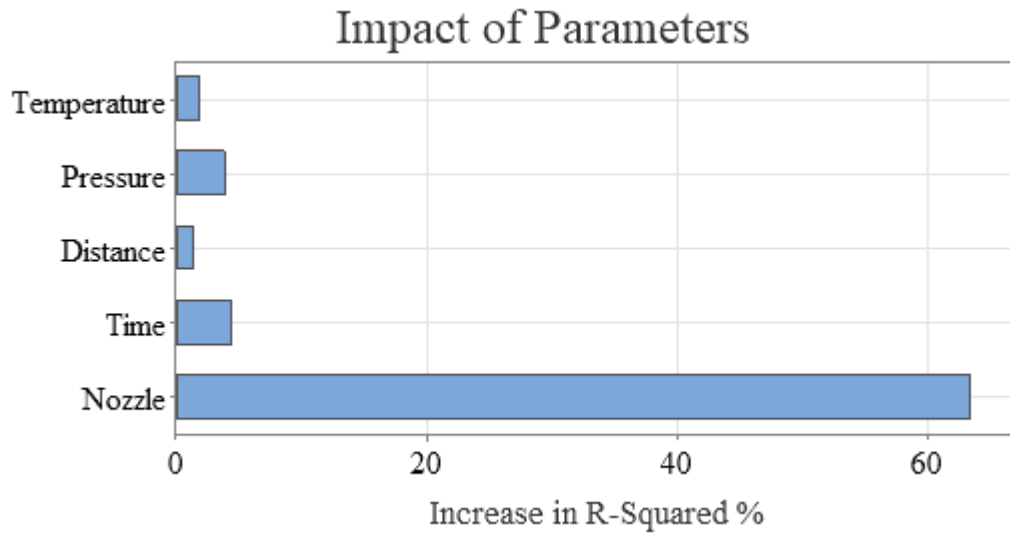
Figure 4. 1: Parameter significance on the depth of cut

Impact of Parameters on Width of Cut
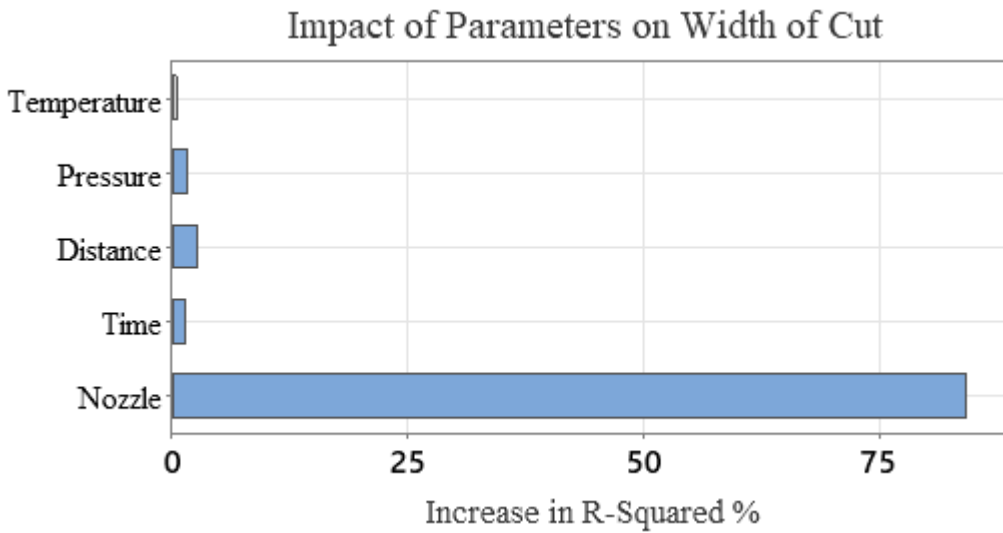
Figure 4. 2: Parameter significance on the width of cut

Similarly, in Figure 4.2, the nozzle geometry has the most influence on the width of cut followed by standoff distance, pump pressure, time of cut and temperature of water jet. The observed phenomenon of the nozzle being the most significant can be attributed to the progressive increase

in the nozzle spray angle, ranging from zero degrees to 40 degrees, which consequently leads to a proportional expansion in the width of the cut.

4.1 Optimum Conditions for Maximum Depth and Width of Cut

The combined impact of the operating parameters of the four nozzles was identified in this study, and the optimum conditions that result in the largest depth and width of cut were determined. We were not particularly interested in the role of specific parametric effects on depth and width of cut because it had already been studied.

Table 4.1, 4.2 and 4.3 show the constraints for optimization and the optimum working conditions necessary to achieve the maximum depth and width of cut for each nozzle.

Table 4. 1: Constraints for optimization

Name	Goal	Lower Limit	Upper Limit	Importance
Nozzle	Is in range	Red	White	3
Temperature	Is in range	10	50	3
Pressure	Is in range	1000	3000	3
Distance	Is in range	5	15	3
Time	Is in range	10	30	3
Depth of cut	Maximize	86	1500	5
Width of cut	Maximize	26	200	5

Table 4. 2: Parametric conditions for maximum predictive depth

Nozzle Type	Temperature	Pressure	Distance	Time	Predictive Depth	Desirability
Red	50	3000	5	30	1356	1
Yellow	50	3000	5	30	689	1
Green	50	3000	5	30	507	1

White	50	3000	5	30	425	1

Table 4. 3: Parametric conditions for maximum predictive width

Nozzle Type	Temperature	Pressure	Distance	Time	Predictive Width	Desirability
Red	50	3000	15	30	54.4	0.378
Yellow	50	3000	15	30	111.8	0.757
Green	50	3000	15	30	150.6	0.913
White	50	3000	15	10	178.3	1.000

The constraints might be established to achieve the desired depth and width of cut depending on the intended aim or purpose. For example, if deicing on a maritime vessel must be done quickly to avoid vessel capsizing, crew members must establish a target for any of the criteria listed in the "Goal" column of Table 4.1 and select any nozzle of choice to estimate the depth and width of cut. Hence, optimization criteria may be determined based on available resources and requirement.

To maximize both depth and width of cut in one cutting operation, the constraints for optimization and the optimum working conditions necessary to achieve that is shown in Table 4.4.

Table 4. 4: Parametric conditions for maximum predictive depth and width of cut

Nozzle Type	Temperature	Pressure	Distance	Time	Depth	Width	Desirability
White	50	3000	5	30	424.7	184.8	0.720

The established regression models may provide cuttability charts for ice block samples frozen to temperatures exceeding -10 degrees Celsius. Table I.2, and I.3 present cuttability charts for

depth and width of cut for each nozzle geometry. Given the temperature, pressure, distance, and time parameters, the red nozzle with a dispersion angle of 0 degrees obtained the maximum depth of cut based on the data presented for the analysis whiles the white nozzle with a dispersion angle of 40 degrees obtained the maximum width of cut.

The optimum operating parameters for depth of cut are a nozzle type red (spray angle of $0°$), pressure of 2371 (psi), temperature of 38.6 (Celsius), distance of 7.7 (cm), and time of cut of 25.9 (s) to obtain a depth of cut of 814 (mm), as stated in Table 4.5.

Table 4. 5: Optimum working parameters for depth of cut

Nozzle Type	Temperature	Pressure	Distance	Time	Optimum Depth	Desirability
Red	38.6	2371	7.7	25.9	814	1

Also, the optimum operating parameters for width of cut are a nozzle type white (spray angle of $40°$), pressure of 2334 (psi), temperature of 33.3 (Celsius), distance of 13.3 (cm), and time of cut of 11.5 (s) to obtain a width of cut of 145 (mm), as stated in Table 4.6.

Table 4. 6: Optimum working parameters for width of cut

Nozzle Type	Temperature	Pressure	Distance	Time	Optimum Width	Desirability
White	33.3	2334	13.3	11.5	145	1

Moreover, the optimum operating parameters for both depth and width of cut are a nozzle type white (spray angle of $40°$), pressure of 2829 (psi), temperature of 28.3 (Celsius), distance of 9 (cm), and time of cut of 20.8 (s) to obtain a width of cut of 145 (mm) and a depth of cut of 186 (mm), as stated in Table 4.7.

Table 4. 7: Optimum working parameters for both depth and width of cut

Nozzle Type	Temperature	Pressure	Distance	Time	Optimum Depth	Optimum Width	Desirability
White	28.3	2829	9	20.8	186	145	1

4.2 Effect of Operating Parameters on Depth of Cut

The effects of temperature of water jet, operating pressure of pump, standoff distance and time of cut were observed on the depth of cut. The effect of each parameter on the depth of cut is not the sole influence, for example the trend of temperature on the depth of cut may increase or decrease while at the same time the effect of operating pump pressure, standoff distance and time of cut is taking place on the depth of cut. The logarithmic trend line was used to predict the optimal curved line in all the plots due to the use of three distinct levels in the data and the rapid increase and decrease observed within these levels.

4.3 Effects of Pressure on Depth of Cut

The mean depth of cut increases as the operating pump pressure increases. The relationship between pressure and mean depth can be understood as follows:

- Increased pressure: When the pressure of the water jet increases, the force exerted by the water on the ice block also increases. The increased force allows the water jet to penetrate deeper into the ice, resulting in a greater mean depth of the cut.

- Water jet velocity: As the pressure increases, the velocity of the water jet also increases. A higher velocity enables the water to cut through the ice more effectively, thereby increasing the mean depth of the cut.

- Ice erosion: The water jet cutting process relies on the erosion of the ice by high-velocity water particles. As the pressure increases, the kinetic energy of the water particles also

increases, which enhances the erosion and cutting mechanism. This, in turn, leads to a deeper cut in the ice block.

The trend of consistent increase in mean depth of cut as pressure increases can be observed from the increase in mean depth from 465.3 mm to 524.7 mm when pressure is increased from 1000 psi to 2000 psi, and further to 745.3 mm when pressure is increased to 3000 psi in Figure 4.3 (a), and 236.7 mm to 291.7 mm when pressure is increased from 1000 psi to 2000 psi, and further to 307 mm when pressure is increased to 3000 psi in Figure 4.3 (b). However, this trend of consistent increase is not prevalent in Figure 4.3 (c-d). This inconsistency is due to parameters settings evidenced in Table I.1. The rows for 2000 psi and 3000 psi for the 25° (green) nozzle and 40° (white) nozzle had standoff distances 5 cm and 15 cm that corresponds to times of cut of 30 seconds and 10 seconds, respectively. Indicating that, the pressure setting of 2000 psi had a closer standoff distance with long duration for cutting than the 3000 psi.

Figure 4. 3: Effect of operating pump pressure on the mean depth of cut (a) 0° (red) nozzle (b) 15° (yellow) nozzle (c) 25° (green) nozzle (d) 40° (white) nozzle

4.4 Effects of Temperature on Depth of Cut

The primary mechanism responsible for water jet cutting process where temperature is an operating factor is the combination of water hammer effect and thermal melting. It is observed that the water jet pressure contributed to ice erosion evidenced by the creation of ice chips from the cutting, while the temperature of the water jet influenced the thermal melting process.

The mean depth of cut increases as temperature of the water jet increase. This can be explained by the following factors:

- Increased thermal melting: With higher water jet temperatures, the water jet can more effectively melt the ice, resulting in a deeper cut. The thermal energy from the hot water

64

jet is transferred to the ice, causing it to melt and allowing the water jet to penetrate further into the ice block.

- Reduced ice strength: As the temperature of the water jet increases, the ice surrounding the cut may also heat up, reducing it overall strength. Warmer ice has a lower resistance to ice erosion, which allows the water jet to cut deeper with the same amount of pressure.

Figure 4.4 (a) shows increase in mean depth is more pronounced from 10°C to 30°C than from 30°C to 50°C, while Figure 4.4 (b-d) show increase in mean depth that is consistent across the temperature range. This suggests that the effect of increasing temperature on the mean depth of the cut might be diminishing as the temperature increases. This could be due to the limitations in the water jet's ability to transfer heat to the ice block or a reduction in the mechanical erosion efficiency at higher temperatures as a result of other parameter settings.
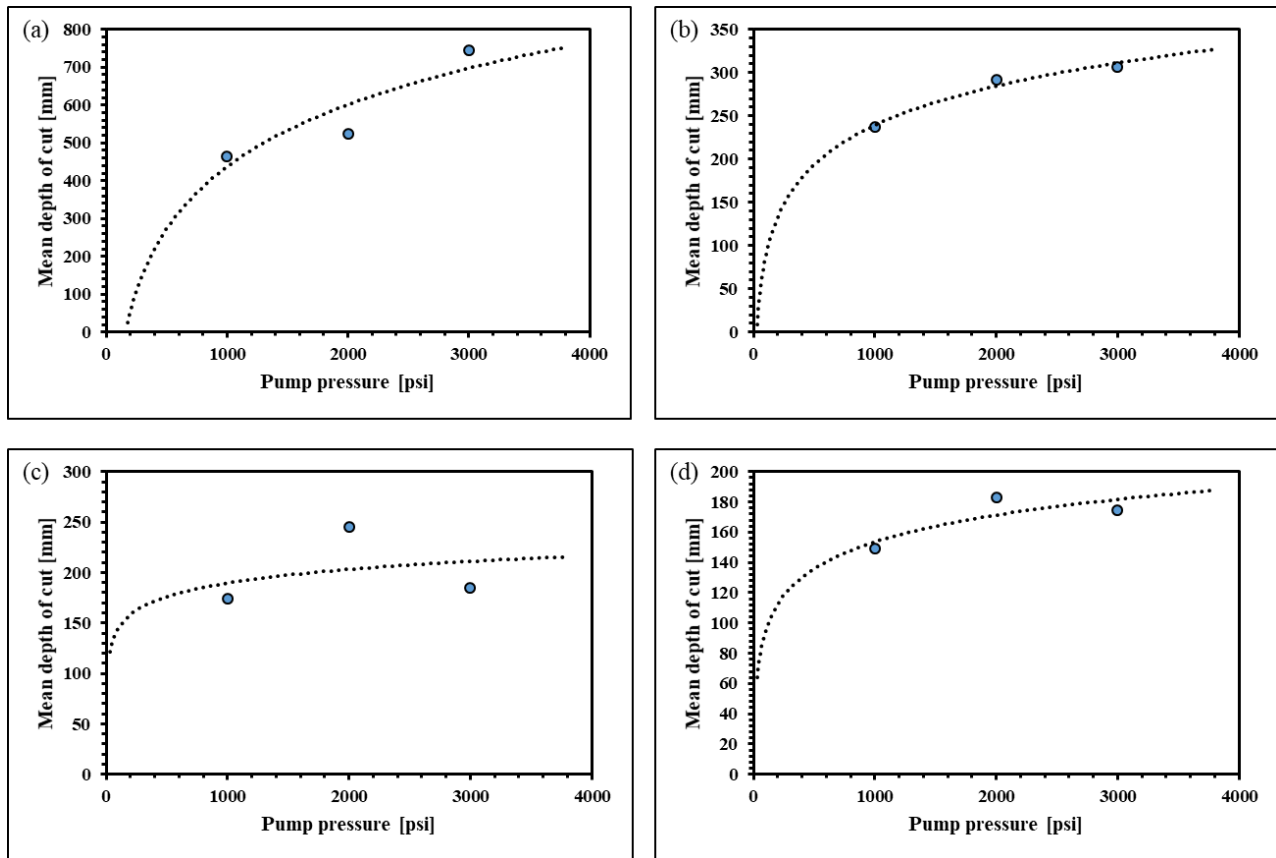
Figure 4. 4: Effect of water jet temperature on the mean depth of cut (a) 0° (red) nozzle (b) 15° (yellow) nozzle (c) 25° (green) nozzle (d) 40° (white) nozzle

4.5 Effects of Stand-off Distance on Depth of Cut

The water jet's cutting power in terms of standoff distance of nozzle is determined by its pressure and flow rate. As the water jet travels through the air, it loses energy due to factors such as air resistance, drag, and the dispersion of the water jet. Therefore, the cutting power of the water jet decreases with an increase in distance from the nozzle. The impact of standoff distance on the depth of cut can be explained as follows:

- Energy dispersion: As the distance from the nozzle to the ice block increases, the water jet loses its kinetic energy due to the dispersion of the water particles. This

leads to a decrease in the energy density at the cutting surface, resulting in a shallower cut.

- Water jet coherence: The coherence of the water jet is crucial for maintaining its cutting power. As the distance between the nozzle and the ice block increases, the jet's coherence is reduced due to the spreading of the water particles, leading to a less focused and less effective cutting action.

- Water pressure drop: With an increase in distance, the water pressure at the cutting surface drops. A higher water pressure is required to cut deeper into the ice block. As the pressure decreases with increased distance, the depth of the cut is reduced.

Figure 4.5 (a) shows increase in depth of cut as standoff distance increases from 5 cm to 10 cm. This could be because the 0° (red) nozzle has no dispersion angle and therefore the effect of increasing standoff distance is not seen immediately. However, as the distance increases further from 10 cm to 15 cm, the mean depth of the cut decreases from 698.7 mm to 527 mm.

Figure 4.5 (b-d), however, shows a consistent decrease in mean depth of cut as standoff distance increases. This is mainly due to the dispersion angles which reduces cutting power due to loss of energy in the water jet as it travels through the air.
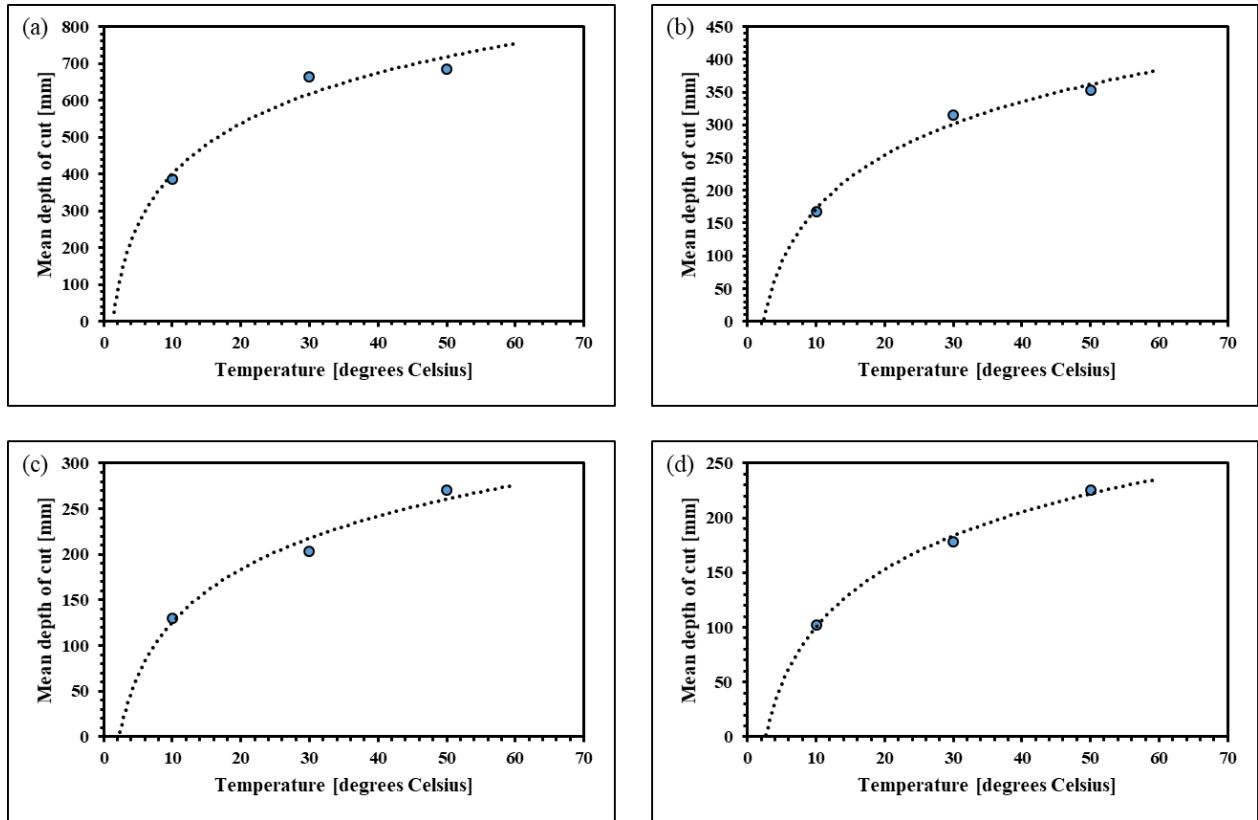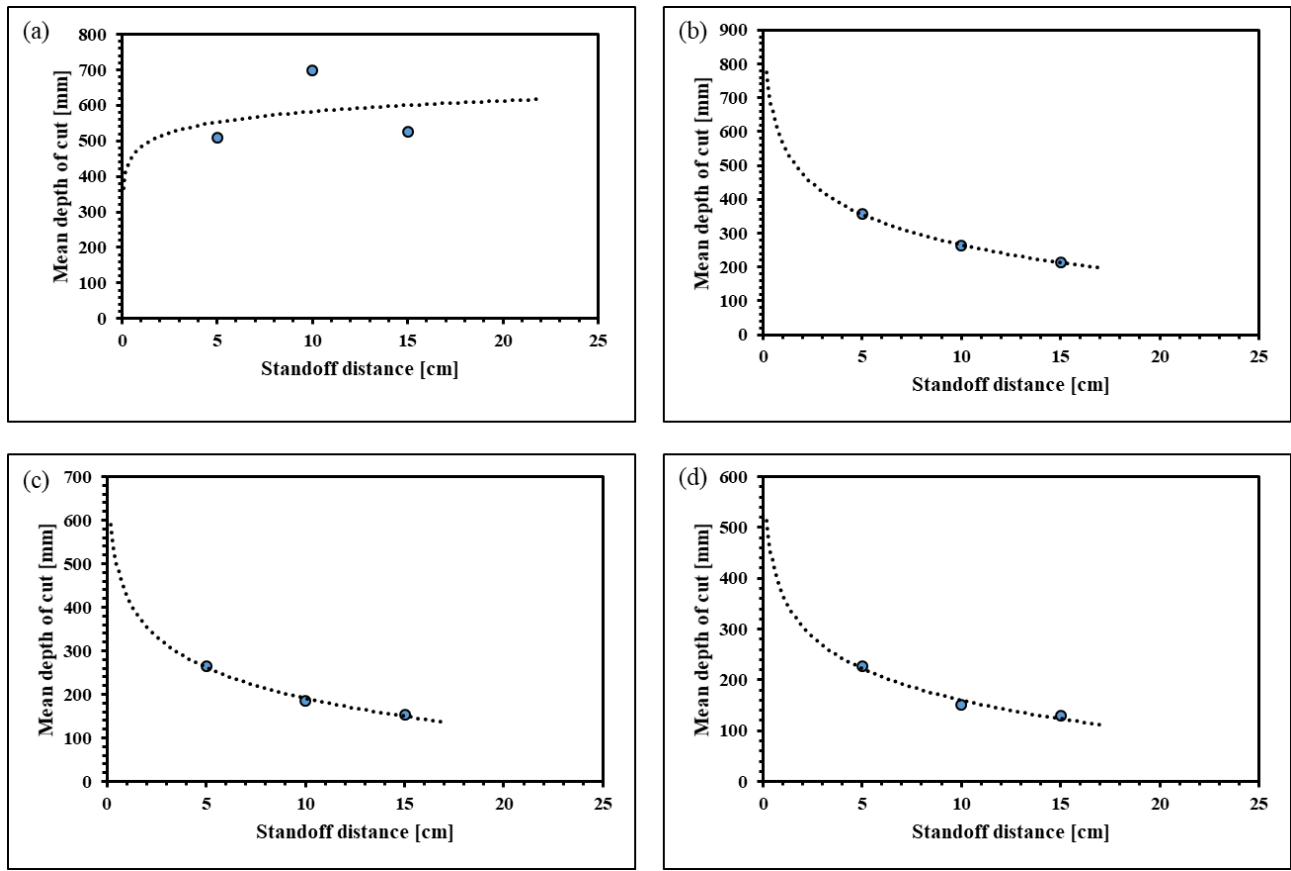
Figure 4. 5: Effect of standoff distance on the mean depth of cut (a) 0° (red) nozzle (b) 15° (yellow) nozzle (c) 25° (green) nozzle (d) 40° (white) nozzle

4.6 Effects of Variation of Time on Depth of Cut

Figure 4.6 (a-d) shows that as the time increases, the mean depth of the cut also increases. The longer the operation of the water jet on the ice block, the deeper the cut. This can be attributed to the fact that the water jet continues to erode the ice as it is being exposed to the high-pressure water jet with elevated temperature for a more extended period. In Figure 4.6 (a), The difference in depth between 10 seconds and 20 seconds is relatively small (17.3 mm), while the difference between 20s and 30s is much larger (250.7 mm). This indicates that there is a non-linear relationship between the cutting time and the mean depth as other parameters are affecting the cutting

performance. However, in Figure 4.6 (b-d), The relationship between the cutting time and the mean depth shows a trend that is closer to linear.

Figure 4. 6: Effect of time of cut on the mean depth of cut (a) 0° (red) nozzle (b) 15° (yellow) nozzle (c) 25° (green) nozzle (d) 40° (white) nozzle

4.7 Combined Influence of Operating Parameters on Depth of Cut based on Nozzle Geometry

The combined influence of the operating parameters of the four nozzles is shown in Figure 4.6. The *x*-axis depicts nominal parameters which is given in equation as:

$$\text{Nominal Parameter} = x \, / \, x_{max} \qquad (4.1)$$

where the parameter could be temperature, pressure, distance or time. x is the value of the parameter and x_{max} is the maximum value of the parameter. Nominal values are used to represent all the parameters on a single graph because it gives a common scale and it is dimensionless.

In Figure 4.7 (a-d), It is observed that the time of cut, pump pressure, and water jet temperature increases as mean depth of cut increased. Temperature of water jet and time of cut show significant effect on the depth of cut than the pump pressure. Apart from the nozzle geometry, which statistical analysis showed would have the greatest impact on the maximum depth of cut, the trends in Figure 4.7 (a-d) follow the projected order of the time of cut, pump pressure, water jet temperature, and stand-off distance being significant.
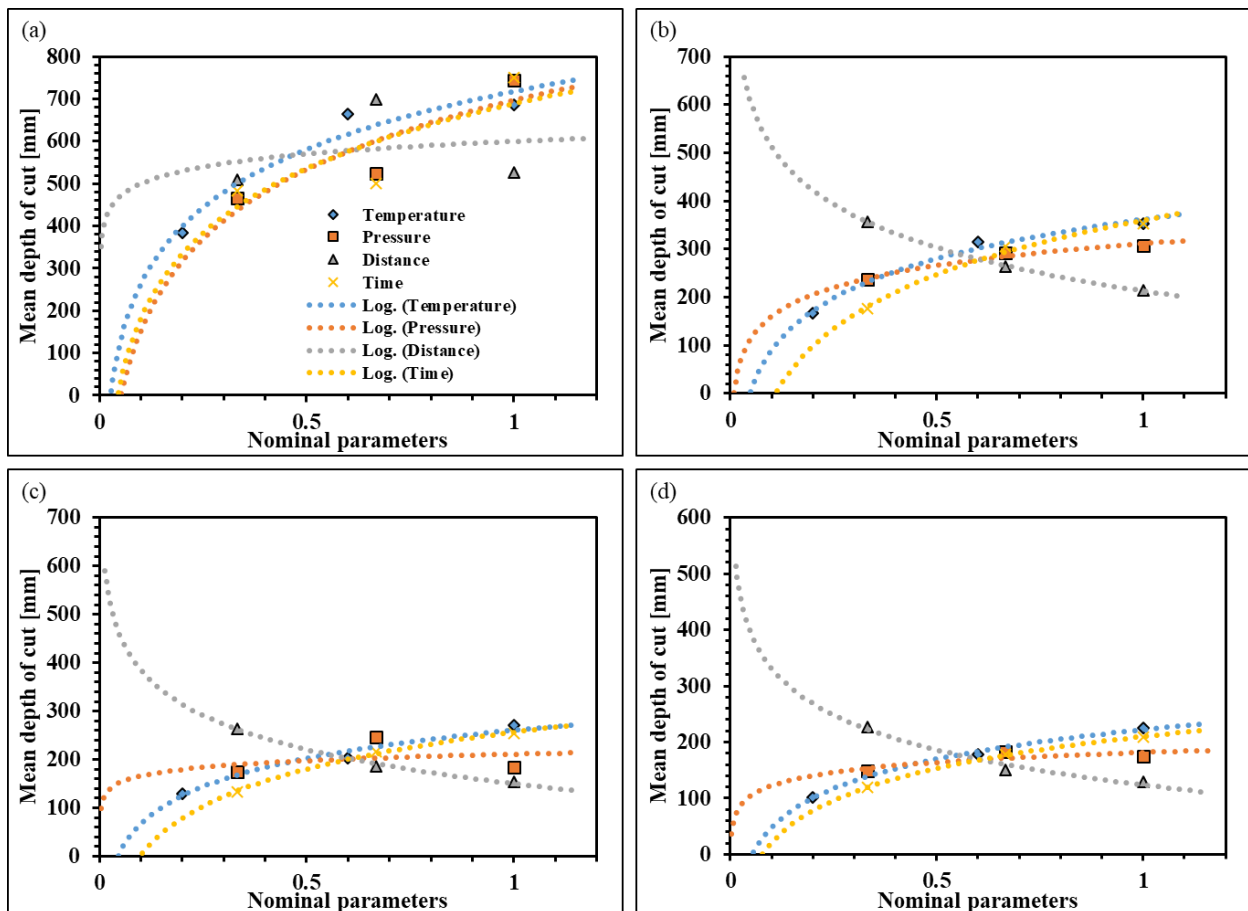
Nominal Parameter $= x / x_{max}$; *x- Parameter*

Figure 4. 7: Effect of nominal parameters on the mean depth of cut (a) 0° (red) nozzle (b) 15° (yellow) nozzle (c) 25° (green) nozzle (d) 40° (white) nozzle

Figure 4.8 shows that mean depth of cut decreases with increased spray angle of dispersion. This due to energy dispersion as a result of atomization of water jet, and also the reduced action of water hammer effect.
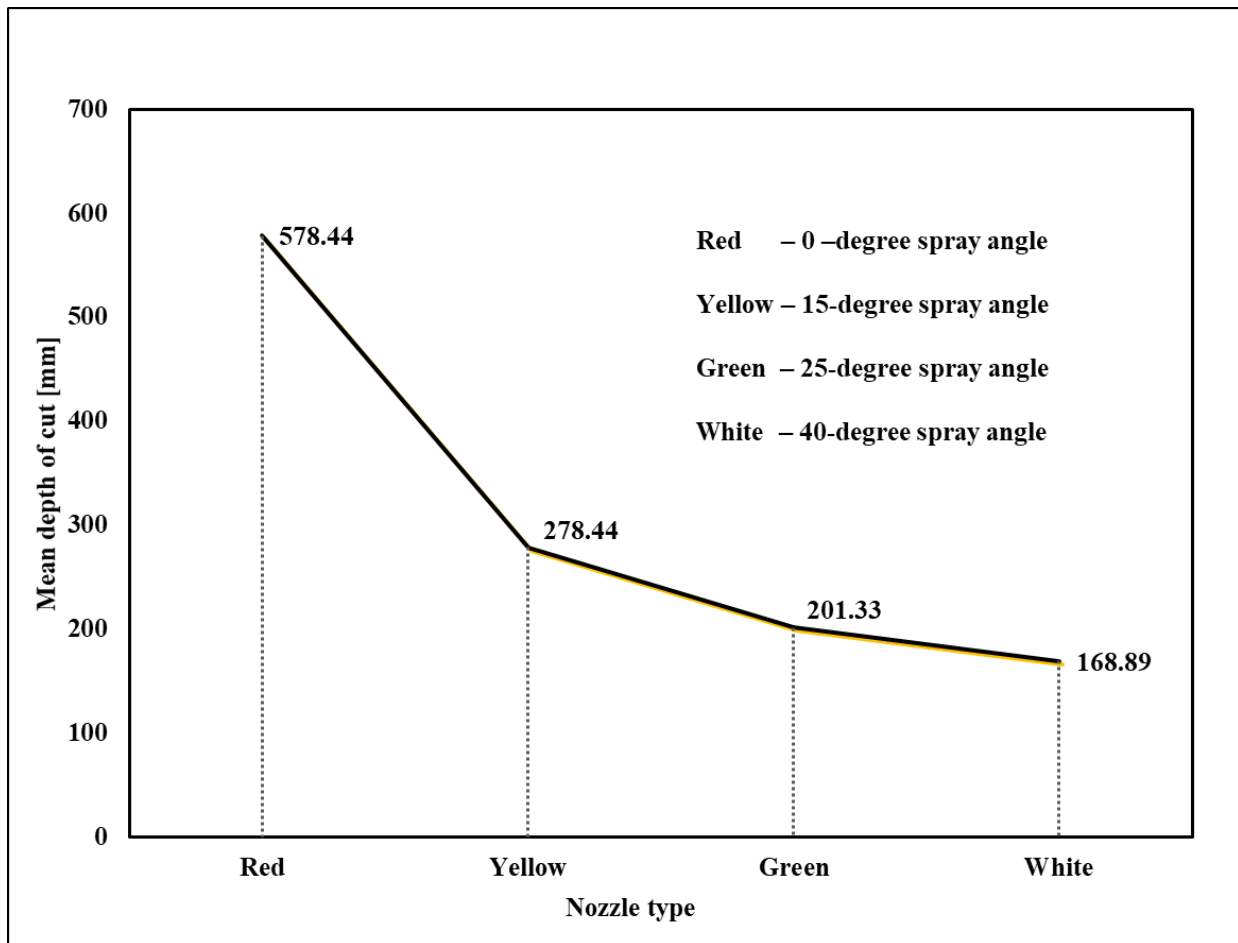
Figure 4. 8: Effect of nozzle geometry on the mean depth of cut

4.8 Effect of Operating Parameters on Width of Cut

The effects of temperature of water jet, operating pressure of pump, standoff distance and time of cut were observed on the width of cut. As aforementioned, the effect of each parameter on the

depth or width of cut is not the sole influence, for example the trend of temperature on the width of cut may increase or decrease while at the same time the effect of operating pump pressure, standoff distance and time of cut is taking place on the width of cut.

The width of the cut must be maximized to enhance crack propagation in order to facilitate ice delamination. This phenomenon makes the analysis of the width of cut equally essential as the depth of cut. When a high-velocity water jet is directed towards an ice surface, it exerts significant pressure on the ice, eventually resulting in fracture initiation. This force permeates the ice structure, causing microscopic fractures to emerge and spread in various directions. More fractures result from a wider jet. These cracks weaken the structural integrity of the ice blocks, eventually leading to large fractures or even complete disintegration.

4.9 Effects of Pressure on Width of Cut

The pressure of the water jet has a direct impact on the ice block. As the pressure increases, the water jet should be able to cut more efficiently and precisely, resulting in narrower cuts. This is because the higher pressure leads to a more focused and faster jet, allowing for better material removal and less widening of the cut. However, the aforementioned phenomenon is not effective when there is a spray angle in the design of the nozzle. In Figure 4.9 (a), the mean width of the cut increases from 35.3 mm to 39.8 mm when the pressure is increased from 1000 psi to 2000 psi, which is opposite of what we would expect. This increase is possible because the 2000 psi has a longer standoff distance than the 3000 psi, creating more dispersed water jet. When the pressure is further increased to 3000 psi, the mean width of the cut decreases to 35.8 mm, which is more in line with the expected relationship. Figure 4.9(d) followed the same pattern as Figure 4.9(a). Figure 4.9 (b-c) on the other hand shows a consistent trend over the pressure range. To better understand

the relationship between pressure and the mean width of the cut in ice blocks using water jet cutting, other parameters would have to be held constant but that is not the focus of this study.
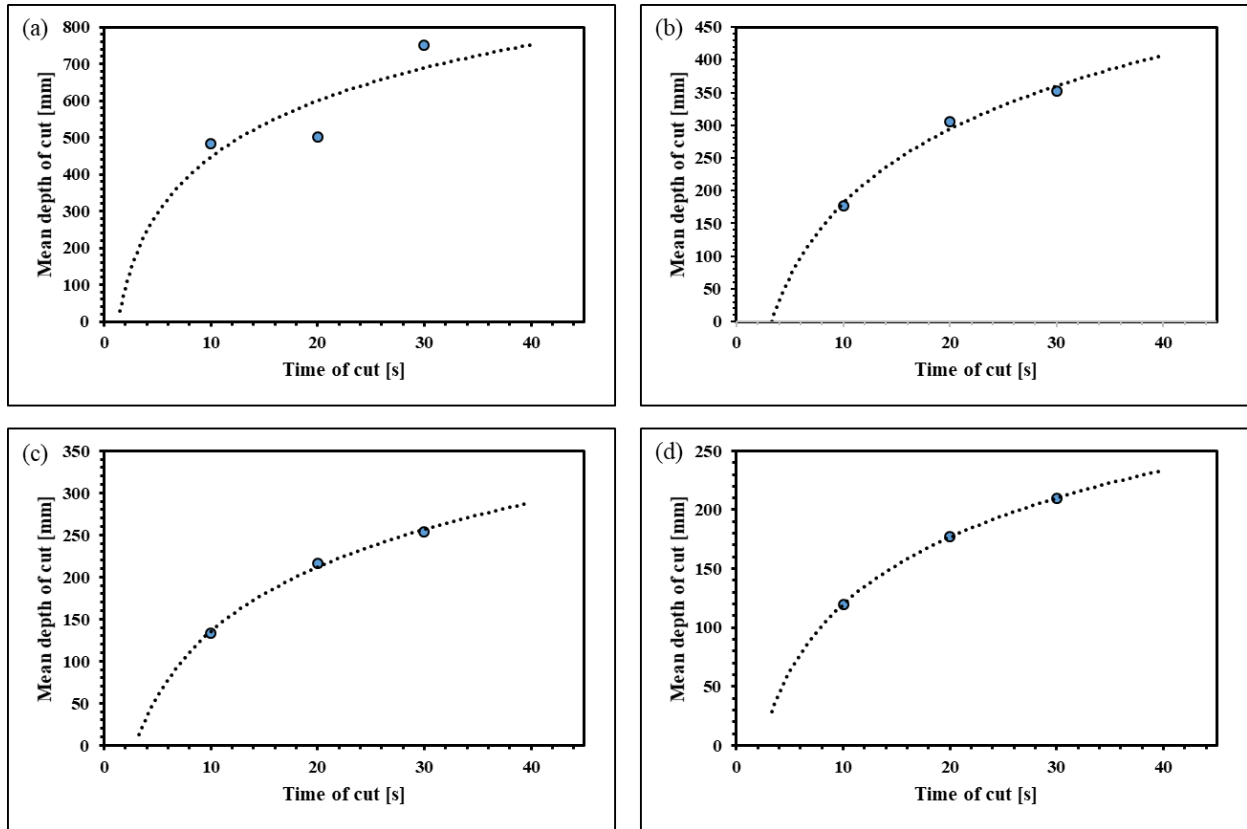

Figure 4. 9: Effect of operating pump pressure on the mean width of cut (a) 0° (red) nozzle (b) 15° (yellow) nozzle (c) 25° (green) nozzle (d) 40° (white) nozzle

4.10 Effects of Temperature on Width of Cut

When a water jet comes into contact with the ice block, heat is transferred from the water to the ice, causing the ice to melt. The rate of heat transfer depends on the temperature difference between the water jet and the ice. The higher the temperature of the water jet, the greater the temperature difference, leading to faster heat transfer and more rapid melting of the ice. Figure 4.10 (a)(c-d) shows a continuous pattern of increasing mean width of cut with increasing water jet temperature. Figure 4.10 (b) showed an inconsistent trend, which might be attributed to the structural integrity

of the ice as well as other operating parameters. As observed in the experiment, the ice surrounding the cut may become weaker and more prone to cracking or breaking, affecting the uniformity and width of the cut.

Figure 4. 10: Effect of temperature of water jet on the mean width of cut (a) 0° (red) nozzle (b) 15° (yellow) nozzle (c) 25° (green) nozzle (d) 40° (white) nozzle

4.11 Effects of Stand-off Distance on Width of Cut

The distance of the water jet from the nozzle can affect the mean width of the cut in the ice block in several ways. The main factors involved are the water jet's energy, the dispersion of the jet, and the stability of the jet over different distances.

- Energy: As the distance between the nozzle and the ice block increases, the energy of the water jet decreases. This is due to a loss of kinetic energy as the water travels through the air, which can lead to a wider and less precise cut in the ice block.

- Dispersion: The water jet disperses as it travels away from the nozzle, leading to a wider spread and potentially a wider cut in the ice block. However, the degree of dispersion can be influenced by various factors such as nozzle design, water pressure, and ambient conditions.

- Stability: A stable water jet is more likely to produce consistent and precise cuts in the ice block. As the distance between the nozzle and the ice block increases, the jet can become more susceptible to environmental factors (e.g., air resistance, wind, etc.), which can lead to instability and ultimately affect the width of the cut.

Figure 4.11 (a-b) shows a decreasing trend of mean width of cut as standoff distance increases. The loss of energy and the increasing instability of the water jet as the distance increases have a greater impact on the mean width of the cut than the dispersion of the water jet. This is probably due to the dispersion angle of the nozzle being less than 15°. We can infer that the optimum spray angle that widens the width of cut starts from 15°. The trends of mean width of cut increase in Figure 4.11 (c-d) as standoff distance increases. Due to the large spray angles, it disperses the water jet, leading to a wider spread. This dispersion effect is primary cause of the increase in the mean width of the cut as the distance increases.
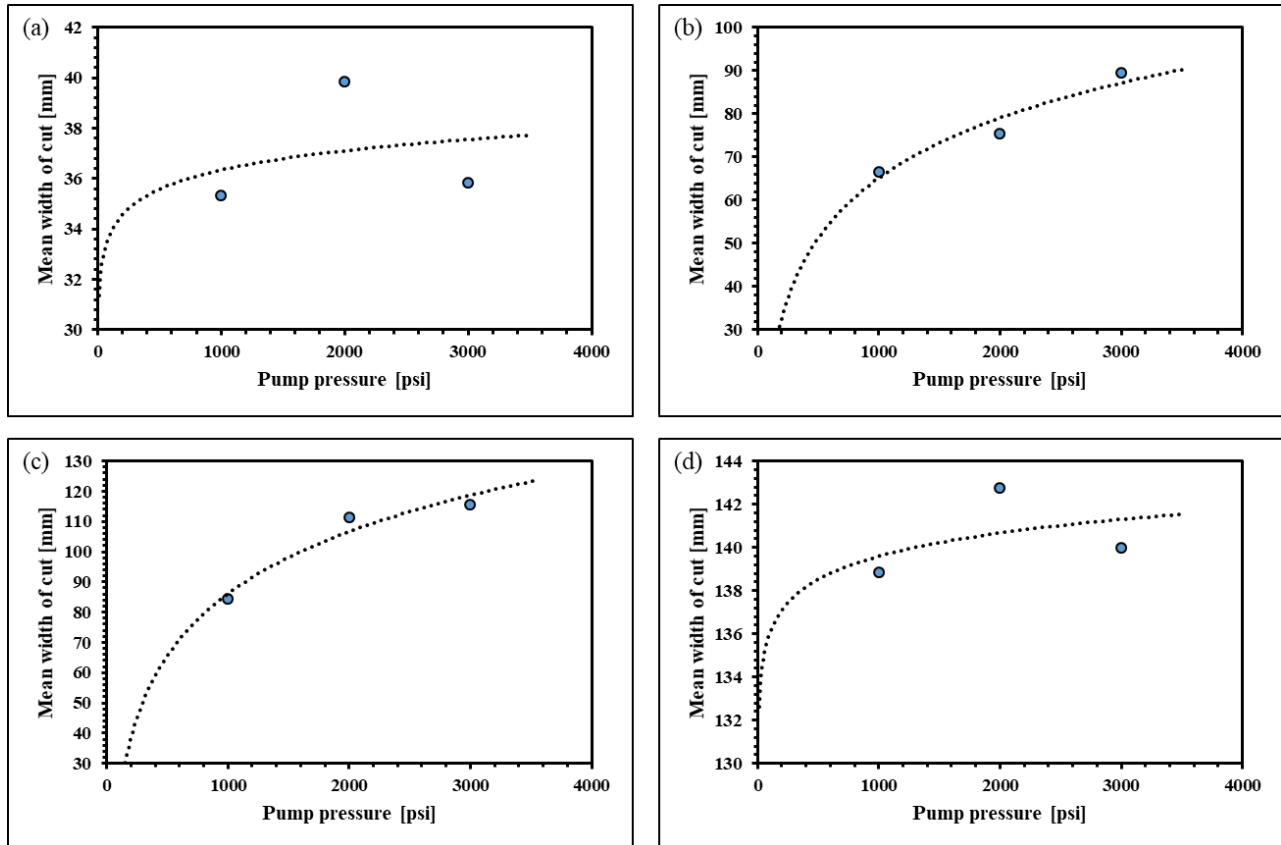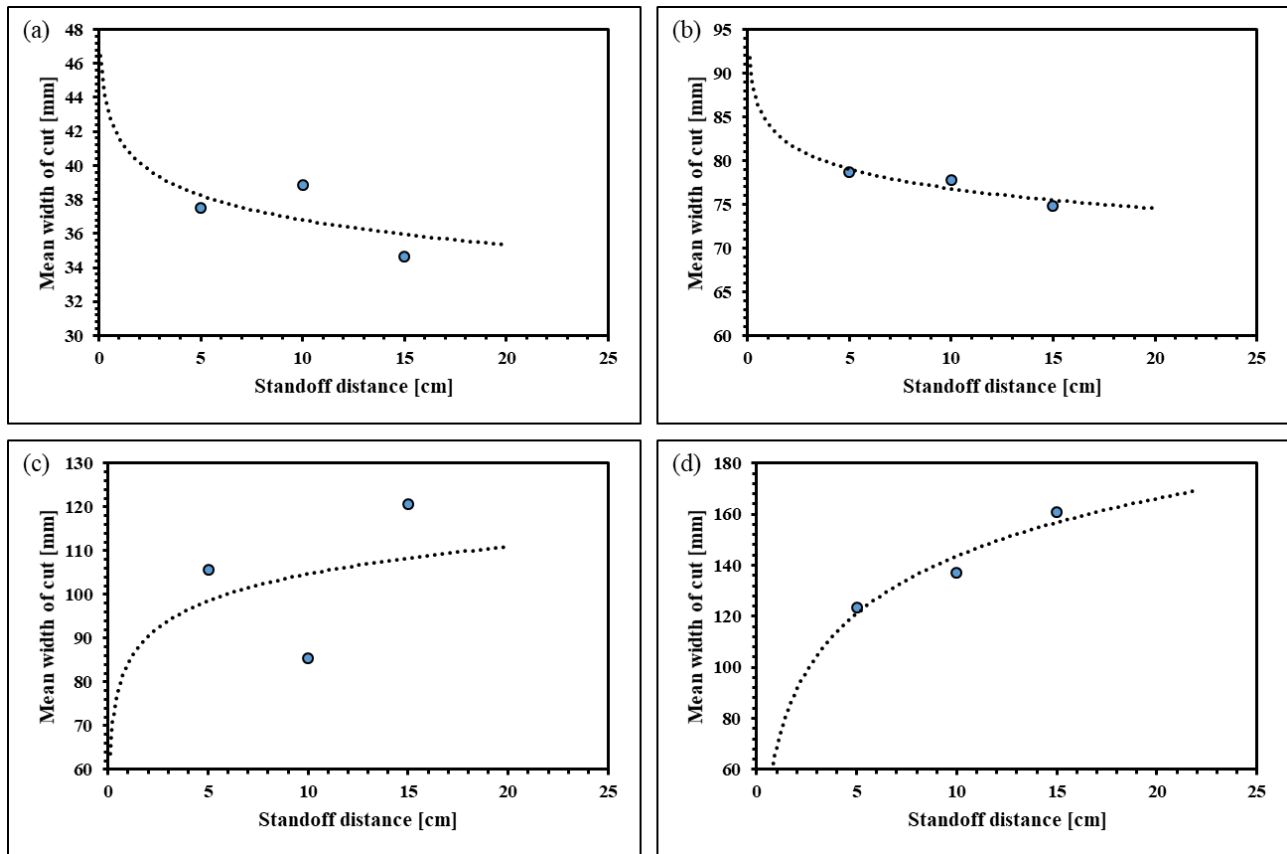
Figure 4. 11: Effect of standoff distance on the mean width of cut (a) 0° (red) nozzle (b) 15° (yellow) nozzle (c) 25° (green) nozzle (d) 40° (white) nozzle

4.12 Effects of Variation of Time on Width of Cut

When the water jet is applied to the ice block, it starts to cut through the ice by melting it. The longer the water jet is applied, the more time the jet has to remove the ice, which in turn increases the width of the cut.

The linear relationship between the time of the water jet and the mean width of the cut can be explained by the constant rate of ice removal by the water jet. As the water jet's intensity, pressure, and temperature remain constant over time, the rate at which it melts the ice is also constant. This leads to a consistent increase in the width of the cut as the time increases as seen in the increasing trend in Figure 4.12 (a-c). The decreasing trend of Figure 4.12 (d) is as a result of the standoff

distance setting. From Table I.1, the time of cut of the white nozzle had a close distance setting. The closer the distance, the narrower the cut, and also the energy of the water jet is dispersed and low in effect due to the large spray angle (40°).
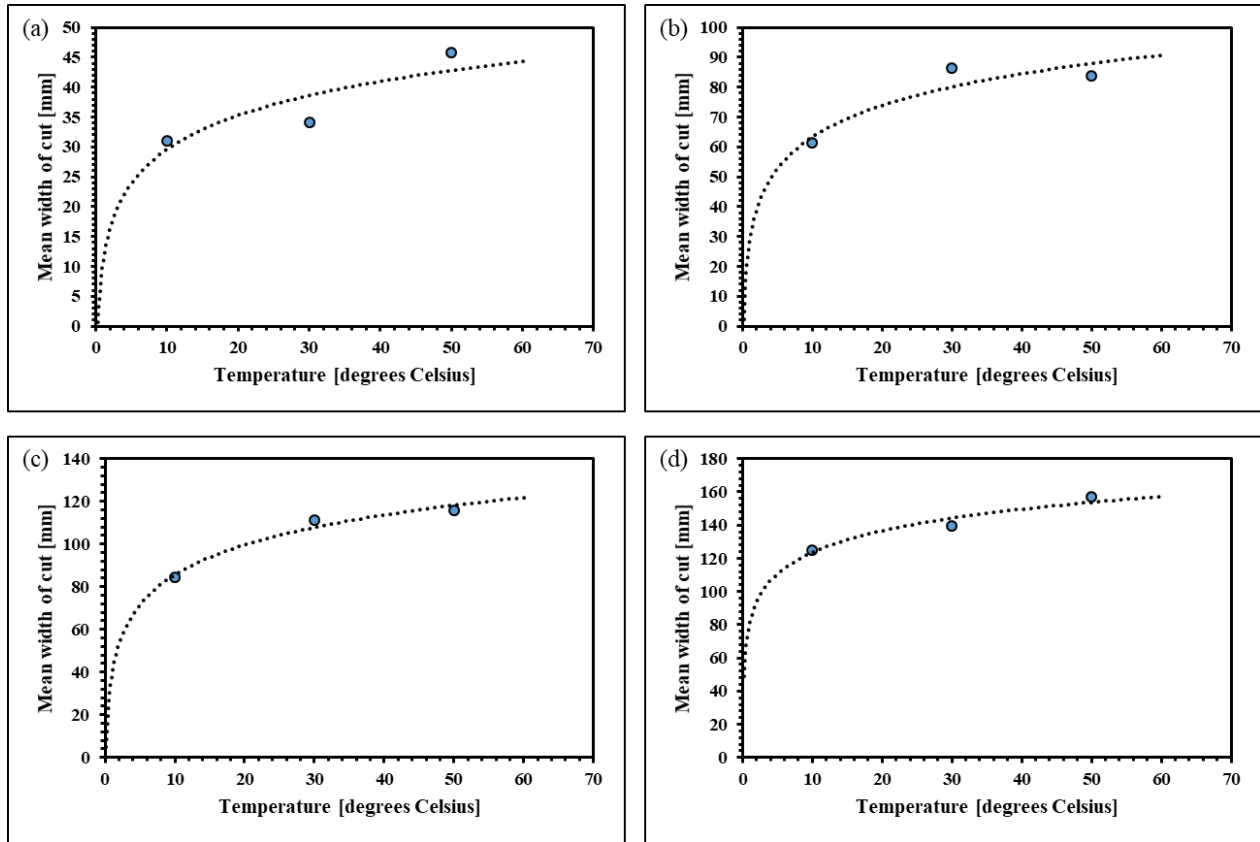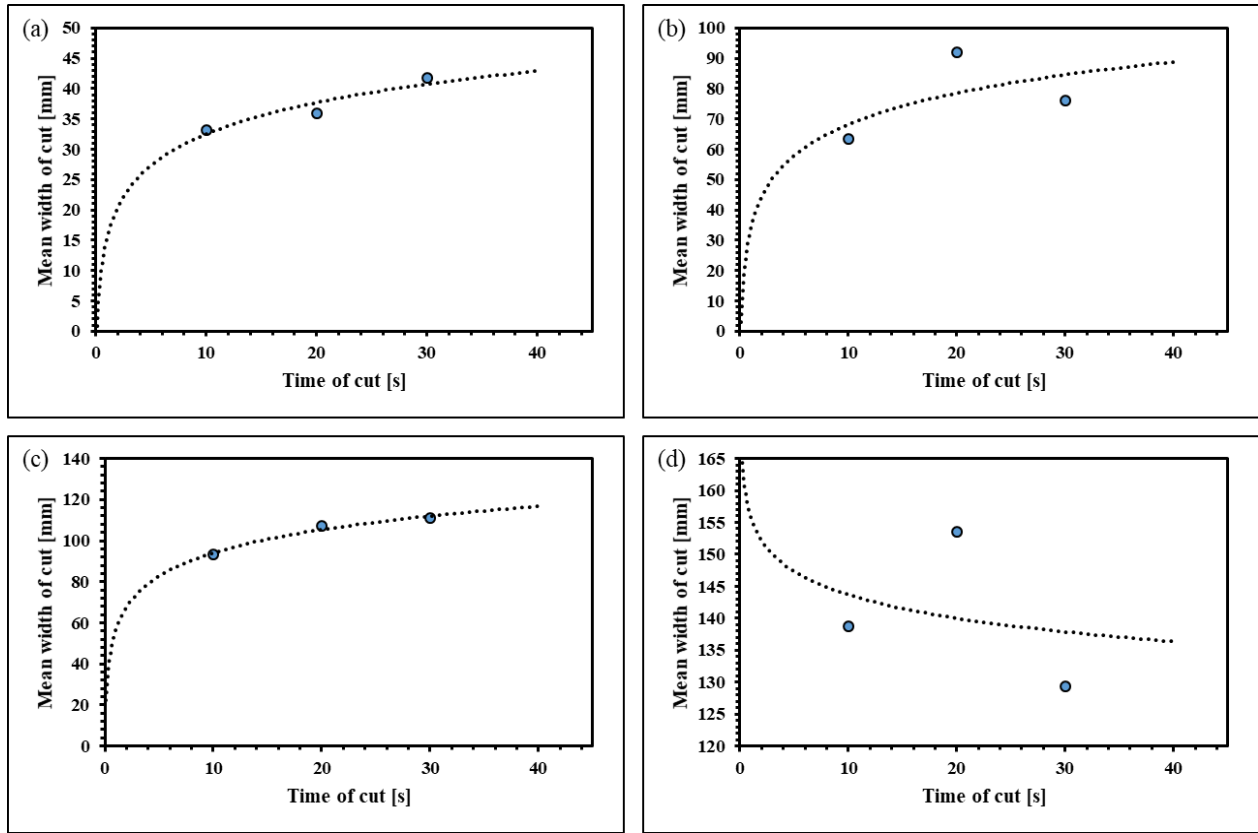

Figure 4. 12: Effect of time of cut on the mean width of cut (a) 0° (red) nozzle (b) 15° (yellow) nozzle (c) 25° (green) nozzle (d) 40° (white) nozzle

4.13 Combined Influence of Operating Parameters on Width of Cut based on Nozzle Geometry

Figure 4.13 (a-d) depicts the mean width of cut of the four distinct nozzles as a function of water jet temperature, operating pump pressure, standoff distance, and time of cut. In Figure 4.13 (a), water jet temperature and time of cut have a stronger impact on the width of cut; in Figure 4.13 (b), water jet temperature, operating pump pressure, and time of cut have a greater influence on

77

the width of cut. In Figure 4.13 (c), all factors have an effect on the width of the cut, and water jet temperature and distance have an effect on the width of the cut in Figure 4.13 (d). These observations are primarily attributable to the spray angles and other parameter settings.
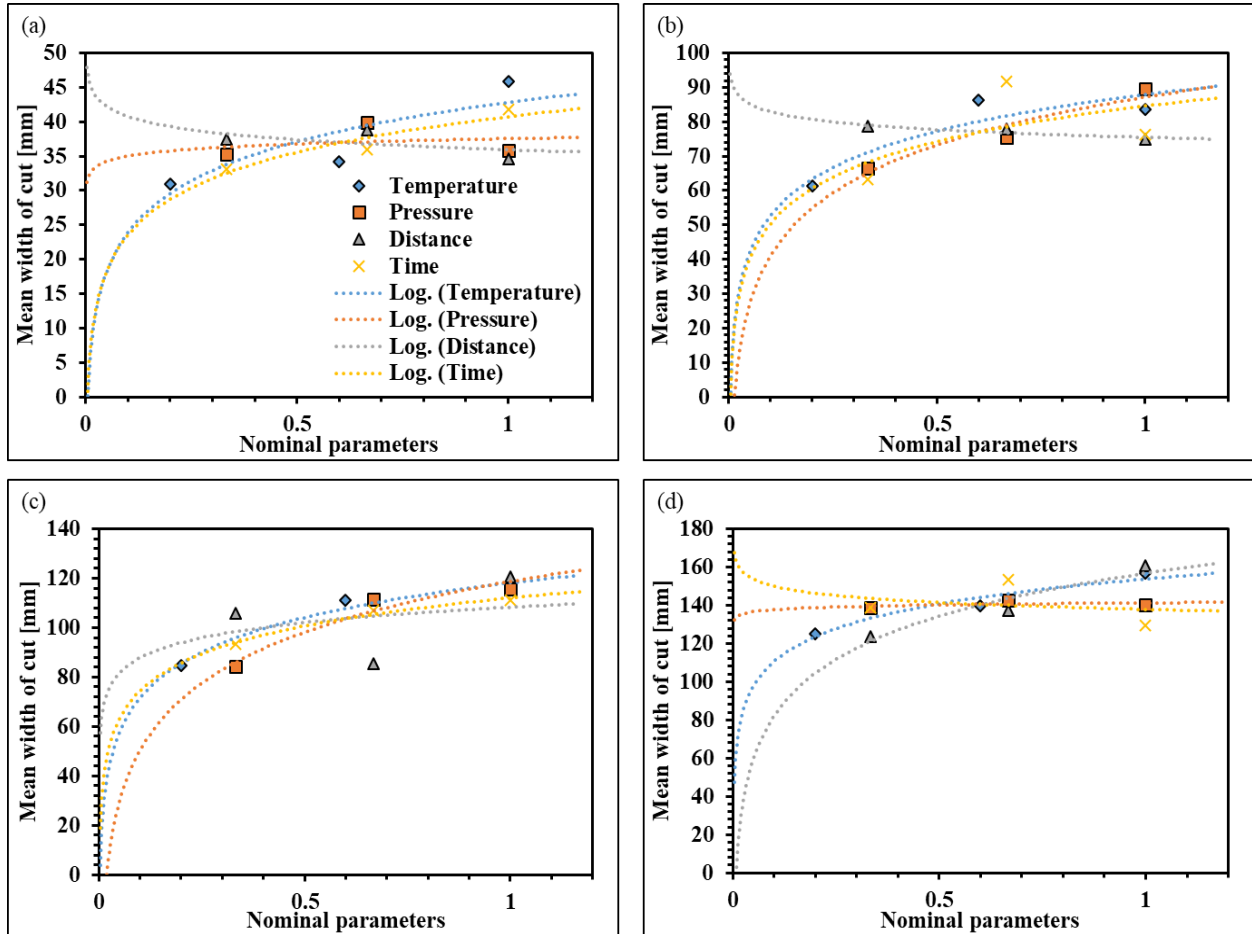
Nominal Parameter $= x / x_{max}$; x- *Parameter*

Figure 4. 13: Effect of nominal parameters on the mean width of cut (a) 0° (red) nozzle (b) 15° (yellow) nozzle (c) 25° (green) nozzle (d) 40° (white) nozzle
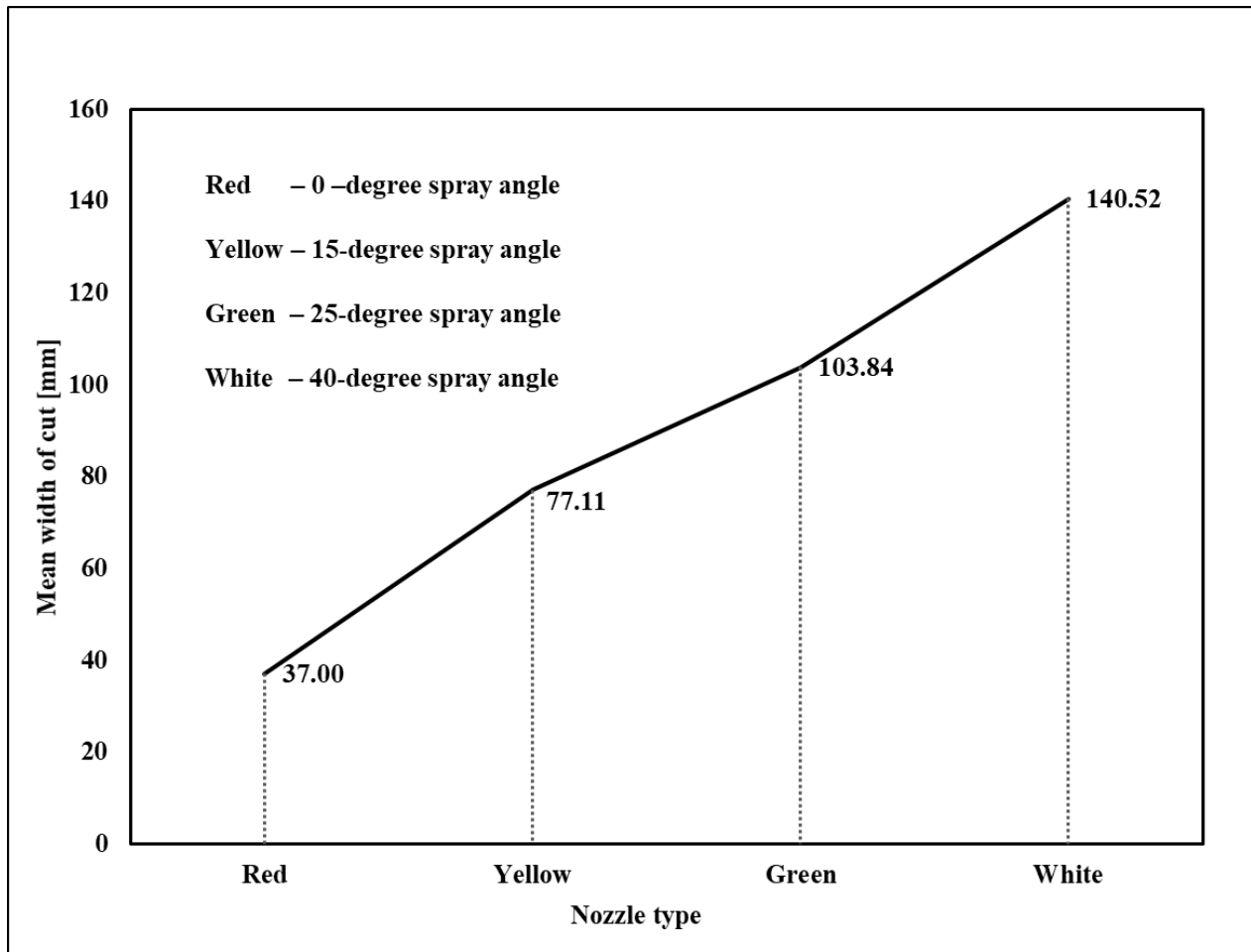
Figure 4. 14: Effect of nozzle geometry on the mean width of cut

Figure 4.14 illustrates that when the spray angle of dispersion rises, so does the mean width of cut. This is due to energy and water jet dispersion as the spray angle increases. The 0° (red) nozzle had a mean width of 37 mm, while the 15° (yellow) nozzle had a mean width of cut of 77.11 mm. The 25° (green) nozzle had a mean width of cut value of 103.84 mm, followed by the 40° (white) nozzle, which had the maximum width of cut value of 140.52 mm.

4.14 Best Parameters for Maximum Cuts

A red nozzle (spray angle of $0°$), operating pump pressure of 2371 psi, water jet temperature of 38.6 Celsius, standoff distance of 7.7 cm, and time of cut of 25.9 s are the best operating conditions for achieving maximum depth of cut. Multiple linear regression analyses, presented in Table 3.7, revealed the following model function between the depth of cut and the jet operating parameters:

$$\ln(\text{depth of cut}) = 4.92654 + 0.019335T + 0.000161P - 0.024211dx + 0.030520t \quad (4.1)$$

Similarly, the best operating conditions for obtaining simultaneous maximum depth and width of cut are a white nozzle (spray angle of $40°$), operating pump pressure of 2829 psi, water jet temperature of 28.3 Celsius, standoff distance of 9 cm, and a time of cut of 20.8 s using the model equation:

$$\ln(\text{jet cut}) = 3.76632 + 0.019335T + 0.000161P - 0.024211dx + 0.030520t \quad (4.2)$$

where T is temperature of water jet, P is operating pump pressure, dx is stand-off distance, and t is time of cut.

5.0 Conclusions and Recommendations

5.1 Conclusions

Ice development on surfaces during winter or in severely cold climates affects several industries, including aviation, hydropower, telecommunications, navigation, electrical distribution, and transportation. The old method of deicing maritime vessels by human labour requires huge effort and long hours for insufficient results in most cases. Current alternative deicing technologies may be too expensive or impossible to implement. Since water is easily accessible to maritime operations and heat energy diverted from the engine to heat up the water, high-pressure water jet (HPWJ) is proving to be a useful deicing technology, which is the focus of our investigation. HPWJ is currently used in high-level precision manufacturing in the automotive, aerospace, building products, electronics, food, paper and steel industries. HPWJ has low efficiency in strong winds, especially when the stand-off distance is long and might damage equipment if the operation parameters are not adjusted appropriately.

The issue of ice accretion has driven the Marine Icing Group of the Memorial University of Newfoundland, to investigate the potential of high-pressure water jets to cut slots in ice blocks, primarily for possible usage as an aid to icebreaking on marine vessels. Deicing is an essential process for ships operating in cold climates or navigating through icy waters. During winter, ice can accumulate on a ship's surface, leading to multiple issues that jeopardize the vessel's safety and efficiency.

One primary concern with ice build-up on a ship is the increased weight. Ice formation on the hull and other areas can add to the ship's mass, reducing maneuverability and fuel efficiency. Furthermore, ice can also impact the ship's stability, making it more susceptible to capsizing or rolling in turbulent waters.

The main objective of this study is to investigate the combined effect of operating parameters including pump pressure, nozzle geometry, water jet temperature, and standoff distance on the depth and width of cut through an ice block. The significance of the main objective is to maximize depth and width of cut in order to facilitate the delamination of ice accrued on surfaces. The depth and width of the cut must be maximized to enhance crack propagation in order to facilitate ice delamination as shown in Fig. 5.1.
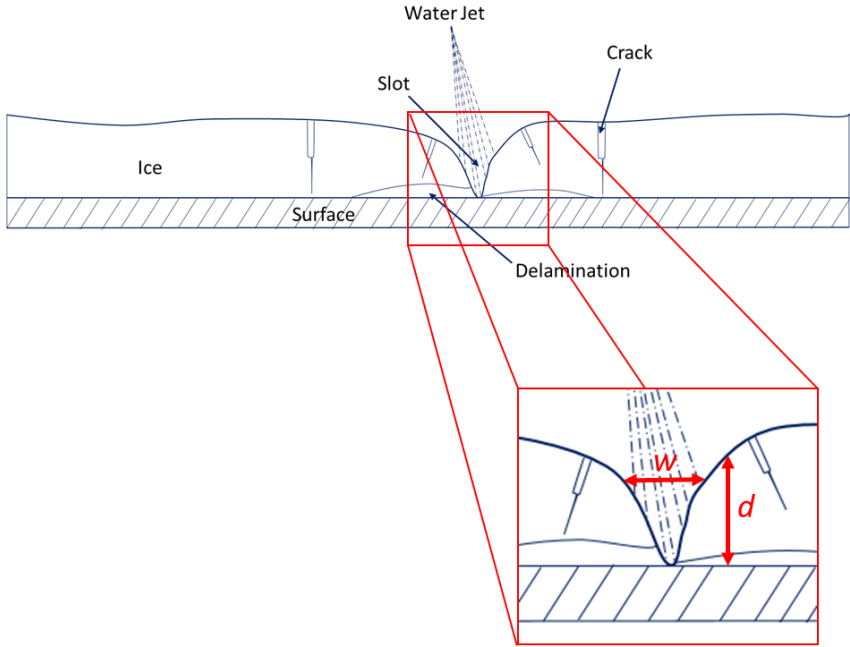
Figure 5.1: Crack propagation and delamination in ice with *w* and *d* representing width and depth of cut, respectively

When a high-velocity water jet is directed towards an ice surface, it exerts significant pressure on the ice, eventually resulting in fracture initiation. This force permeates the ice structure, causing microscopic fractures to emerge and spread in various directions. More fractures result from a

wider jet and a deeper cut. These cracks weaken the structural integrity of the ice blocks, eventually leading to large fractures or even complete disintegration.

This study was conducted experimentally in a cold room with an ambient temperature of 10 °C. Ice was simulated in the lab by making ice blocks that were kept at -10 °C throughout the experiment. Preliminary cases were acquired using a factorial design of experiment at different levels with five parameters, including the nozzle type, yielding biased results. New cases were developed, and the measured responses were used to generate regression model equations for the four nozzle types. The models predicted depth of cut with a P-value less than 0.0001 and an F-value of 23.26 with 99% confidence, showing that the models are significant. Also, the Predicted R^2 of 0.7473 is in reasonable agreement with the Adjusted R^2 of 0.8166; i.e. the difference is less than 0. 2. According to the findings, the nozzle geometry has the greatest impact on the maximum depth of cut, followed by the time of cut, pump pressure, water jet temperature, and stand-off distance. Whereas the models predicted width of cut with a P-value less than 0.0001 and an F-value of 44.67 with 99% confidence, showing that the models are significant. The respective Predicted and Adjusted R^2 values of the width of cut are 0.8635 and 0.8973 and are in reasonable agreement with a difference of less than 0.2. Also, the nozzle geometry has the greatest impact on the maximum width of cut, followed by the stand-off distance, pump pressure, time of cut and water jet temperature.

The multiple regression analysis of the model for the depth and width of cut are given in Tables 3.7 and 3.11, respectively. The model equation for the depth and width of cut are obtained in Tables 3.8 and 3.12, respectively, from Tables 3.7 and 3.11.

This study investigated the effectiveness of HPWJ deicing on maritime vessels. I discovered that HPWJ efficiently cut slots in ice blocks, reaching depth of 825 mm and width of 175 mm. These values are good enough to create slots and cracks in accumulated ice on marine vessels. The

process of ice sheet delamination on vessel surfaces has been demonstrated by Derbidge et al. (1989), indicating that this approach can effectively facilitate HPWJ deicing. In their study, Derbidge et al. (1989) presented a high-pressure flash flow system for de-icing, which was tested experimentally under conditions of 517-862 kPa and temperatures ranging from 122 to 133°C. A photograph of the system can be found in Ryerson's (2008) work on page 84. The design of the system was aimed at utilizing a ship's fire main as its source of operation, while incorporating a portable heater to elevate the temperature of water without transforming it into steam, thereby facilitating the use of seawater. The results of the tests indicate that the equipment demonstrated the capacity to eliminate ice with a thickness of 10 cm and a removal rate of up to 186 cm2 of ice per second without causing damage to the substrate (vessel deck).

The optimization of operational parameters is used to develop a cuttability chart (attached in the appendix) for various thicknesses of accumulated ice on the deck and various vessel surfaces. Also, a chart to obtain width slots between 30 mm and 210 mm is developed.

To the best of authors' knowledge, this is the first research on the combined effect of operating pump pressure, water jet temperature, stand-off distance of the different nozzle geometries ($0°, 15°, 25°$ and $40°$) on the depth and width of cut in ice blocks.

5.2 Recommendations for future work

Although this study provided valuable insight into the effectiveness of the combined effect of operating pump pressure, water jet temperature, and stand-off distance of the various nozzle geometries ($0°, 15°, 25°$ and $40°$) on the depth and width of cut in ice blocks, there are some recommendations for future research.

Some recommendations for future work are summarized below:

➢ Examining depth and width of water jet cut in ice blocks through the combined effects of operational parameters.

- Simulate the temperature of the cold room to be like the ambient condition of the artic or cold regions marine vessels normal operate.

- Include traverse velocity of the water jet within a certain cutting width. This could increase cutting width leading to more fracture and crack propagation to facilitate delamination, and ultimately increasing deicing efficiency.

- Use of saline/seawater to simulate ice block and water jet

➢ Multiphase interaction of water jet cutting in ice blocks

- Numerical verification and validation of experimental results

➢ Evolution of interface boundary between water jet and ice blocks

- Analytical studies using Stefan problem to validate numerical and/or experimental results

References

Adriaens, Han, Koning, & Banning. (2000). Modeling piezoelectric actuators. *IEEE/ASME Transactions on Mechatronics*, *5*, 331–341.

Andrei, C. (1975). *Constanta Maritime University Annals: CONSIDERATIONS REGARDING ICE ACCRETION ON BOARD SHIPS AND THE INFLUENCE ON INTACT STABILITY*. *28*, 28.

Bajaj, A. K., & Garg, V. K. (1977). Linear Stability of Jet Flows. *American Society of Mechanical Engineers (Paper)*, *77-WA/APM-10*, 378–384.

Baller. (1983). Rig winterization to allow year-round drilling off northern Norway. *Oil and Gas*.

Begenir, A., Tafreshi, H. V., & Pourdeyhimi, B. (2004). Effect of Nozzle Geometry on Hydroentangling Water Jets: Experimental Observations. *Textile Research Journal*, *74*(2), 178–184. https://doi.org/10.1177/004051750407400215

Borisenkov, & Panov. (1972). *Osnovnyye rezultaty i perspektivy issledovaniy gidrometeorologicheskikh usloviy obledeneniya sudov* . *Technical Report Trudy No. 298, Arkticheskii i Antarkticheskii NauchnoIssledovatielSkii lnstitut*.

Boston. (1985). *Engineering Progrsm on Anti/De-icing of the Rast Track. In Proceeding of rhe 1985 US Navy Symposium of the Artic/Cold Weather Operations of Ships, 3-4 December*. *December*, 201–214.

Brown, Mitten, & Hansen. (1988). *Ice accretion on drilling platforms off the east coast of Canada*.

Bruno Arab, P., & Barreto Celestino, T. (2020). A microscopic study on kerfs in rocks subjected to abrasive waterjet cutting. *Wear*, *448–449*, 203210. https://doi.org/10.1016/J.WEAR.2020.203210

Brunton, J. H. (1966). The Physics of Impact and Deformation: Single Impact, I. High Speed Liquid Impact. *Philosophical Transactions of The Royal Society A*, *260*(1110).

Cammaert. (2013). Impact of marine icing on Arctic offshore operations. *Arctic Marine Operations Challenges & Recommendations*, *5*.

Carstens. (1983). Special hazards in open waters at high latitudes. *Cold Regions Science and Technology*, 293–295.

Chanson, H. (2004). *The hydraulics of open channel flow : an introduction ; basic principles, sediment motion, hydraulic modelling, design of hydraulic structures*. Elsevier Butterworth Heinemann.

Coveney, D. B. (1981). *Cutting Ice With High Pressure Water Jets*. 50.

Coveney, D. B., & Brierley, W. H. (1978). *The Cutting of Ice With Water Jets*. 42.

Crowley. (1988). *Cold water effects upon marine operations*. 543–548. https://doi.org/10.1109/OCEANS.1988.794867

Cui, D., Li, H., He, J., Wang, Q., Lu, C., Hu, H., Cheng, X., & Wang, C. (2022). Applications of Water Jet Cutting Technology in Agricultural Engineering: A Review. *Applied Sciences (Switzerland)*, *12*(18). https://doi.org/10.3390/app12188988

Dehghani, S. R., Muzychka, Y. S., & Naterer, G. F. (2016). Droplet trajectories of wave-impact sea spray on a marine vessel. *Cold Regions Science and Technology*, *127*, 1–9. https://doi.org/10.1016/j.coldregions.2016.03.010

Deo, R. C., Mi, J., & Nathan, G. J. (2007). The influence of nozzle-exit geometric profile on statistical properties of a turbulent plane jet. *Experimental Thermal and Fluid Science*, *32*(2), 545–559. https://doi.org/10.1016/j.expthermflusci.2007.06.004

Deo, R. C., Nathan, G. J., & Mi, J. (2007). Comparison of turbulent jets issuing from rectangular nozzles with and without sidewalls. *Experimental Thermal and Fluid Science*, *32*(2), 596–606. https://doi.org/10.1016/j.expthermflusci.2007.06.009

Derbidge, T. C., Schweizer, S. E., & Powars, C. A. (1989). Ice removal using low-pressure flashing flow. *US Navy Symposium on Arctic/Cold Weather Operations of Surface Ships*, 327–338.

Deshpande, S., Sæterdal, A., & Sundsbø, A. (2021). Sea spray icing: The physical process and review of prediction models and winterization techniques. *Journal of Offshore Mechanics and Arctic Engineering*, *143*(6), 1–12. https://doi.org/10.1115/1.4050892

Donald, G., Kenneth, B., Ronald, C., Arthur, G., Janet, P., & Craig, W. (2009). *Assessment of Undiscovered Oil and Gas in the Arctic*. *51*(6), 1401–1403.

Dyment, A. (2015). Compressible Liquid Impact Against a Rigid Body. *Journal of Fluids Engineering*,

3(3), 031102. https://doi.org/10.1115/1.4028597

Engin, I. C. (2012). A correlation for predicting the abrasive water jet cutting depth for natural stones. *South African Journal of Science*, *108*(9–10), 1–11. https://doi.org/10.4102/sajs.v108i9/10.692

Esoy, Henry, & Palmer. (2019). Anti-Icing and De-Icing of Pipe Structures on Marine Vessels Using Waste Heat Recovery. *Proceedings of the ASME 2019 38th International Conference on Ocean, Offshore and Artic Engineering*, *58875*, V008T07A006.

Fagan. (2004). Safety of well testing. *MMS JIP Report*, *4514774*.

Farzaneh, M., & Ryerson, C. C. (2011). Anti-icing and deicing techniques. *Cold Regions Science and Technology*, *65*(1), 1–4. https://doi.org/10.1016/j.coldregions.2010.08.012

Fett, R. W., Englebretson, R. E., P. (1993). *Forecasters handbook for the Bering Sea, Aleutian Islands and Gulf of Alaska*. 302.

Field, J. E., Camus, J. J., Tinguely, M., Obreschkow, D., & Farhat, M. (2012). Cavitation in impacted drops and jets and the effect on erosion damage thresholds. *Wear*, *290–291*, 154–160. https://doi.org/10.1016/J.WEAR.2012.03.006

Foldyna, J., Sitek, L., Ščučka, J., Martinec, P., Valíček, J., & Páleníková, K. (2009). Effects of pulsating water jet impact on aluminium surface. *Journal of Materials Processing Technology*, *209*(20), 6174–6180. https://doi.org/10.1016/j.jmatprotec.2009.06.004

Frankenstein, S., & Tuthill, A. M. (2002). Ice Adhesion to Locks and Dams: Past Work; Future Directions? *Journal of Cold Regions Engineering*, *16*(2), 83–96. https://doi.org/10.1061/(asce)0887-381x(2002)16:2(83)

Garry, T., & Ivana, K. (1963). NRC Publications Archive Archives des publications du CNRC concrete cl. *NRC Publications Record*, 1–15.

Gentz, G., Thelen, B., Gholamisheeri, M., Litke, P., Brown, A., Hoke, J., & Toulson, E. (2015). A study of the influence of orifice diameter on a turbulent jet ignition system through combustion visualization and performance characterization in a rapid compression machine. *Applied Thermal Engineering*, *81*, 399–411. https://doi.org/10.1016/j.applthermaleng.2015.02.026

Gilpin, R. R. (1973). The Ablation of Ice by a Water Jet. *Transactions of CSME*, *2*, 91–96.

Gold, L. W. (1971). Use of ice covers for transportation. *Canadian Geotechnical Journal*, *8*(2), 170–181. https://doi.org/10.1139/t71-018

Goraj, Z. (2014). Flight dynamics models used in different national and international projects. *Aircraft Engineering and Aerospace Technology*, *86*(3), 166–178. https://doi.org/10.1108/AEAT-02-2013-0036

Gryc, R., Hlaváč, L. M., Mikoláš, M., Šancer, J., & Daněk, T. (2014). Correlation of pure and abrasive water jet cutting of rocks. *International Journal of Rock Mechanics and Mining Sciences*, *65*, 149–152. https://doi.org/10.1016/j.ijrmms.2013.11.001

Guo, Z., Long, X., Liu, Q., & Zhang, M. (2014). EXPERIMENTAL STUDY ON WATER-JET DEICING. *IEEE*, 12–15.

Haavasoja, T., Haavisto, V., Engineer, E., Turunen, M. J., Nylander, P., Engineer, S., Helsinki, V., Traffic, S., & Centre, M. (2002). *A Field Trial of Vehicle Grip Compared to RWS Data*. 28–30.

Hansen, E. S. (2012). *Numerical modelling of marine icing on offshore structures and vessels*. *June*.

Heydari, G., Thormann, E., Järn, M., Tyrode, E., & Claesson, P. M. (2013). Hydrophobic surfaces: Topography effects on wetting by supercooled water and freezing delay. *Journal of Physical Chemistry C*, *117*(42), 21752–21762. https://doi.org/10.1021/jp404396m

Holman, J. P. (2001). Experimental Methods for Engineers. In *McGraw Hills* (Vols. s1-VIII, Issue 193). https://doi.org/10.1093/nq/s1-VIII.193.43-b

Holman, J. P. (Jack P. (1994). *Experimental methods for engineers*. 616.

Hsu, C. Y., Liang, C. C., Teng, T. L., & Nguyen, A. T. (2013). A numerical study on high-speed water jet impact. *Ocean Engineering*, *72*, 98–106. https://doi.org/10.1016/j.oceaneng.2013.06.012

Hu, Y., Kang, Y., Wang, X. C., Li, X. H., Long, X. P., Zhai, G. Y., & Huang, M. (2014). Mechanism and experimental investigation of ultra high pressure water jet on rubber cutting. *International Journal of Precision Engineering and Manufacturing*, *15*(9), 1973–1978. https://doi.org/10.1007/s12541-014-0553-0

Huang, F., Mi, J., Li, D., & Wang, R. (2020). Impinging Performance of High-Pressure Water Jets Emitting from Different Nozzle Orifice Shapes. *Geofluids*, *2020*. https://doi.org/10.1155/2020/8831544

Hussein, J., Capp, S. P., & George, W. K. (1994). Velocity measurments in a H-Re-number, etc turbolent jet. In *Journal of Fluid Mechanics* (Vol. 258, pp. 31–75).

Jerman, M., Orbanić, H., & Valentinčič, J. (2022). CFD analysis of thermal fields for ice abrasive water jet. *International Journal of Mechanical Sciences*, *220*(February), 0–13. https://doi.org/10.1016/j.ijmecsci.2022.107154

Jones, K. F., & Andreas, E. L. (2012). Sea spray concentrations and the icing of fixed offshore structures. *Quarterly Journal of the Royal Meteorological Society*, *138*(662), 131–144. https://doi.org/10.1002/qj.897

Jorgensen, T. S. (1982). *Influence of Ice Accretion on Activity in the Northern Part of the Norwegian Continental Shelf*.

Kalaaji, A., Lopez, B., Attané, P., & Soucemarianadin, A. (2003). Breakup length of forced liquid jets. *Physics of Fluids*, *15*(9), 2469–2479. https://doi.org/10.1063/1.1593023

Kenzhebayeva, A., Bakbolat, B., Sultanov, F., & Daulbayev, C. (2021). *A Mini-Review on Recent Developments in Anti-Icing Methods*.

Kulyakhtin, A., & Tsarau, A. (2014). A time-dependent model of marine icing with application of computational fluid dynamics. *Cold Regions Science and Technology*, *104–105*, 33–44. https://doi.org/10.1016/j.coldregions.2014.05.001

Lagerveld, S., Tamis, J., Bolman, B., Geelhoed, S. C. V., Jak, R., Scheidat, M., Benda-Beckmann, S. V., Faidutti, D., & Vries, P. D. (2013). Arctic Operations Handbook: Generic Framework for Environmental Assessments. *Undefined*.

Li, S., & Ye, X. (2009). Study on the Bridge Surface Deicing System in Yuebei Section of Jingzhu Highway. *International Journal of Business and Management*, *3*(12), 116–121. https://doi.org/10.5539/ijbm.v3n12p116

Liljestrom, & Lindgren. (1983). Ice weight a hazard to loaded semi. *Offshore*, *43*(4), 133.

Liu, J. liang, Xu, J. yu, Huang, H., & Chen, H. (2020). Microwave deicing efficiency and dielectric

property of road concrete modified using different wave absorbing material. *Cold Regions Science*

and Technology, *174*(March 2019), 103064. https://doi.org/10.1016/j.coldregions.2020.103064

Liu, X., Tang, P., Geng, Q., & Wang, X. (2019). Effect of Abrasive Concentration on Impact

Performance of Abrasive Water Jet Crushing Concrete. *Shock and Vibration*, *2019*.

https://doi.org/10.1155/2019/3285150

Lu, Shouqing, Wang, C., Wang, W., Li, M., & Zhang, D. (2021). Analysis on the Shape and Impact

Pressure of the High-Pressure Water Jet during the Hydraulic Flushing Cavity Technique. *Geofluids*,

2021. https://doi.org/10.1155/2021/7496540

Lu, Song, Xu, J., Bai, E., Liu, J., & Luo, X. (2017). Investigating microwave deicing efficiency in

concrete pavement. *RSC Advances*, *7*(15), 9152–9159. https://doi.org/10.1039/c6ra27109j

Lu, W., Lubbad, R., & Løset, S. (2015). Out-of-plane failure of an ice floe: Radial-crack-initiation-

controlled fracture. *Cold Regions Science and Technology*, *119*, 183–203.

https://doi.org/10.1016/j.coldregions.2015.08.009

Makkonen, L. (1984). *Atmospheric Icing on Sea Structures*. 04–01.

Makkonen, L. (1987). Salinity and growth rate of ice formed by sea spray. *Cold Regions Science and*

Technology, *14*(2), 163–171. https://doi.org/10.1016/0165-232X(87)90032-2

Makkonen, L. (2012). Ice adhesion—theory, measurements and countermeasures. *Journal of Adhesion*

Science and Technology, *26*, 413–445.

Masterson, D. M. (2009). State of the art of ice bearing capacity and ice construction. *Cold Regions*

Science and Technology, *58*(3), 99–112. https://doi.org/10.1016/J.COLDREGIONS.2009.04.002

Mellor, M., Road, P. R., Va, S., & Peg, D. (1973). *Cutting Ice With High Pressure Water Jets*.

Mi, J., Deo, R. C., & Nathan, G. J. (2005). Characterization of turbulent jets from high-aspect-ratio

rectangular nozzles. *Physics of Fluids*, *17*(6), 1–4. https://doi.org/10.1063/1.1928667

Miller, R. K. (1990). *Waterjet cutting: Technology and industrial applications*.

Mintu, S., Molyneux, D., & Oldford, D. (2016). State-of-the-art review of research on ice accretion

measurements and modelling. *Arctic Technology Conference 2016*, *March 2017*.

https://doi.org/10.4043/27422-ms

Murti, V. S., & Philip, P. K. (2007). A comparative analysis of machining characteristics in ultrasonic

assisted EDM by the response surface methodology.

Http://Dx.Doi.Org/10.1080/00207548708919838, *25*(2), 259–272.

https://doi.org/10.1080/00207548708919838

Nauman, J. (1984). *Superstructure icing observations on the semisubmersible Ocean Bounty in lower

Cook Inlet, Alaska*. 19–21.

Ni, B., & Wu, Q. (2020). Auxiliary Icebreaking Methods. *Encyclopedia of Ocean Engineering*, 1–7.

https://doi.org/10.1007/978-981-10-6963-5_103-1

Ni, B. Y., Pan, Y. T., Yuan, G. Y., & Xue, Y. Z. (2021). An experimental study on the interaction

between a bubble and an ice floe with a hole. *Undefined*, *187*.

https://doi.org/10.1016/J.COLDREGIONS.2021.103281

Nyantekyi-Kwakye, B. (2016). Experimental Investigation on the Flow Characteristics of Three-

Dimensional Turbulent Offset Jets. *Thesis*, *7*(6), 2016.

Ozcelik, Y., Gursel, M., Ciccu, R., Costa, G., & Bortolussi, A. (2012). Optimization of working

parameters of water jet cutting in terms of depth and width of cut. *Proceedings of the Institution of

Mechanical Engineers, Part E: Journal of Process Mechanical Engineering*, *226*(1), 64–78.

https://doi.org/10.1177/0954408911407706

Palacios, J., Smith, E., Rose, J., & Royer, R. (2011). Instantaneous de-icing of freezer ice via ultrasonic

actuation. *AIAA Journal*, *49*(6), 1158–1167. https://doi.org/10.2514/1.J050143

Parsons, S. C., January, R., & May, R. (1928). *Erosion by Water-hammer. CXIX*.

Paul Zakrzewski, W., Lozowski, E. P., & Muggeridge, D. (1988). Estimating the extent of the spraying

zone on a sea-going ship. *Ocean Engineering*, *15*(5), 413–429. https://doi.org/10.1016/0029-

8018(88)90008-X

Pingping, W., A-Man, Z., Yuxiang, P., Zifei, M., Pingping, W., A-Man, Z., Yuxiang, P., & Zifei, M. (2022). NUMERICAL SIMULATION OF TRANSIENT STRONGLY-NONLINEAR FLUID-STRUCTURE INTERACTION IN NEAR-FIELD UNDERWATER EXPLOSION BASED ON MESHLESS METHOD. *Chinese Journal of Theoretical and Applied Mechanics, 2022, Vol. 54, Issue 8, Pages: 2194-2209*, *54*(8), 2194–2209. https://doi.org/10.6052/0459-1879-22-271

Pommier-Budinger, V., Budinger, M., Rouset, P., Dezitter, F., Huet, F., Wetterwald, M., & Bonaccurso, E. (2018). Electromechanical resonant ice protection systems: Initiation of fractures with piezoelectric actuators. *AIAA Journal*, *56*(11), 4400–4411. https://doi.org/10.2514/1.J056662

Pope, S. (2000). Turbulent flows. *The Finite Element Method Set*, 248–273. https://doi.org/10.1016/b978-075066431-8/50214-9

Rashid, T., Khawaja, H. A., & Edvardsen, K. (2016). Review of marine icing and anti-/de-icing systems. *Journal of Marine Engineering and Technology*, *15*(2), 79–87. https://doi.org/10.1080/20464177.2016.1216734

Raudensky, M., Horak, A., Horsky, J., Pohanka, M., & Kotrbacek, P. (2007). Hydraulic descaling improvement, findings of jet structureon water hammer effect. *Revue de Metallurgie. Cahiers D'Informations Techniques*, *104*(2), 84–90. https://doi.org/10.1051/metal:2007133

Reitz, R. D., & Bracco, F. V. (1982). Mechanism of atomization of a liquid jet. *Physics of Fluids*, *25*(10), 1730–1742. https://doi.org/10.1063/1.863650

Ryerson, C. C. (1995). Superstructure spray and ice accretion on a large U.S. Coast Guard cutter. *Atmospheric Research*, *36*(3–4), 321–337. https://doi.org/10.1016/0169-8095(94)00045-F

Ryerson, C. C. (2008). Assessment of superstructure ice protection as applied to offshore oil operations safety, problems, hazards, needs, and potential transfer technologies. U. S. Army Cold Regions Research and Engineering Laboratory. *U. S. Army Cold Regions Research and Engineering Laboratory*, 156.

Ryerson, Charles C. (2011). Ice protection of offshore platforms. *Cold Regions Science and Technology*, *65*(1), 97–110. https://doi.org/10.1016/j.coldregions.2010.02.006

Ryerson, Charles C. (2013). Icing Management for Coast Guard Assets Cold Regions Research and

Engineering Laboratory. *US Army Corps of Engineers*, *April 2013*.

Samuelsen, E. M., Løset, S., & Edvardsen, K. (2015). Marine icing observed on KV Nordkapp during a

cold air outbreak with a developing polar low in the Barents sea. *Proceedings of the International

Conference on Port and Ocean Engineering under Arctic Conditions, POAC*, *2015-Janua*(195153).

https://doi.org/10.13140/RG.2.1.2678.8006

Semenov, Y. A., Wu, G. X., & Oliver, J. M. (2013). Splash jet generated by collision of two liquid

wedges. *Journal of Fluid Mechanics*, *737*, 132–145. https://doi.org/10.1017/JFM.2013.529

Sharma, V. S., Dogra, M., & Suri, N. M. (2009). Cooling techniques for improved productivity in turning.

International Journal of Machine Tools and Manufacture, *49*(6), 435–453.

https://doi.org/10.1016/j.ijmachtools.2008.12.010

Shvaishtein, Z. I. (1973). *CUTTING ICE WITH A CONTINUOUS HIGH-PRESSURE WATER JET*.

August.

Sodhi, D. S. (1995). Breakthrough Loads of Floating Ice Sheets. *Journal of Cold Regions Engineering*,

9(1), 4–22. https://doi.org/10.1061/(asce)0887-381x(1995)9:1(4)

Sollén, S., Kumar Eppanapelli, L., Casselgren, J., Pettersson, J., Ukonsaari, J., & Attermo, P. (2022).

Experimental Investigation of an Infrared Deicing System for Wind Power Application in a Cold

Climate. *Journal of Cold Regions Engineering*, *36*(4), 1–9. https://doi.org/10.1061/(asce)cr.1943-

5495.0000284

Srivastava, M., Tripathi, R., Hloch, S., Chattopadhyaya, S., & Dixit, A. R. (2016). Potential of using

water jet peening as a surface treatment process for welded joints. *Procedia Engineering*, *149*(June),

472–480. https://doi.org/10.1016/j.proeng.2016.06.694

Sun, S. L., Hu, J., & Hu, J. Z. (2013). Impact of a compressible water column on an elastic plate. *Chuan

Bo Li Xue/Journal of Ship Mechanics*, *17*(9), 1031–1037. https://doi.org/10.3969/J.ISSN.1007-

7294.2013.09.007

Takahashi, K., Usami, N., Shibata, T., Goto, K., Uehara, T., Kondo, H., Ishikawa, R., & Saeki, H. (2004).

Experimental study on a deicing method using a water jet. *Bridges across the Oceans - Conference Proceedings*, *3*, 1668–1673. https://doi.org/10.1109/oceans.2004.1406374

Thakur, P., Raut, D. N., & Siddiqui, F. (2022). *Recent Applications, Developments and Challenges in Waterjet Technology*. 141–155. https://doi.org/10.1007/978-981-16-9236-9_14

Tijsseling, A. S., Lambert, M. F., Simpson, A. R., Stephens, M. L., Vítkovský, J. P., & Bergant, A. (2008). Skalak's extended theory of water hammer. *Journal of Sound and Vibration*, *310*(3), 718–728. https://doi.org/10.1016/j.jsv.2007.10.037

Timco, G. W., & Weeks, W. F. (2010). A review of the engineering properties of sea ice. *Cold Regions Science and Technology*, *60*(2), 107–129. https://doi.org/10.1016/J.COLDREGIONS.2009.10.003

Villeneuve, E., Harvey, D., Zimcik, D., Aubert, R., & Perron, J. (2015). Piezoelectric deicing system for rotorcraft. *Journal of the American Helicopter Society*, *60*(4), 1–13. https://doi.org/10.4050/JAHS.60.042001

Wang, F., Wang, R., Zhou, W., & Chen, G. (2017). Numerical simulation and experimental verification of the rock damage field under particle water jet impacting. *International Journal of Impact Engineering*, *102*, 169–179. https://doi.org/10.1016/J.IJIMPENG.2016.12.019

Wang, X. (2008). *Convective Heat Transfer and Experimental Icing Aerodynamics of Wind Turbine Blades*. 1–212.

Willberg, C., Vivar-Perez, J. M., Ahmad, Z., & Gabbert, U. (2009). Simulation of piezoelectric induced Lamb waves in plates. *Structural Health Monitoring 2009: From System Integration to Autonomous Systems - Proceedings of the 7th International Workshop on Structural Health Monitoring, IWSHM 2009*, *2*, 2299–2306. https://doi.org/10.1002/pamm.200910224

Xue, Y., Liu, R., Li, Z., & Han, D. (2020). A review for numerical simulation methods of ship–ice interaction. *Ocean Engineering*, *215*, 107853. https://doi.org/10.1016/J.OCEANENG.2020.107853

Yehia, S., & Tuan, C. Y. (1998). Bridge Deck Deicing. *Transportation Conference Proceedings*, 51–57.

Yu, L., Guo, W., Pan, X., & Chen, H. (2021). Analysis and Research on Cold Proof Design of Polar Marine Machinery. *Journal of Physics: Conference Series*, *2125*(1). https://doi.org/10.1088/1742-

6596/2125/1/012060

Yuan, G. Y., Ni, B. Y., Wu, Q. G., Xue, Y. Z., & Han, D. F. (2021). Ice breaking by a high-speed water jet impact. *Journal of Fluid Mechanics*, *934*, A1. https://doi.org/10.1017/JFM.2021.999

Yuan, G. Y., Ni, B. Y., Wu, Q. G., Xue, Y. Z., & Zhang, A. M. (2020). An experimental study on the dynamics and damage capabilities of a bubble collapsing in the neighborhood of a floating ice cake. *Journal of Fluids and Structures*, *92*. https://doi.org/10.1016/J.JFLUIDSTRUCTS.2019.102833

Yuvaraj, N., & Kumar, M. P. (2016). Investigation of process parameters influence in abrasive water jet cutting of D2 steel. *Http://Dx.Doi.Org/10.1080/10426914.2016.1176183*, *32*(2), 151–161. https://doi.org/10.1080/10426914.2016.1176183

Zaki, R., & Barabadi, A. (2014). *Application of De-icing Techniques for Artic Offshore Production Facilities.* 1–8.

Zakrzewski, W. P. (1987). Splashing a ship with collision-generated spray. *Cold Regions Science and Technology*, *14*(1), 65–83. https://doi.org/10.1016/0165-232X(87)90045-0

Zdobyslaw Goraj. (2004). An Overview of the Deicing and Antiicing Technologies With Prospects for the Future. *24Th International Congress of the Aeronautical Sciences*, 1–11.

Zhao, J., Zhang, G., Xu, Y., Lin, A., Zhao, J., & Yang, D. (2019). Enhancing rate of penetration in a tight formation with high-pressure water jet (HPWJ) via a downhole pressurized drilling tool. *Journal of Petroleum Science and Engineering*, *174*(November 2018), 1194–1207. https://doi.org/10.1016/j.petrol.2018.11.042

Zhao, S., He, Z., & Li, Y. (2021). Impact pressure evaluation of water jet peening on typical concave surfaces: Theoretical and finite element analysis. *Journal of Pressure Vessel Technology, Transactions of the ASME*, *143*(3). https://doi.org/10.1115/1.4049713/1096377

Zhao, Z., Chen, H., Liu, X., Wang, Z., Zhu, Y., & Zhou, Y. (2020). Novel sandwich structural electric heating coating for anti-icing/de-icing on complex surfaces. *Surface and Coatings Technology*, *404*(October), 126489. https://doi.org/10.1016/j.surfcoat.2020.126489

Zhaolong, G., Xudong, M., Yajie, J., Yiyu, L., & Binwei, X. (2014). Influence radius of slotted borehole

drainage by high pressure water jet. *Journal of Mining and Safety Engineering*, *31*(4), 657.

Zhou, L., Liu, R., & Yi, X. (2022). Research and development of anti-icing/deicing techniques for vessels: Review. *Ocean Engineering*, *260*(January), 112008. https://doi.org/10.1016/j.oceaneng.2022.112008

Appendix I

Table I. 1: Design of Experiment Cases

Cases	Nozzle Type	Temperature (°C)	Pressure (psi)	Distance (cm)	Time(s)	Depth (cm)	Width (mm)
1	Red	10	1000	5	10	10.8	26
2	Red	10	2000	15	20	20.2	30.5
3	Red	10	3000	10	30	82.5	36.5
4	Red	30	1000	15	30	67.3	35
5	Red	30	2000	10	10	63.6	35
6	Red	30	3000	5	20	67.5	32.5
7	Red	50	1000	10	20	61.5	45
8	Red	50	2000	5	30	73.6	54
9	Red	50	3000	15	10	70.6	38.5
10	Yellow	10	1000	5	10	10.3	38.5
11	Yellow	10	2000	15	20	14.5	72
12	Yellow	10	3000	10	30	25.5	73.5
13	Yellow	30	1000	15	30	28.4	72.5
14	Yellow	30	2000	10	10	21.1	71.5
15	Yellow	30	3000	5	20	45.0	115
16	Yellow	50	1000	10	20	32.3	88.5
17	Yellow	50	2000	5	30	51.9	82.5
18	Yellow	50	3000	15	10	21.6	80
19	Green	10	1000	5	10	9.8	56.5
20	Green	10	2000	15	20	14.2	112
21	Green	10	3000	10	30	15.0	85
22	Green	30	1000	15	30	18.1	115.6
23	Green	30	2000	10	10	16.5	90
24	Green	30	3000	5	20	26.5	128
25	Green	50	1000	10	20	24.3	81
26	Green	50	2000	5	30	42.5	132.5
27	Green	50	3000	15	10	13.8	134
28	White	10	1000	5	10	9.1	104.5
29	White	10	2000	15	20	8.6	160.7
30	White	10	3000	10	30	13.0	110
31	White	30	1000	15	30	16.1	147
32	White	30	2000	10	10	12.5	136.5
33	White	30	3000	5	20	25.0	135
34	White	50	1000	10	20	19.6	165
35	White	50	2000	5	30	33.8	131
36	White	50	3000	15	10	14.3	175

Table I. 2: Cuttability chart for depth of cut between 100 mm and 1500 mm

Nozzle Type	Temperature (°C)	Pressure (psi)	Distance (cm)	Time(s)	Depth (mm)
Red	10.0	1000	15.0	10	193.5
Red	10.7	1006	12.5	10	208.7
Red	11.0	2150	14.8	19	313.0
Red	26.5	1319	12.4	21	417.2
Red	33.9	1767	8.5	18	521.7
Red	33.5	2132	7.9	22	626.1
Red	32.3	1871	7.3	29	730.4
Red	38.5	2605	8.9	27	834.7
Red	49.6	1806	11.5	30	939.1
Red	39.7	2899	5.9	29	1043.4
Red	49.2	2713	6.5	28	1147.8
Red	49.8	2592	5.2	30	1252.1
Red	50.0	3000	5.0	30	1356.2
Yellow	12.0	1131	15.0	10	104.3
Yellow	23.0	1164	6.0	18	208.7
Yellow	26.0	2361	10.3	27	313.0
Yellow	48.2	2964	10.8	20	417.4
Yellow	48.8	1815	5.6	28	521.7
Yellow	49.0	2742	5.8	29	626.1
Yellow	50.0	3000	5.0	30	688.7
Green	11.0	1740	9.5	13	104.3
Green	41.7	2126	13.3	17	208.7
Green	34.1	2861	9.3	28	313.0
Green	48.3	2112	5.4	30	417.4
Green	50.0	3000	5.0	30	506.5
White	28.7	1880	13.9	10	104.3
White	46.6	2607	10.7	15	208.7
White	47.4	2751	12.0	28	313.0
White	49.8	2954	5.2	30	417.4
White	50.0	3000	5.0	30	425.1

Table I. 3: Cuttability chart for width of cut between 30 mm and 210 mm

Nozzle Type	Temperature (°C)	Pressure (psi)	Distance (cm)	Time(s)	Width (mm)
Red	27.0	1035	9.7	10	30.5
Red	50.0	3000	15.0	30	54.4
Yellow	10.0	1000	5.0	10	51.3
Yellow	10.1	1155	9.4	24	61.0
Yellow	45.9	1436	13.5	29	91.4
Yellow	50.0	3000	15.0	30	111.8
Green	10.0	1000	5.0	10	69.0
Green	28.3	1084	5.2	26	91.4
Green	37.4	2533	10.5	28	121.9
Green	50.0	3000	15.0	30	150.5
White	10.0	1000	5.0	10	95.4
White	14.8	1709	13.8	15	121.9
White	35.0	2985	7.4	17	152.4
White	49.3	2699	7.6	30	182.9
White	50.0	3000	15.0	30	207.9

Table I. 4: Mean depth of cut based on temperature

Nozzle	Temperature	Nominal Temperature	Mean Depth
Red	10	0.2	385.0
Red	30	0.6	664.7
Red	50	1	685.7
Yellow	10	0.2	167.7
Yellow	30	0.6	315.0
Yellow	50	1	352.7
Green	10	0.2	130.0
Green	30	0.6	203.7
Green	50	1	270.3
White	10	0.2	102.3

White	30	0.6	178.7
White	50	1	225.7

Table I. 5: Mean depth of cut based on pressure

Nozzle	Pressure	Nominal Pressure	Mean Depth
Red	1000	0.3333	465.3
Red	2000	0.6667	524.7
Red	3000	1	745.3
Yellow	1000	0.3333	236.7
Yellow	2000	0.6667	291.7
Yellow	3000	1	307.0
Green	1000	0.3333	174.0
Green	2000	0.6667	245.7
Green	3000	1	184.3
White	1000	0.3333	149.3
White	2000	0.6667	183.0
White	3000	1	174.3

Table I. 6: Mean depth of cut based on standoff distance

Nozzle	Distance	Nominal Distance	Mean Depth
Red	5	0.3333	509.7
Red	10	0.6667	698.7
Red	15	1	527.0
Yellow	5	0.3333	357.3
Yellow	10	0.6667	263.0
Yellow	15	1	215.0
Green	5	0.3333	264.3
Green	10	0.6667	186.0
Green	15	1	153.7
White	5	0.3333	226.3
White	10	0.6667	150.3

Nozzle			
White	15	1	130.0

Table I. 7: Mean depth of cut based on time of cut

Nozzle	Time	Nom Time	Mean Depth
Red	10	0.3333	483.3
Red	20	0.6667	500.7
Red	30	1	751.3
Yellow	10	0.3333	176.7
Yellow	20	0.6667	306.0
Yellow	30	1	352.7
Green	10	0.3333	133.7
Green	20	0.6667	216.7
Green	30	1	253.7
White	10	0.3333	119.7
White	20	0.6667	177.3
White	30	1	209.7

Table I. 8: Mean width of cut based on temperature

Nozzle	Temperature	Nominal Temperature	Mean Width
Red	10	0.2	31.0
Red	30	0.6	34.2
Red	50	1	45.8
Yellow	10	0.2	61.3
Yellow	30	0.6	86.3
Yellow	50	1	83.7
Green	10	0.2	84.5
Green	30	0.6	111.2
Green	50	1	115.8
White	10	0.2	125.1

White	30	0.6	139.5
White	50	1	157.0

Table I. 9: Mean width of cut based on pressure

Nozzle	Pressure	Nominal Pressure	Mean Depth
Red	1000	0.3333	35.3
Red	2000	0.6667	39.8
Red	3000	1	35.8
Yellow	1000	0.3333	66.5
Yellow	2000	0.6667	75.3
Yellow	3000	1	89.5
Green	1000	0.3333	84.4
Green	2000	0.6667	111.5
Green	3000	1	115.7
White	1000	0.3333	138.8
White	2000	0.6667	142.7
White	3000	1	140.0

Table I. 10: Mean width of cut based on standoff distance

Nozzle	Distance	Nominal Distance	Mean Width
Red	5	0.3333	37.5
Red	10	0.6667	38.8
Red	15	1	34.7
Yellow	5	0.3333	78.7
Yellow	10	0.6667	77.8
Yellow	15	1	74.8
Green	5	0.3333	105.7
Green	10	0.6667	85.3
Green	15	1	120.5

White	5	0.3333	123.5
White	10	0.6667	137.2
White	15	1	160.9

Table I. 11: Mean width of cut based on time of cut

Nozzle	Time	Nominal Time	Mean Width
Red	10	0.3333	33.2
Red	20	0.6667	36.0
Red	30	1	41.8
Yellow	10	0.3333	63.3
Yellow	20	0.6667	91.8
Yellow	30	1	76.2
Green	10	0.3333	93.5
Green	20	0.6667	107.0
Green	30	1	111.0
White	10	0.3333	138.7
White	20	0.6667	153.6
White	30	1	129.3

Table I. 12: Nozzle types and their corresponding mean depth and width of cut

Nozzle Type	Mean Depth	Mean Width
Red	575.1	37.0
Yellow	278.4	77.1
Green	200.8	103.8
White	168.9	140.5